

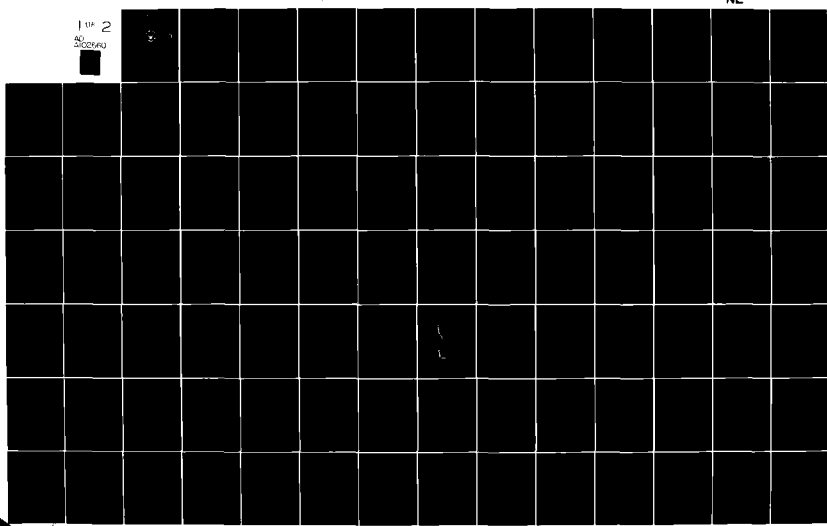
AD-A102 660    NAVAL POSTGRADUATE SCHOOL MONTEREY CA  
RADAR TARGET IMAGING BY TIME-DOMAIN INVERSE SCATTERING.(U)  
MAR 81 M MORAG.

F/G 17/9

UNCLASSIFIED

NL

110 2  
60  
SICARD



LEVEL

2

NAVAL POSTGRADUATE SCHOOL  
Monterey, California



DTIC FILE COPY

AD A102650

THESIS

RADAR TARGET IMAGING BY TIME-DOMAIN  
INVERSE SCATTERING

by

Meir Morag

March 1981

Thesis Advisor:

M. A. Morgan

Approved for public release; distribution unlimited.

813 21 049

## UNCLASSIFIED

SECURITY CLASSIFICATION OF THIS PAGE (When Data Entered)

REPORT DOCUMENTATION PAGE		READ INSTRUCTIONS BEFORE COMPLETING FORM
1. REPORT NUMBER	2. GOVT ACCESSION NO.	3. RECIPIENT'S CATALOG NUMBER
	AD-A102	660
4. TITLE (and Subtitle)	5. TYPE OF REPORT & PERIOD COVERED	
Radar Target Imaging by Time-Domain Inverse Scattering	Master's Thesis; March 1981	
6. AUTHOR(S)	7. PERFORMING ORG. REPORT NUMBER	
Meir/Morag		
8. PERFORMING ORGANIZATION NAME AND ADDRESS	9. CONTRACT OR GRANT NUMBER(S)	
Naval Postgraduate School Monterey, California 93940		
10. CONTROLLING OFFICE NAME AND ADDRESS	11. PROGRAM ELEMENT, PROJECT, TASK AREA & WORK UNIT NUMBERS	
Naval Postgraduate School Monterey, California 93940	12. REPORT DATE	
	March 1981	
13. MONITORING AGENCY NAME & ADDRESS (if different from Controlling Office)	14. NUMBER OF PAGES	
	140	
15. DISTRIBUTION STATEMENT (of this Report)	16. SECURITY CLASS. (of this report)	
Approved for public release; distribution unlimited.	Unclassified	
17. DISTRIBUTION STATEMENT (of the abstract entered in Block 20, if different from Report)	18. DECLASSIFICATION/DOWNGRADING SCHEDULE	
19. SUPPLEMENTARY NOTES		
20. KEY WORDS (Continue on reverse side if necessary and identify by block number)		
Radar Target Imaging Time-Domain Inverse Scattering		
21. ABSTRACT (Continue on reverse side if necessary and identify by block number)		
This thesis describes the study and development of a workable inverse scattering method for imaging and identification of radar targets. The space-time integral approach is used for iterative target shape reconstruction.		
Following an overview of transient electromagnetics, the integral equation is applied for thin-wire transient response computation.		

UNCLASSIFIED

SECURITY CLASSIFICATION OF THIS PAGE WHEN DATA ENTERED:

#20 - ABSTRACT - (CONT.)

The analytical time domain integral equation is derived and solved numerically, for general conducting bodies of revolution. Finally the algorithm for an inverse scattering computer solution is derived and tested under simulation of physical environments.

Acceptance Date	
Initial Release	✓
Classification	
Declassification	
Redistribution	
Storage	
Handling	
Disposition	
Final Disposal	

A

Approved for public release; distribution unlimited.

Radar Target Imaging by Time-Domain  
Inverse Scattering

by

Meir Morag  
Lieutenant Commander, Israeli Navy  
B.S., Technion, Israel Institute of Technology, Haifa, 1970

Submitted in partial fulfillment of the  
requirements for the degree of

MASTER OF SCIENCE IN ELECTRICAL ENGINEERING

from the

NAVAL POSTGRADUATE SCHOOL

March 1981

Author

M. Morag

Approved by:

W. A. M. Karan  
Thesis Advisor

Second Reader

D. Kirk

Chairman, Department of Electrical Engineering

William M. Toller  
Dean of Science and Engineering

ABSTRACT

This thesis describes the study and development of a workable inverse scattering method for imaging and identification of radar targets. The space-time integral approach is used for iterative target shape reconstruction.

Following an overview of transient electromagnetics, the integral equation is applied for thin-wire transient response computation.

The analytical time domain integral equation is derived and solved numerically for general conducting bodies of revolution. Finally, the algorithm for an inverse scattering computer solution is derived and tested under simulation of physical environments.

TABLE OF CONTENTS

I.	INTRODUCTION -----	9
	A. OVERVIEW -----	9
	B. PRACTICAL CONSIDERATIONS -----	13
	C. SURVEY OF THE LITERATURE -----	13
	D. THESIS OBJECTIVES -----	15
II.	GENERAL SOLUTION OF THE TIME DOMAIN INTEGRAL EQUATIONS -----	16
	A. THE INTEGRAL EQUATIONS -----	16
	B. NUMERICAL SOLUTION AND CONSIDERATIONS -----	19
	C. APPLICATION TO THE TIME DOMAIN SCATTERING BY A THIN-WIRE -----	23
III.	THE TIME DOMAIN RESPONSE OF PERFECTLY CONDUCTING BODY OF REVOLUTION -----	30
	A. INTRODUCTION -----	30
	B. THE MAGNETIC FIELD INTEGRAL EQUATION -----	30
	C. FAR ZONE SCATTERED FIELD -----	37
	D. NEAR ZONE BACK-SCATTERED FIELD -----	41
IV.	NUMERICAL SOLUTION OF THE TIME DOMAIN RESPONSE OF THE BODY OF REVOLUTION -----	44
	A. DIVIDING THE BODY INTO PATCHES -----	44
	B. NUMERICAL SOLUTION OF THE INTEGRAL EQUATIONS -----	48
	C. NUMERICAL EXAMPLES -----	54
V.	INVERSE SCATTERING -----	68
	A. PROBLEM DEFINITION -----	68
	B. FORMULATION OF THE PROBLEM -----	68

C. INVERSE SCATTERING SOLUTION PROCEDURE -----	71
D. NUMERICAL SOLUTION AND EXAMPLES -----	73
E. INFLUENCE OF NOISE -----	82
VI. SUMMARY -----	96
A. SUMMARY OF RESULTS -----	96
B. RECOMMENDATIONS -----	97
C. AREAS FOR FURTHER STUDIES -----	99
APPENDIX A: DERIVATION OF THE SCALAR INTEGRAL EQUATIONS -----	101
APPENDIX B: DEMONSTRATION OF THE SINUSOIDAL VARIATION OF THE CURRENTS WITH $\phi$ -----	105
APPENDIX C: SIMPLIFICATION OF THE SCALAR INTEGRAL EQUATIONS -----	107
APPENDIX D: COMPUTER PROGRAM FOR THE TRANSIENT RESPONSE OF A STRAIGHT THIN-WIRE -----	110
APPENDIX E: COMPUTER PROGRAM FOR THE TIME DOMAIN RESPONSE AND INVERSE SCATTERING FOR THE BODY OF REVOLUTION -----	117
APPENDIX F: RELATIONSHIP BETWEEN RAMP RESPONSE AND THE SHAPE -----	136
LIST OF REFERENCES -----	138
INITIAL DISTRIBUTION LIST -----	140

LIST OF FIGURES

2.1	Space-time sampling diagram -----	21
2.2	Geometry of the thin-wire scatterer -----	25
2.3	Current induced at the center of a thin-wire by a gaussian incident pulse. ( $A = 6 \cdot 10^8$ , $a/L = 0.0008$ ) -----	27
2.4	Backscattered field from a thin-wire. ( $A = 6 \cdot 10^8$ , $a/L = 0.0008$ ) -----	28
2.5	Backscattered field from a thin-wire. ( $A = 3.25 \cdot 10^9$ , $a/L = 0.0067$ ) -----	29
3.1	Geometry of the scattering by a body of revolution -----	33
3.2	Body contour -----	35
3.3	Geometry of the far-zone scattered field -----	38
3.4	Geometry of the near-zone backscattered field -	42
4.1	Geometry of the contour sampling -----	46
4.2	Space sampling of whole body -----	47
4.3	Gaussian shaped pulse incident on a sphere ---	55
4.4	Smoothed impulse response of a 1 meter radius sphere -----	57
4.5	Ramp response of a 1 meter radius sphere -----	58
4.6	Measured impulse response of a 30 cm diameter sphere -----	61
4.7	Geometry of the cone sphere target -----	62
4.8	Smoothed impulse response of the cone sphere --	63
4.9	Ramp response of the cone sphere -----	64
4.10	Geometry of the capped cylinder -----	65
4.11	Smoothed impulse response of the capped cylinder -----	66

4.12	Ramp response of the capped cylinder -----	67
5.1	Inverse scattering geometry -----	69
5.2	Contour estimates of the sphere -----	76
5.3	6th estimate of the contour of the sphere -----	77
5.4	Contour estimates of the cone-sphere (cut to 12 segments) -----	78
5.5	6th estimate of the contour of the cone-sphere (cut to 12 segments) -----	79
5.6	Estimates of the contour of the cone sphere (cut to 11 segments) -----	80
5.7	6th estimate of the contour of the cone sphere (cut to 11 segments) -----	81
5.8	Contour estimates of the capped cylinder -----	83
5.9	4th estimate of the contour of the capped cylinder -----	84
5.10	Ramp response of the sphere with noise added (S/N = 10 dB) -----	86
5.11	Ramp response of the sphere with noise added (S/N = 20 dB) -----	87
5.12	Ramp response of the sphere with noise added (S/N = 30 dB) -----	88
5.13	Ramp response of the sphere with noise added (S/N = 40 dB) -----	89
5.14	Estimates of the sphere shape (S/N = 20 dB) ---	90
5.15	6th estimate of the sphere shape (S/N = 20 dB) -----	91
5.16	Estimates of the sphere shape (S/N = 30 dB) ---	92
5.17	8th estimate of the sphere shape (S/N = 30 dB) -----	93
5.18	Estimates of the sphere shape (S/N = 40 dB) ---	95

## I. INTRODUCTION

### A. OVERVIEW

The classification of radar targets, has become increasingly important in the past two decades. In military applications, the need to distinguish between friendly, enemy, and neutral targets, is vital.

In most radar applications, the only properties that are measured are range, angle, velocity and elevation. The methods that are used by radars to provide some classification of the target generally involve the examination of the echo signal. Some of these techniques can be summarized briefly as follows:

1. High range resolution radar, which uses a very short pulse that can provide sufficient range resolution to obtain a rough profile of the illuminated part of the target shape.
2. Cross section fluctuations analysis which can provide information on the size of the target.
3. Synthetic aperture radar that gives a high angular resolution. This method is typically employed in ground mapping.
4. Analysis of the backscattered polarization from a target can provide a means for discrimination between types of targets.
5. Use of nonlinear effects due to junction of metals.

The backscattered spectrum is analyzed and checked for

harmonics appearing in the received signal, that are typical for certain type of targets.

6. Doppler modulation by propellers, the rotary wing in helicopters or even hull vibrations in armored vehicles.

None of the methods cited can be used to obtain all the information on the target shape and size, they only can be used to discriminate to a certain extent between different types of targets. Other methods currently used involve passive reception of radiation by targets.

Elint receivers or IR detectors can be used to monitor radiation from targets, and, based on previous intelligence, or signature catalog, associate a type of radiation to a type of target.

The inverse scattering technique, that is the subject of study in this thesis, uses the basic properties of the transient response to an impulse excitation (impulse response) in order to obtain information on the size, shape and also material composition of the target.

In principle, the smoothed impulse response can be obtained by measuring the backscattered fields at all frequencies up to some upper limit. In most cases this would be impractical so, instead, the target is illuminated by a very short pulse (with a very wide band frequency spectrum ranging from the low frequencies in the Rayleigh region up to higher resonance region frequencies).

The impulse response contains all the information needed to characterize the target. The higher frequencies give the information about the structure. This is related to the optical theory of diffraction which is a good approximation, under certain conditions, for shape prediction up to the shadow boundary. Physical optics, however, fails to predict the phenomena appearing in the shadow region, such as the creeping wave which is due to lower frequency waves travelling around the body.

A different approach that has been used to retrieve target configuration information is related to the singularity expansion method (S.E.M.). This method seeks to classify scatterers through the complex residues and poles of their time domain signatures. Briefly, in this method the transient E.M. response of a conducting body is characterized as a series of complex exponentials (or damped sinusoids): [1], [2]

$$f(t) = \sum_{m=1}^N R_m e^{s_m t}$$

where  $R_m$  is the amplitude (residue) of each mode of complex frequency  $s_m$ . The true function has a complex frequency representation of the form:

$$F(s) = \sum_{m=1}^N \frac{R_m}{s - s_m} .$$

The poles  $s_m$  depend only on the geometry (independently of the orientation), and the residue  $R_m$  depends on both

excitation and geometry [3]. Thus, once the poles and residues are known, they provide a means for target classification. The problem is to find the poles and residues.

A method is suggested using Prony's algorithm in [2] for extraction of poles and residues from time-domain signatures. The method has been tried successfully on wire geometries and simple shapes.

Another important application of the impulse response of a target is the study of its radar cross section (RCS), since the Fourier transform of the impulse response, (the frequency response) is directly related to the RCS by the following relationship:

$$\sigma = \pi c^2 |F(\omega)|^2$$

where

$$F(\omega) = \int_{-\infty}^{\infty} F_I(t) e^{j\omega t} dt$$

and

$F_I(t)$  is the impulse response of the target.

Finally the time-domain analysis of the impulse response of a body is of great importance in the study of the electro-magnetic pulse (E.M.P.) response of targets.

## B. PRACTICAL CONSIDERATIONS

The practical study and measurement of the impulse response involves the building of a time-domain scattering range. The availability of generators having very short pulse-widths, fast rise time, and high voltage outputs, together with fast sampling oscilloscopes and small computers makes the task feasible.

For the solution of the inverse scattering problem the time domain scattering range developed at the Naval Post-graduate School [4], was employed to measure the impulse response and demonstrate the validity of the theories developed in this thesis. The transient response data measured by using pulse generators with very fast rise times can validate the calculation of the time domain integral equation solution. More important, it provides a vehicle for testing various target imagery and I.D. schemes, as well as investigating broad-band RCS reduction.

## C. SURVEY OF THE LITERATURE

One of the first efforts to determine physical properties of electromagnetic scatterers from time-domain analysis was due to Kennaugh and Cosgriff [5], who employed the physical optics approximation to calculate the approximate backscattered impulse response of a flat spheroid.

A summary of this work was reported by Kennaugh and Moffatt [6], who extended the physical optics approximation to transient response calculations. At this stage the computation of the

impulse response was approximated by using the physical optics approach or the inverse transform of the frequency domain solution. Then, in 1968, Bennett derived in his Ph.D. thesis [7] an approach for solving the time domain integral equation directly by using a time-stepping method. Bennett used a form of the equation called the magnetic field integral equation (or M.F.I.E.) for two and three-dimensional surfaces.

Sayre and Harrington [8] used the same time-stepping technique to derive the transient response of a wire, but they employed another type of equation called the electric field integral equation (EFIE).

Additional work in time-domain electromagnetics has been reported in several more recent papers as, for example, the report by Miller, Poggio and Burke [9] on time-domain analysis of thin-wires. Summaries and review of the time-domain electromagnetics are due to Mittra [2] and [10] and Miller [11].

A comprehensive review on the subject and its application has been published by Bennett [12], which gives the reader an introduction and initiation to time-domain electromagnetics. Literature dealing with the inverse scattering problem is due to Young [13] and Shubert, Young and Moffatt [14], which describes the image generation of a target from the ramp response waveform.

Moffatt and Mains [15] describe a method of detection and discrimination of radar targets using the idea of ramp response but with multiple harmonic radar frequencies. Finally, a very

recent report by Bennett [16] gives the general approach to the time domain inverse scattering solution. The method suggested in that report is being used in this thesis to approach the problem of transient target imaging. This list of efforts is by no means exhaustive, as many other authors have published papers dealing with transient electromagnetics and target imaging.

#### D. THESIS OBJECTIVES

The objective of this effort is to develop the analytical and numerical solution of time-domain inverse scattering problem. It follows the development of the time-domain scattering range at the NPS [4].

The main effort has been conducted toward the formulation and numerical solution of the time-domain integral equations for conducting bodies of revolution.

A computer program is developed to solve for direct and inverse scattering. The algorithm was used for experimental display of the shape of the target under test.

## II. GENERAL SOLUTION OF THE TIME DOMAIN INTEGRAL EQUATIONS

This chapter is a review of the development of time domain integral equations, their solutions and the associated numerical considerations. Detailed development of the equations can be found in [2,10,11].

### A. THE INTEGRAL EQUATIONS (E.F.I.E. and M.F.I.E.)

The basis for derivation of the equations are the general time dependent forms of Maxwell's equations:

$$\nabla \times \vec{E}(\vec{r}, t) = - \frac{\partial}{\partial t} \mu_0 \vec{H}(\vec{r}, t)$$

$$\nabla \times \vec{H}(\vec{r}, t) = \frac{\partial}{\partial t} \epsilon_0 \vec{E}(\vec{r}, t) + \vec{J}(\vec{r}, t)$$

$$\nabla \cdot \vec{E}(\vec{r}, t) = \sigma(\vec{r}, t) / \epsilon_0$$

$$\nabla \cdot \vec{H}_0(\vec{r}, t) = 0$$

Starting from these equations, and using the expressions for the magnetic vector potential,  $\vec{A}$ , and the electric scalar potential,  $\phi$ , which are related to the fields by

$$\vec{H}(\vec{r}, t) = \frac{1}{\mu_0} \nabla \times \vec{A}(\vec{r}, t)$$

$$\vec{E}(\vec{r}, t) = - \nabla \phi(\vec{r}, t) - \frac{\partial \vec{A}}{\partial t}(\vec{r}, t)$$

one can obtain the expression of the magnetic field integral equation (M.F.I.E.) for a perfect conductor [2]

$$\vec{J}_s(\vec{r}, t) = 2\hat{n} \times \vec{H}^{inc}(\vec{r}, t) + \frac{1}{2\pi} \hat{n} \cdot \int_S \left[ \frac{1}{c} \frac{\partial}{\partial \tau} + \frac{1}{R} \right] \vec{J}_s(\vec{r}, \tau) \times \frac{\vec{R}}{R^2} dS' \quad (2.1)$$

and the electric field integral equation (EFIR)

$$\hat{n} \times \vec{E}^{inc}(\vec{r}, t) = \frac{\hat{n}}{2\pi} \times \int_S \left[ \frac{\mu_0}{R} \frac{\partial}{\partial \tau} \vec{J}_s(\vec{r}', \tau) - \frac{\sigma(\vec{r}', \tau)}{\epsilon_0 R^2} \left( \frac{1}{R} + \frac{1}{c} \frac{\partial}{\partial \tau} \right) \vec{R} \right] dS' \quad (2.2)$$

In equations (2.1) and (2.2),

$\hat{n}$  is the unit vector normal to the conductor at the observation point  $\vec{r}$ .

$\vec{J}_s(\vec{r}', \tau)$  is the current density at the source point  $\vec{r}'$  at a retarded time  $\tau$ .

$\sigma(\vec{r}', \tau)$  is the charge density at source point at the retarded time  $\tau$ .

Here : is given by

$$\tau = t - R/c$$

and

$R$  is the distance from the observation point  $\vec{r}$  to the source point  $\vec{r}'$ , i.e.,

$$\vec{R} = \vec{r} - \vec{r}'$$

$\vec{E}^{\text{inc}}(\vec{r}, t)$  and  $\vec{H}^{\text{inc}}(\vec{r}, t)$  are the incident electric and magnetic fields at the observation point. Because of numerical constraints, the equation most suitable for closed surfaces is the MFIE equation (2.1) while for thin wires and open structures the EFIE equation (2.2) is used.

Equation (2.1) states that the current induced on a point  $\vec{r}$  of a body at a time  $t$  is due to the incident field  $\vec{H}^{\text{inc}}$  at that point and the sum of scattered fields there from earlier, more distant locations of the body. The interactions between the samples of the body are displaced in time by an amount equal to the transit time of the fields between them.

In the integral, the observation point ( $R = 0$ ) is excluded since this "self-term" is included in the incident field portion of the equation. This determines the general solution for the MFIE equation which is solved directly by marching on in time. The solution is started at a certain time ( $t = 0$ ), and due to causality the integral part of the equation will be zero since there are no past currents. Then, as  $t$  increases, the integral is solved with previous currents already computed. This technique is a time-stepping procedure for solving initial value problems.

For the EFIE, equation (2.2), the method is slightly different but uses the same time stepping procedure. The solution of this equation is applied to the problem of transient scattering by a thin wire, in the next chapter.

The solution of equations (2.1) and (2.2) gives the currents induced on the body by the incident field. Once the

currents are known, it is a straightforward step to compute the scattered fields. For the far-field case the field is given by:

$$\hat{H}^{\text{scatt}}(\vec{r}_o, t) = \frac{1}{4\pi r_o c} \int_S \frac{\partial}{\partial \tau} \vec{J}(r', \tau) \times \hat{a}_R ds' \quad (2.3)$$

where  $\hat{a}_R$  is the unit vector from the source  $r'$  to the far observation point and  $r_o$  is the separation distance.  $\vec{J}_s(r', \tau)$  is the current at the source point at a previous (retarded) time  $\tau = t - r_o/c$ .

#### B. NUMERICAL SOLUTION AND CONSIDERATIONS

The solution of the integral equations implies finding the currents induced on the body once illuminated by an incident field. Since the solution is to be carried out numerically, the first step is to represent the currents by their space and time samples  $J_{ij}(s, t)$  in a discrete manner.  $J_{ij}(s, t)$  is the current at the  $i^{\text{th}}$  segment  $\Delta s$  (or patch) at the  $j^{\text{th}}$  time increment  $\Delta t$ . The total current will be approximated in terms of all samples at all times and spatial segments via the basis function expansion:

$$J(r, t) = \sum_{i=1}^{N_S} \sum_{j=1}^{N_T} J_{ij}(s, t) U(t_j) V(s_i) \quad (2.4)$$

where  $N_S$  is the number of space samples on the body while  $N_T$  is the total number of time increments, and the pulse basis functions are:

$$U(t_j) = \begin{cases} 1 & \text{at the center of the } j\text{th time interval} \\ 0 & \text{elsewhere} \end{cases}$$

$$V(s_i) = \begin{cases} 1 & \text{at the center of the } i\text{th space patch} \\ 0 & \text{elsewhere.} \end{cases}$$

The space time sampling is shown in figure 2.1. The sampling of the currents already suggests that the body is divided into segments (or patches)  $\Delta S$  and the time is sampled at  $\Delta T$  intervals, while the total observation time goes up to  $N_T \times \Delta T$ .

It is very important at this point, before attempting to solve this equation, to define the basic criteria for proper selection of the space and time sampling as well as their relationship to the shape of the exciting pulse and the body size.

The incident field is chosen here to be represented by a gaussian impulse due to its rapidly decreasing features and also because most of the short pulse generators will produce such a waveform.

The gaussian impulse is given by

$$g(t) = e^{-A^2 t^2}$$

Its amplitude falls to 1/10 of its maximum value at  $t_{\max} = 1.5/A$ . Its frequency spectrum is given by [2]

$$G(f) = F\{g(t)\} = e^{-\pi^2 f^2 / A^2}.$$

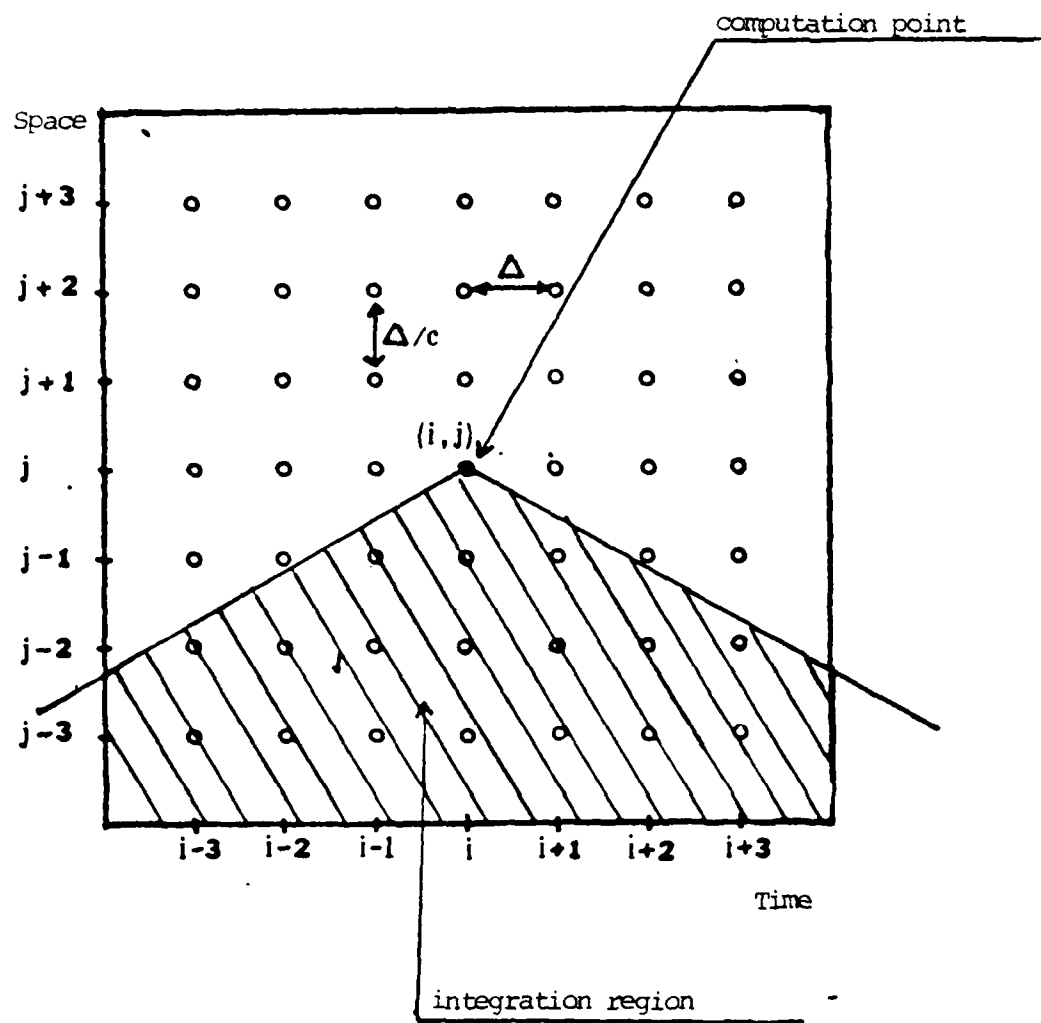


Figure 2.1. Space-time sampling diagram

This response reduces to 1/10 of its maximum value at  $f_{\max} \approx 0.5A$ . The time sampling  $\Delta T$  must exceed the Shannon rate to avoid aliasing problems if FFT's are employed later, i.e.,

$$\Delta T_{\min} \geq \frac{1}{2f_{\max}} = \frac{1}{A}$$

Usually  $\Delta T$  will be taken smaller,

$$\Delta T \approx \frac{1}{5f_{\max}} = \frac{1}{2.5A} \quad (2.5)$$

The spatial sampling  $\Delta S$  must be chosen such that

$$\Delta S \geq \Delta T \times C \quad (2.6)$$

otherwise there will be coupling between the currents of adjacent patches. Violation of (2.6) will also mean that the stepping procedure for solving the equations, which assumes that during one time interval the currents at one patch are not influenced by adjacent currents, will no longer be satisfied, thus producing an incorrect solution.

Another consideration is that the space sample points must be close enough to resolve adequately the spatial variation of the incident field over the body. From Eq. (2.5) and (2.6) we have:

$$\Delta S \geq \frac{C}{5f_{\max}}$$

$$\Delta s \geq \frac{\lambda_{\min}}{5}$$

This latter relationship imposes some minimum ratio of the size  $L$  of the body to the minimum wavelength (or equivalently the minimum pulse width). The ratio  $L/\lambda_{\min}$  determines the resolution and the usefulness of the time domain analysis, and it must be kept high enough to maintain adequate resolution. If the body is to be represented with good fidelity with a certain minimum number of samples  $N_s$  we will need

$$L \geq \frac{N_s \lambda_{\min}}{5}$$

This means that if  $\lambda_{\min}$  increases (i.e., wider pulse)  $L$  must increase or equivalently for a small size target  $\lambda_{\min}$  must decrease (i.e., shorter pulse).

Having presented the equations, their general solution and the requirements for the various parameters involved we can move on to the implementation.

### C. APPLICATION TO THE TIME-DOMAIN SCATTERING BY A THIN-WIRE

The first application that was studied was the computation of the impulse response of a straight thin wire. This example was chosen since it gives a good understanding of the physical processes and the numerical techniques used in the solution of time domain integral equations. The basis for this computation is given by Sayre and Harrington in [8].

The problem is formulated as follows: a thin-wire of length  $L$  and radius  $a$  aligned with the  $z$  axis is illuminated

by an impulse field of the form

$$E^{inc}(t) = e^{-A^2(t-t_{max})^2}$$

The basic formulas are in terms of the retarded potentials:

The boundary condition :

$$E_z^{inc}(t, z) = \frac{\partial A_z}{\partial t} + \frac{\partial \phi}{\partial z}$$

where the retarded magnetic potential is given by :

$$A_z(t, z) = \frac{\mu}{4\pi} \int_{\text{Axis}} \frac{I(z', \tau)}{R} dz'$$

and the retarded electric potential is

$$\phi = \frac{1}{4\pi\epsilon_0} \int_{\text{Axis}} \frac{q(z', \tau)}{R} dz'$$

where the continuity equation between charge and current is

$$\frac{\partial I}{\partial z} = - \frac{\partial q}{\partial t}$$

In these equations  $I(z', \tau)$  and  $q(z', \tau)$  are the current and charge at source point  $z'$  at time  $\tau = t - R/c$ , while  $R$  is the distance between the source and observation points. The geometry is described in figure 2.2.

Using the numerical formulation expressed in [8], and applying the time stepping procedure, a computer program was written (Appendix D) to compute the scattered field from a thin wire of length 1 meter and radius 0.8 mm. The wire was divided into 40 segments and the sampling time  $\Delta T = \Delta z/c = L/40c$ .

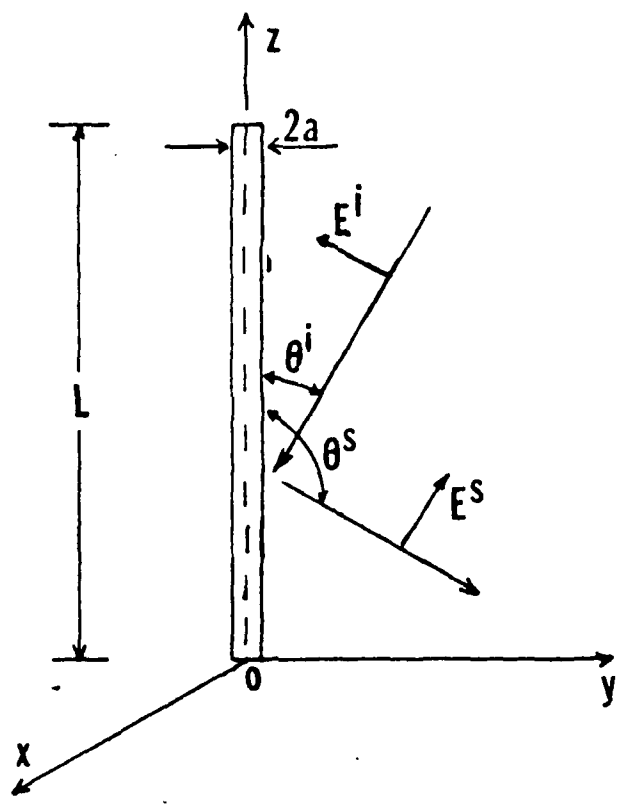


Figure 2.2. Geometry of the thin-wire scatterer

The incident field was taken to be similar to the pulse transmitted by the generator of the NPS transient scattering range, with linear polarization parallel to the wire and incidence normally on it.

$$E^{inc} = e^{-A^2(t-t_{max})^2}$$

$$A = 6 \cdot 10^8 \text{ sec}^{-1}$$

$$t_{max} = 18 \cdot \Delta T \text{ (about half transit time along the wire)}$$

The program computes the currents at each spatial segment with up to 400 time samples. This corresponds to 10 transit times across the wire. The current at the center of the wire is given in figure 2.3. The backscattered field is given in figure 2.4.

No significant change was obtained for 20 segments and 200 time increments. Comparison of this computation with lab measurement was done by Hammond [4] and very good agreement was found.

Similarly, comparison of the computed results found in [11] with a ratio of  $L/a = 0.00667$  and  $A = 3.25 \cdot 10^9$  gave exact agreement. The backscattered field for this case is shown in figure 2.5.

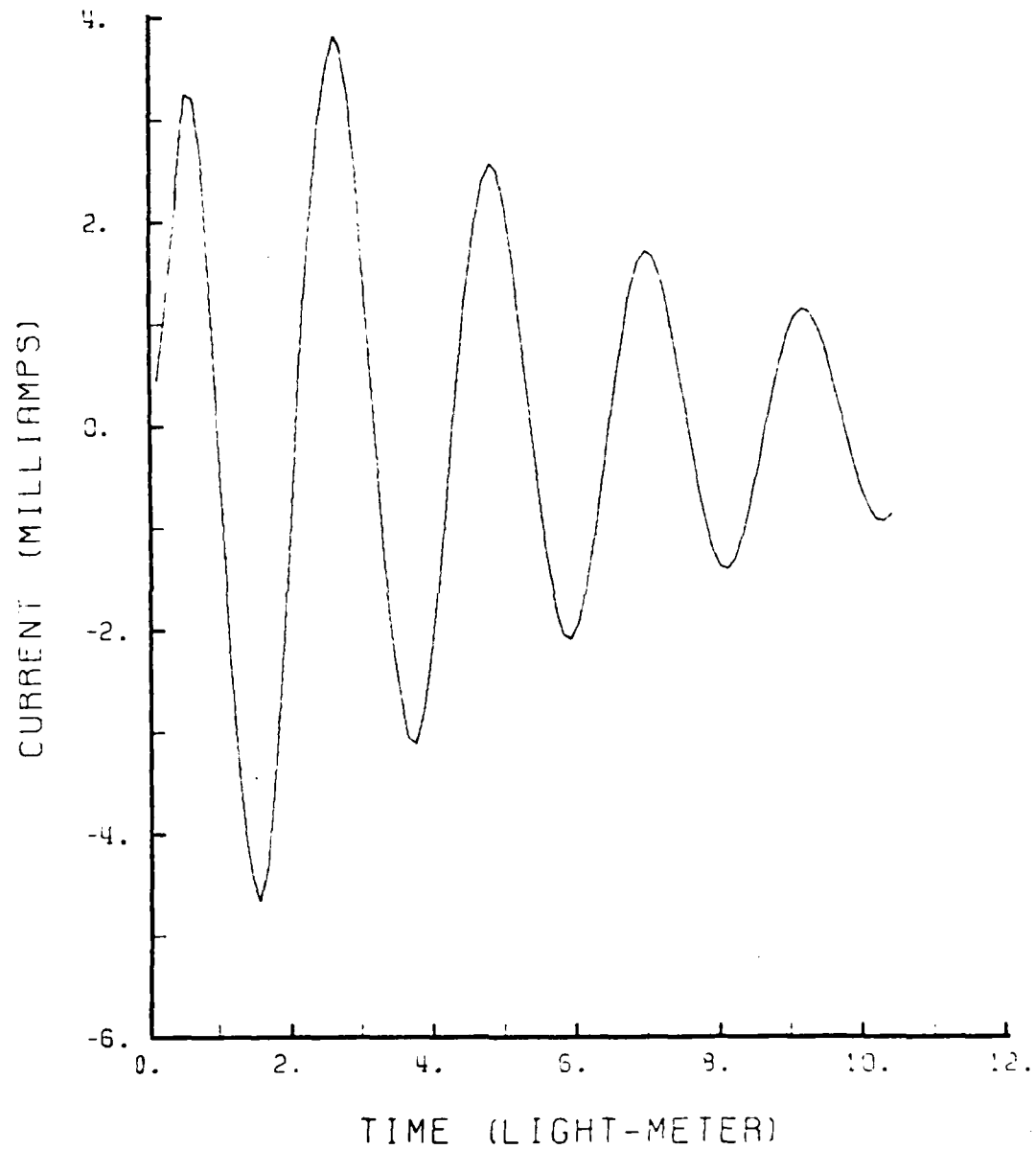


Figure 2.3. Current induced at the center of a thin-wire by a gaussian incident pulse ( $A = 6 \cdot 10^8$  and  $a/L = 0.0008$ )

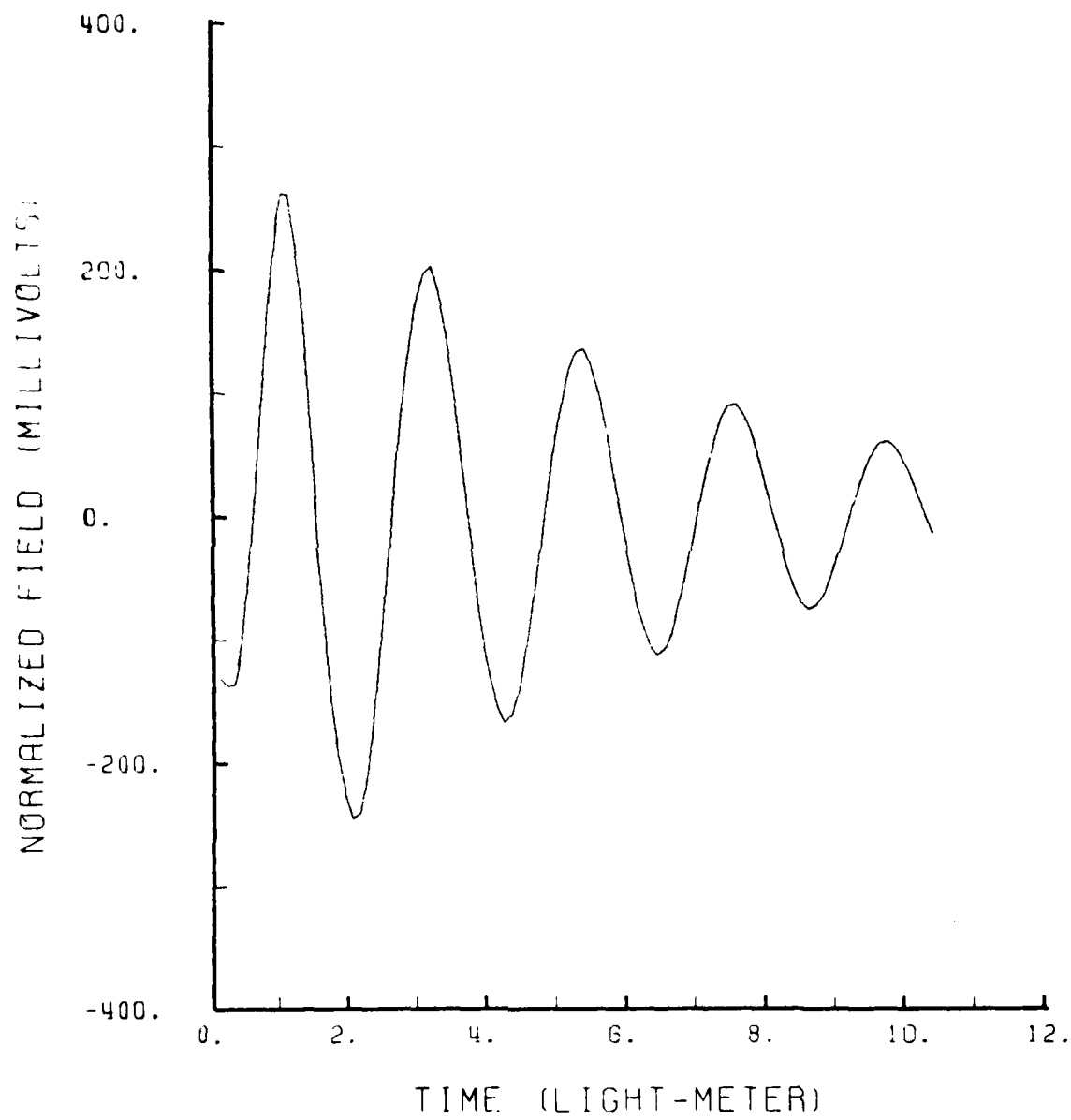


Figure 2.4. Backscattered field from a thin-wire  
( $A = 6 \cdot 10^8$ ,  $a/L = 0.0008$ )

Q [11] Figure 58

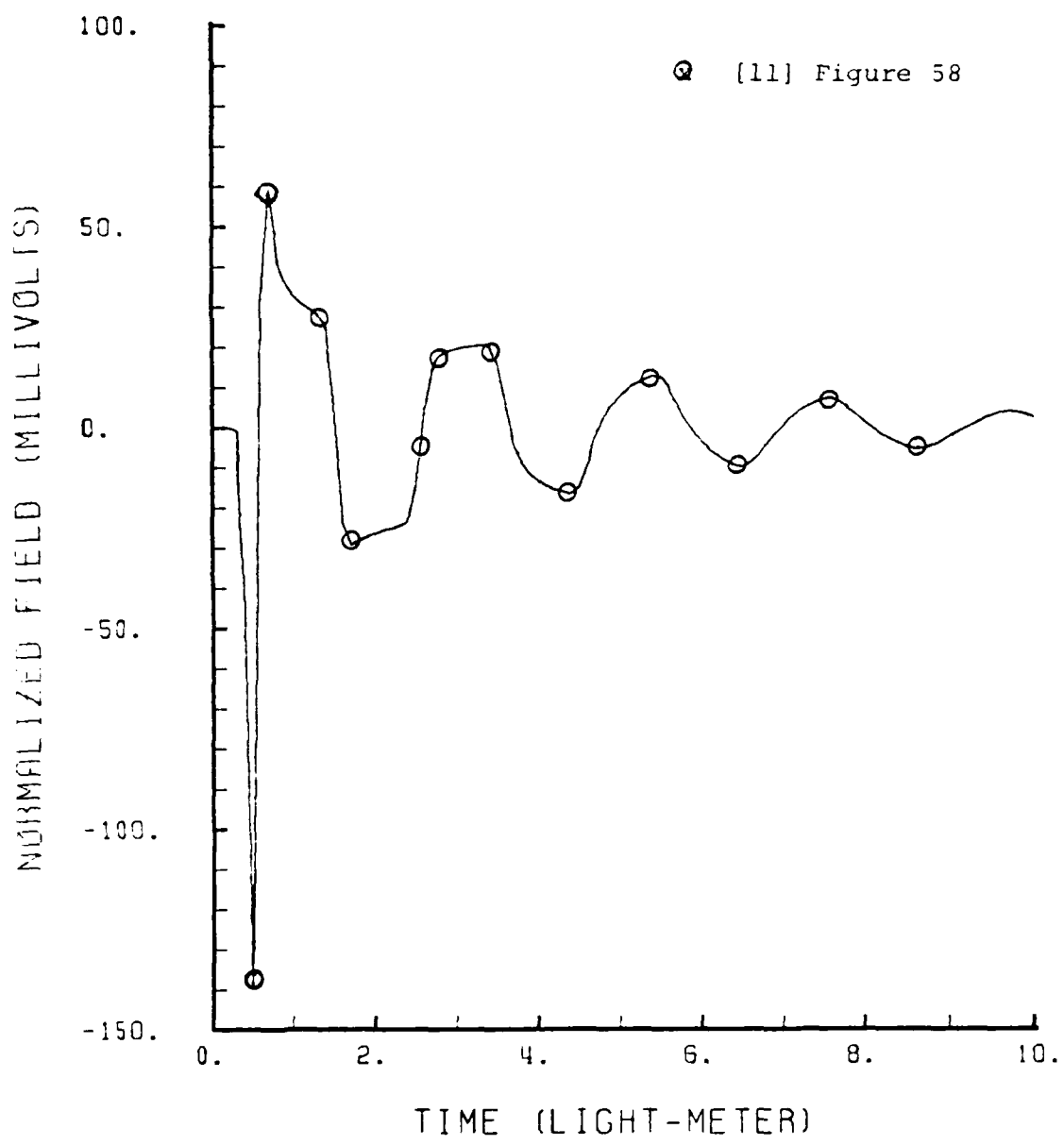


Figure 2.5. Backscattered field from a thin-wire  
( $A = 3.25 \cdot 10^9$  and  $a/L = 0.0067$ )

### III. TIME DOMAIN RESPONSE OF PERFECTLY CONDUCTING BODY OF REVOLUTION

#### A. INTRODUCTION

This section considers the solution of the time domain response for a body of revolution, when the exciting wave is propagated along the axis of symmetry of the body.

The use of the axial symmetry of the body will result in considerable simplification of the computation of both the induced currents on the body surface and the field scattered from the body. The algorithm developed in this section will be used later for the solution of the inverse scattering problem.

#### B. THE MAGNETIC FIELD INTEGRAL EQUATION

In [7] Bennett derives the integro-differential equation for three dimensional scatterers:

$$\vec{J}(\vec{r}, t) = 2\hat{a}_n \times \vec{H}^i(\vec{r}, t) + \frac{1}{2\pi} \int_A [\hat{a}_n \times (\frac{1}{R^2} + \frac{1}{RC} \frac{\partial}{\partial \tau}) \vec{J}(\vec{r}', \tau) \times \frac{\vec{R}}{R}] dA' \quad (3.1)$$

where:

$$\tau = t - R/C \text{ (retarded time)}$$

$\vec{r}$  is the observation point

$\vec{r}'$  is the source (or integration) point

$$R = |\mathbf{r} - \mathbf{r}'|$$

$A$  is the surface of the scatterer

$\mathbf{H}^i(\mathbf{r}, t)$  is the incident magnetic field at the observer's point.

The geometry for the body of revolution is given in figure 3.1.

For the actual problem the incident magnetic field is propagating along the  $z$ -axis (axis of rotation of the body), and is directed towards the positive  $x$ -axis. The body lies completely to the right of the positive  $z$ -axis, and is defined by the continuous contour function,  $\rho(z)$ , which is the radius of the body at a point  $z$ .

The prime coordinates denote the source or integration point, while the unprimed denote the observation point for which the current is desired. At each point on the body, there is defined the triad of orthogonal unit vectors,  $(\hat{\mathbf{a}}_n, \hat{\mathbf{a}}_\phi, \hat{\mathbf{a}}_s)$  where:

$\hat{\mathbf{a}}_n$ : unit vector normal to the surface

$\hat{\mathbf{a}}_\phi$ : unit vector tangent to the surface and directed towards the positive  $\phi$  direction

$\hat{\mathbf{a}}_s$ : unit vector tangent to the surface and directed along the curve representing the longitudinal contour of the body.

For the following derivation we will define the angle  $\alpha$  (or  $\alpha'$ ) as that sustained by  $\hat{\mathbf{a}}_s$  (or  $\hat{\mathbf{a}}'_s$ ) with the  $z$  axis,  $\alpha$  (or  $\alpha'$ ) being positive when  $\hat{\mathbf{a}}_s$  (or  $\hat{\mathbf{a}}'_s$ ) points outward from the  $z$  axis

and negative if it points towards it. The angle  $\phi$  (or  $\phi'$ ) is the angle defined by  $\hat{r}$  (or  $\hat{r}'$ ) with the  $(x, y)$  plane. Equation (3.1) states that the current density at the observation point  $\hat{r}$  at time  $t$  is due to:

1. The current induced by the incident field at  $(\hat{r}, t)$ .

This part represents the physical optics approximation,

$$2a_n \times \vec{H}^i(\hat{r}, t).$$

2. The current due to the flow of currents at all other points of the body at a retarded time  $\tau = t - R/C$ , where  $R$  is the distance from the integration point to the observation point.

According to the geometry described in figure 3.1 we can write

$$R = (\rho^2 + \rho'^2 - 2\rho\rho' \cos(\phi' - \phi) + (z' - z)^2)^{1/2}$$

The current on the body will flow only in the  $\hat{s}$  and  $\hat{\phi}$  directions and can be expressed (for both primed and unprimed coordinates), as

$$\vec{J}(\hat{r}, t) = J_s(\rho, z, t, \phi) \cdot \hat{a}_s + J_\phi(\rho, z, t, \phi) \cdot \hat{a}_\phi$$

where  $J_s(\rho, z, t, \phi)$  and  $J_\phi(\rho, z, t, \phi)$  are the scalar values of the current components and are functions of the position on the scatterer. We will denote them simply by  $J_s$  and  $J_\phi$  so that

$$\vec{J}(\hat{r}, t) = J_s \hat{a}_s + J_\phi \hat{a}_\phi.$$

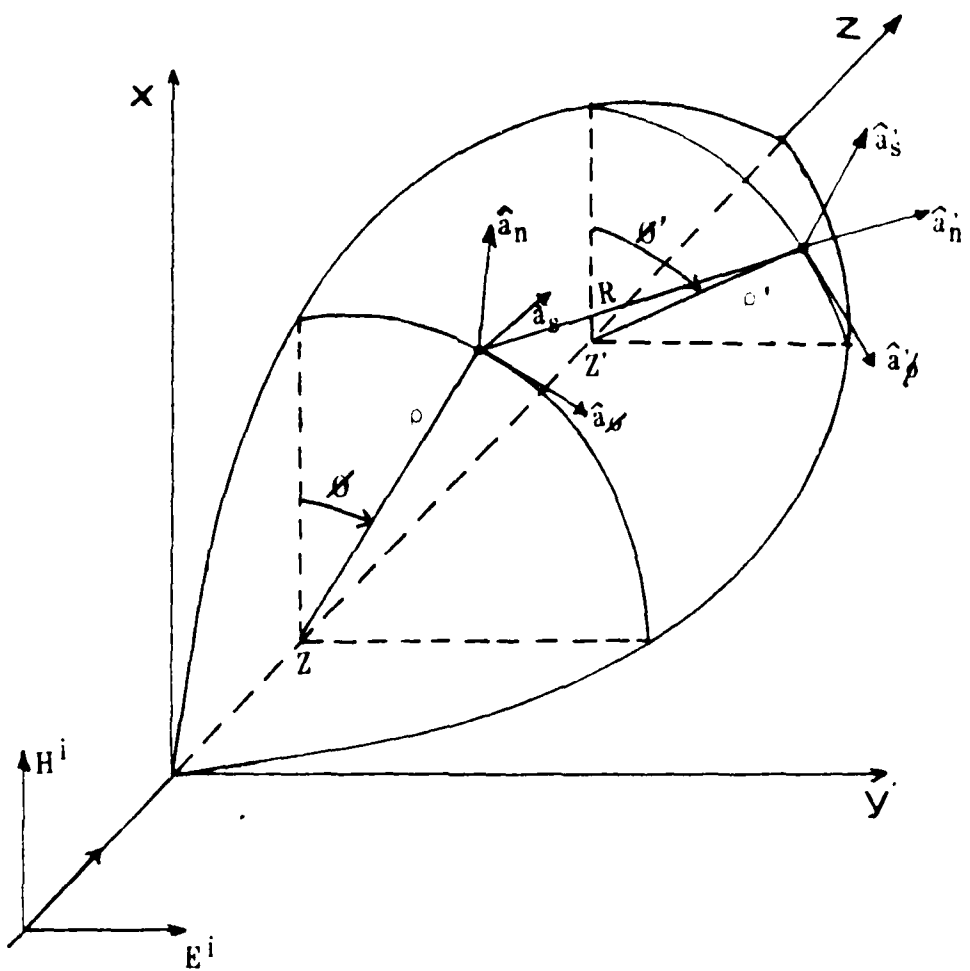


Figure 3.1. Geometry of the scattering by a body of revolution

Eq. (3.1) can be written in terms of its components in the  $\hat{s}$  and  $\hat{\phi}$  direction, i.e.,

$$J_s(r, t) = [2\hat{a}_n \times \vec{H}^i(r, t)]_s + \frac{1}{2\pi} \int \frac{1}{A} \frac{1}{R^2} \left[ \frac{1}{R} + \frac{1}{C} \frac{\partial}{\partial \tau} \right] [\hat{a}_n \times \vec{J}' \times \vec{R}]_s dA' \quad (3.2)$$

$$J_\phi(r, t) = [2\hat{a}_n \times \vec{H}^i(r, t)]_\phi + \frac{1}{2\pi} \int \frac{1}{A} \frac{1}{R^2} \left[ \frac{1}{R} + \frac{1}{C} \frac{\partial}{\partial \tau} \right] [\hat{a}_n \times \vec{J}' \times \vec{R}]_\phi dA' \quad (3.3)$$

In order to obtain the scalar expressions of the two last equations we have to perform the vector multiplications: This is done in Appendix A and as a result, equations (3.2) and (3.3) become:

$$J_s = -2H^i(z, t) \sin \phi + \frac{1}{2\pi} \int \frac{1}{A} \frac{1}{R^2} \left[ \frac{1}{C} \frac{\partial}{\partial \tau} + \frac{1}{R} \right] [J'_s \cdot F_1 - J'_\phi V \sin \beta] dA' \quad (3.4)$$

$$J_\phi = -2H^i(z, t) \cos \phi \sin \alpha + \frac{1}{2\pi} \int \frac{1}{A} \frac{1}{R^2} \left[ \frac{1}{C} \frac{\partial}{\partial \tau} + \frac{1}{R} \right] [J'_s U \sin \beta + J'_\phi F_2] dA' \quad (3.5)$$

where:

$$\beta = \phi' - \phi$$

$$F_1 = (z' - z) \cos \beta \sin \alpha' + (\rho - \rho' \cos \beta) \cos \alpha'$$

$$V = z' - z$$

$$F_2 = (\rho \cos \beta - \rho') \cos \alpha + \sin \alpha \cos \beta (z' - z)$$

$$U = (z' - z) \sin \alpha \cdot \sin \alpha' + \rho \cos \alpha \sin \alpha' - \rho' \sin \alpha \cdot \cos \alpha'$$

We note that the incident field  $H^i$  is dependent only on  $z$  and  $t$  (independnet of  $\phi$  due to symmetry). We also note that:

$$dA' = \rho' d\phi' ds' = \rho' d\phi ds'$$

The integrals in Eq. (3.4) and (3.5) can then be divided into two parts: integration over  $\phi$  from 0 to  $2\pi$ , and integration over  $ds'$  from 0 to  $S$  ( $S$  being the contour curve as shown in figure 3.2).

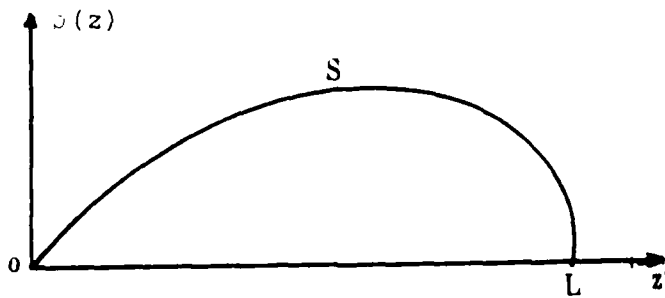


Figure 3.2. Body contour

The next step is to obtain further simplification of the integral equations (3.4) and (3.5).

The currents in these equations are functions of their position on the body:

$$J_s = J_s(z, \rho, \phi, t)$$

$$J_\phi = J_\phi(z, \rho, \phi, t)$$

But we remark that the currents due to the incident field have a sinusoidal variation with  $\phi$ , as follows:

$$J_\phi = H^i(z, t) \cos \phi \cdot \sin \alpha$$

$$J_s = H^i(z, t) \sin \phi$$

so that we can assume that the currents will have the same respective relationships with  $\phi$ .

$$J_s(z, \rho, t, \phi) = J_s(z, \rho, t) \sin \phi = J_s \cdot \sin \phi \quad (3.6)$$

$$J_\phi(z, \rho, t, \phi) = J_\phi(z, \rho, t) \cos \phi = J_\phi \cdot \cos \phi \quad (3.7)$$

This assumption is demonstrated in Appendix B, using Maxwell's equation.

After substitution of equations (3.6) and (3.7) into the integrals (3.4) and (3.5), the integrals over the angle  $\beta$  can be simplified as shown in Appendix C, so that the scalar integral equations reduce to their final expressions:

$$J_s = -2H^i(z, t) + \frac{1}{2\pi} \int_0^S \rho' ds' \int_0^{2\pi} \frac{1}{R^2} \left[ \frac{1}{R} + \frac{1}{C} \frac{\partial}{\partial \tau} \right] \cdot [J'_s F_1 \cos \beta + V \sin^2 \beta J'_\phi] d\beta \quad (3.8)$$

$$J_\phi = -2H^i(z, t) \sin \alpha + \frac{1}{2\pi} \int_0^S \rho' ds' \int_0^{2\pi} \frac{1}{R^2} \left[ \frac{1}{R} + \frac{1}{C} \frac{\partial}{\partial \tau} \right] \cdot [J'_s U \sin^2 \beta + F_2 \cos \beta J'_\phi] d\beta \quad (3.9)$$

in which the currents  $J_s$  and  $J_\phi$  ( $J'_s$  and  $J'_\phi$ ) are only functions of  $\rho$ ,  $z$ , and  $t$  ( $\rho', z', \tau$ ) and independent of the angle  $\phi$ .

The significance here is that the surface distribution of the unknown currents is reduced to a one-dimensional variation of current along the generating arc of the surface of revolution.

This will allow considerable reduction in computer time and storage when carrying out the numerical solution of the equations.

Once the currents along the contour of the body are known, the currents at any other point (at some time  $t$  and some  $z$  position) will be given by

$$J_s(\rho, z, t, \phi) = J_s(\rho, z, t) \cdot \sin \phi$$

$$J_\phi(\rho, z, t, \phi) = J_\phi(\rho, z, t) \cdot \cos \phi.$$

### C. FAR-ZONE SCATTERED FIELD

In most cases we are interested in the far scattered field. At a large distance from the body the scattered field is given by:

$$H^s(\vec{r}, t) = \frac{1}{4\pi r_0 C} \int_A \frac{\partial}{\partial \tau} [\vec{J}(\vec{r}', \tau) \times \hat{a}_R] dA' \quad (3.8)$$

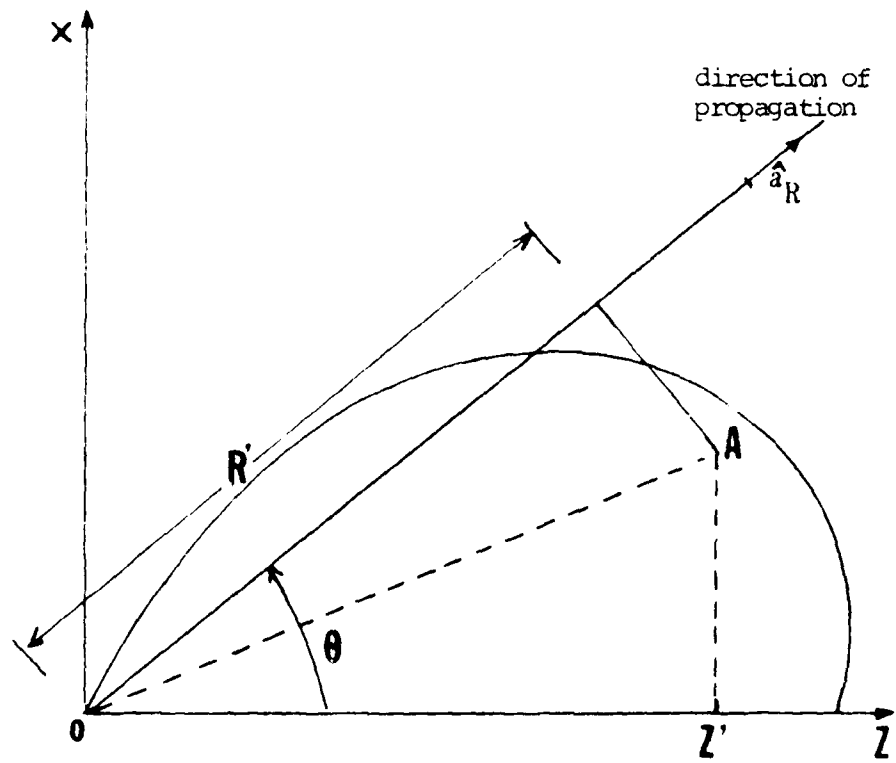
where

$\tau$  is the retarded time  $t - R'/C$ .

$R'$  is the path difference between the integration point to the observer and the origin to the observer.

$\vec{J}(\vec{r}', \tau)$  is the current at the surface integration point retarded in time, while  $\hat{a}_R$  is the unit vector pointing from the source point towards the observation point. The geometry is described in figure 3.3.

$r_0$  is the distance from the origin to the observation point.



A is the projection of the source point on the plane  $(x, z)$

Figure 3.3. Geometry for the far-zone scattered field

In the following, the scattered field will be derived for an arbitrary elevation angle  $\alpha$ . Due to symmetry with  $\phi$  there is no loss of generality if we observe the scattered field in the plane  $(x, z)$  where  $\phi = 0$ .

According to the geometry:

$$R' = -[z' \cos \theta + r' \cos \phi' \sin \theta]$$

$$t = t - R/C.$$

$R'$  is negative whenever the observation point is closer to the source than the origin, and positive otherwise.

$$\hat{a}_R = \sin \theta \hat{a}_x + \cos \theta \hat{a}_z$$

Performing the vector multiplication in equation (3.8) and separating the field into its cartesian components, gives the following set of three scalar equations:

$$H_x^s(\theta, t) = \frac{1}{4\pi r_o C} \int_A \frac{\partial}{\partial \tau} [J_s \sin^2 \phi' \sin \alpha' + J_\phi \cos^2 \phi'] \cos \theta dA' \quad (3.9)$$

$$H_y^s(\theta, t) = \frac{1}{4\pi r_o C} \int_A \frac{\partial}{\partial \tau} [(J_\phi - J_s \sin \alpha') \sin \phi' \cos \phi' \cos \theta + J_s \sin \phi' \sin \theta \cos \alpha'] dA' \quad (3.10)$$

$$H_z^s(\theta, t) = \frac{1}{4\pi r_o C} \int_A \frac{\partial}{\partial \tau} [-\sin \theta (J_s \sin^2 \phi' \sin \alpha' + J_\phi \cos^2 \phi')] dA' \quad (3.11)$$

After substitution of  $dA' = \rho' d\phi' ds'$ , and using the odd properties of some of the terms appearing in the integral on

(as it has been done previously in Appendix C), the three scalar equations representing the components of the scattered field reduce to the following expressions:

$$H_x^S(\theta, t) = \cos \theta H_o^S(t) \quad (3.12)$$

$$H_z^S(\theta, t) = -\sin \theta H_o^S(t) \quad (3.13)$$

$$H_y^S(\theta, t) = 0 \quad (3.14)$$

where the common term  $H_o^S(t)$  is given by the following integral:

$$H_o^S(t) = \frac{1}{4\pi r_o C} \int_0^S \int_0^{2\pi} \frac{\partial}{\partial \tau} (J_s \sin^2 \phi' \sin \chi' + J_d \cos^2 \phi') d\phi' \quad (3.15)$$

Equations (3.12) to (3.15) represent the scattered field for an arbitrary elevation angle  $\theta$ . The special case of interest is the backscattered field where  $\theta = \pi$ . For this case there is only one component of the scattered field, which is

$$H_x^S(t) = -H_o^S(t)$$

and the retarded time is:

$$\tau = t - R'/C$$

where

$$R' = z'.$$

All the terms appearing inside the integral in equation (3.15) are independent of  $t'$  so that the integration on  $t'$  can be carried out analytically. Doing this yields the following expression for the backscattered field:

$$H_s^s(t) = -\frac{1}{4r_0C} \int_0^S \frac{\partial}{\partial \tau} [J_s(s', z', \tau) \sin \omega t' + J_s(s', z', \tau)] s' ds' \quad (3.16)$$

In equation (3.16), the currents  $J_s$  and  $J_s$  are those given by equations (3.8) and (3.9) respectively, used at time  $\tau = t - z'/C$  ( $z' \geq 0$ ), where  $z'/C$  is the retardation time relative to the origin. The backscattered field equation is independent of  $t$  which means that we can integrate the time derivative of the currents, along a line on the contour of the body.

#### D. NEAR ZONE BACKSCATTERED FIELD

In the Time Domain Scattering Range developed at NPS, the distance from the antenna to the target under test is not long enough to be considered for all frequencies of interest as a far region. Consequently, it is needed to develop a formulation of the scattered field in the near zone. For this case the geometry is described in figure 3.4.

The general equation for the scattered field is given by:

$$\vec{H}^s(\vec{r}, t) = \frac{1}{4\pi} \int_A \left[ \frac{1}{R^2} + \frac{1}{RC} \frac{\partial}{\partial \tau} \right] [\vec{J}(\vec{r}', \tau) \times \vec{R}] \frac{dA'}{R} \quad (3.17)$$

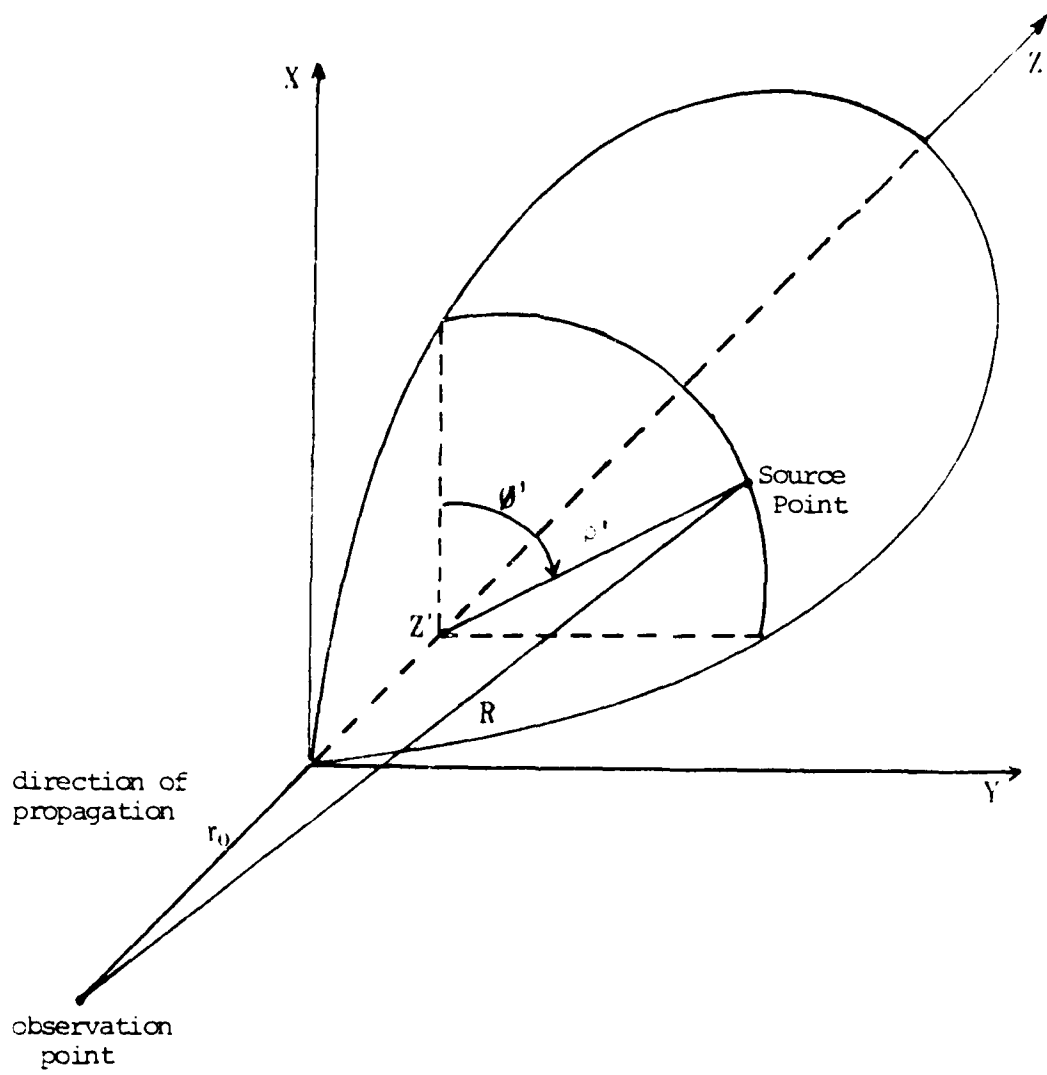


Figure 3.4. Geometry of the near-zone backscattered field

where

$$\tau = t - R/C, \text{ and}$$

$$dA' = \rho' d\phi' ds'$$

$$R'^2 = (r_o^2 + z'^2) + \rho'^2$$

After carrying out the vectorial multiplication, dividing the field vector into its cartesian components, again dropping all the odd terms in  $\phi'$  and integrating analytically on  $\phi'$ , equation (3.17) reduces to:

$$H_x^s(r_o, t) = \frac{1}{4} \int_0^s \frac{1}{R'^2} \left[ \frac{1}{R'} + \frac{1}{C} \frac{\partial}{\partial \tau} \right] [J_s(\rho' \cos \alpha' - (r_o + z') \sin \alpha' - J_\phi(r_o + z'))] \rho' ds' \quad (3.18)$$

Equation (3.18) is the expression of the near backscattered field where:

$$R' = ((r_o + z')^2 + \rho'^2)^{1/2}$$

The currents  $J_s(\rho', z', \tau)$  and  $J_\phi(\rho', z', \tau)$  are given by equations (3.8) and (3.9), being used at the retard time  $\tau$ .

$$\tau = t - (R' - r_o)/C \quad (\text{referred to the origin})$$

#### IV. NUMERICAL SOLUTION OF THE TIME DOMAIN RESPONSE OF THE BODY OF REVOLUTION

In the previous section the analytical equations for the currents and scattered field were derived. The equation obtained will have to be solved numerically, and the first step will be to divide the body into patches of approximately equal curvilinear surface area. This is followed by the setup of the algorithm for the solution.

##### A. DIVIDING THE BODY INTO PATCHES

The geometry of the body is completely specified by the function  $s(z)$ , ( $0 < z \leq L$ ); which represents the body contour function  $S$ . Since the integration is to be carried over  $S$ , the contour will be divided into  $NS$  segments of equal length  $\Delta S$ . Consequently, the body contour function is fully defined by  $NS+1$  points.

$$s_i(z_i) \quad i = 1 \text{ to } NS+1$$

The space samples of each segment  $\Delta S$  is at the middle of the segment and is given by

$$\begin{aligned} s_i &= (s_{i+1} + s_i)/2 & i = 1, \dots, NS & (4.1) \\ z_i &= (z_{i+1} + z_i)/2 \end{aligned}$$

The angle  $\alpha$  for each sample point is the slope of the curve at that point and is approximated linearly by

$$\alpha_i = \text{Arctan} \left( \frac{r_{i+1} - r_i}{z_{i+1} - z_i} \right), \quad i = 1, \dots, NS \quad (4.2)$$

Figure 4.1 shows the geometry of the contour sampling. Each segment  $\Delta S$  defines a ring at  $z_i$  with radius  $r_i$ . All the rings will be divided into patches of approximately equal surface area,  $dA_i$ , according to the following formulas:

$$dA_i \approx \Delta S \cdot r_i \cdot \Delta \beta_i = \Delta S^2$$

where  $\Delta \beta_i$  is the angle between two adjacent sample points on the same ring.

$$\Delta \beta_i = \frac{\Delta S}{r_i}$$

This suggests a division of each ring into an even number of patches NPI which will be

$$NPI = 2 \times \text{INT} \left( \frac{\pi r_i}{\Delta S} \right) \quad (4.3)$$

The function INT means the integer value of its argument so that the increment angle for the  $i^{\text{th}}$  ring becomes

$$\Delta \beta_i = \frac{2\pi}{NPI} \quad (4.4)$$

Thus, following this procedure, any arbitrarily shaped body of revolution can be subdivided into patches of approximately equal surface area. Figure 4.2 shows the geometry of the space sampling on the whole body.

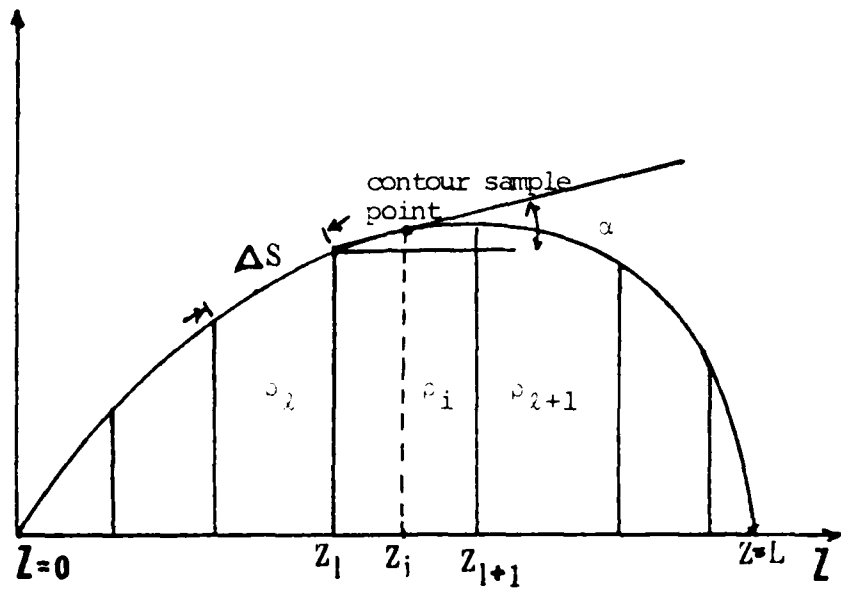


Figure 4.1. Geometry of the contour sampling

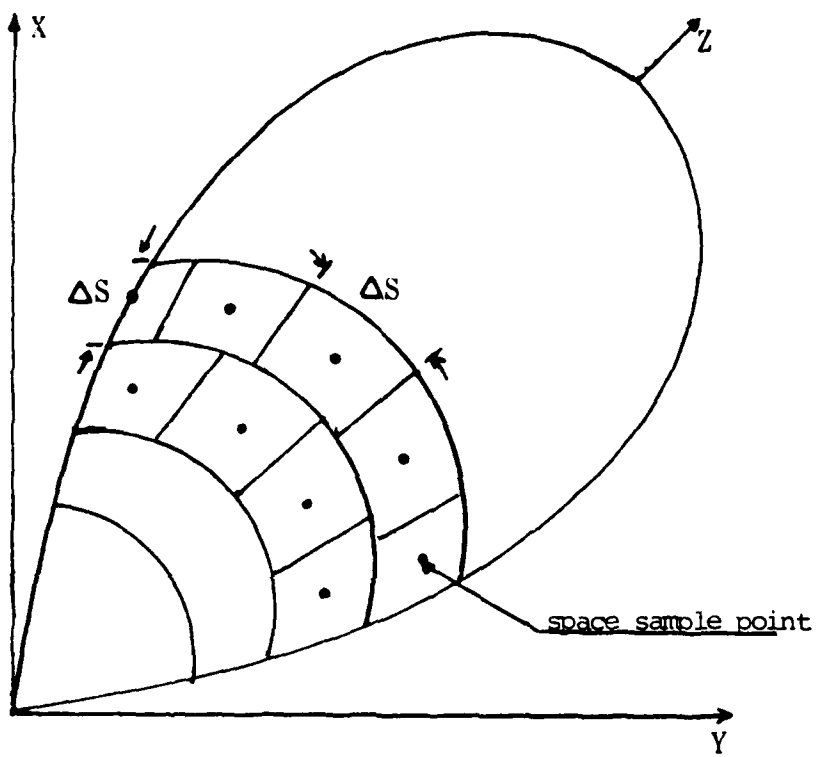


Figure 4.2. Space sampling of the whole body

## B. NUMERICAL SOLUTION OF THE INTEGRAL EQUATIONS

The equations to be solved are given by Eq. (3.8) and (3.9) in previous sections.

For the numerical solution the currents will be represented by their space-time samples:

$$J(\rho, z, t) = J(i, n)$$

where  $i$  is the  $i^{\text{th}}$  space sample on the contour function and  $n$  is the  $n^{\text{th}}$  time sample

$$i = 1, \dots, NS$$

$$n = 1, \dots, NT$$

$$t = n \cdot \Delta T$$

The time being sampled at a rate  $\Delta T$ . Similarly the incident field is sampled and will be denoted by its  $n^{\text{th}}$  time sample at the  $i^{\text{th}}$  segment:

$$H^i(z, t) = H^i(i, n)$$

The general procedure for the numerical procedure was already mentioned in Chapter II, and will be reviewed in more detail here. The incident field,  $H$ , is assumed to be zero at all times less than some reference value (which will be set equal to  $t_0$ ). Hence the total current on the surface of the scatterer is also zero prior to time  $t_0$ .

At the next time interval  $t_1 = t_0 + \Delta t$  the incident field reaches the scatterer at  $z = z_1$  (first space sample), thus at

time  $t_1$  the current will be simply twice the tangential component of the incident field. As time marches on, the incident field covers more of the body and the current will be due to the incident field plus the fields due to currents at other points on the scatterer at earlier times. So, by marching on in time, the currents at each space sample, for each time increment, can be computed.

The currents appearing inside the integrals in equations (3.8) and (3.9) are the retarded currents, and are given by

$$J'_{S,k}(\rho', z', \tau) = J'_{S,k}(\rho', z', t - R/C)$$

The point  $(\rho', z')$  is represented by the  $k$ -th space sample while the time  $\tau$  will be:

$$\tau = t - R/C = n \cdot \Delta t - R/C = g \Delta T.$$

In the general case  $\tau$  will not be an integer multiple of  $\Delta T$ , so that the current cannot be represented by any of the previously computed samples. In order to find the value of the current at time  $\tau$ , there is a need to interpolate between the sampled known, discrete values.

For a better accuracy use was made of the four point Lagrangian interpolation formula using two samples at each side of the value  $g \Delta T$  if  $t_1, t_2, t_3, t_4$  are the four samples used for interpolation, such that:

$$t_4 = t_3 + \Delta t = t_2 + 2\Delta t = t_1 + 3\Delta t$$

$$t_4 = g_4 \Delta t$$

$$t_3 = g_3 \Delta t$$

$$t_2 = g_2 \Delta t$$

$$t_1 = g_1 \Delta t$$

$g_1, g_2, g_3, g_4$  are integer values, and

$$\tau = g \Delta t \quad (g \text{ real number})$$

such that

$$t_1 < t_2 < \tau < t_3 < t_4$$

The interpolation formula using those four points will be given by: [17]

$$J_{s,\phi}(\tau) = \sum_{n=1}^4 \left[ \prod_{\substack{i=1 \\ i \neq n}}^4 \left( \frac{\tau - t_i}{t_n - t_i} \right) J_{s,\phi}(t_n) \right] \quad (4.5)$$

This interpolation formula must be adjusted in two cases:

1. Whenever  $t_3$  or  $t_4$  is greater than the actual time of computation  $t$  (in order not to interpolate in the future).
2. Whenever  $t_1$  or  $t_2$  are less than the beginning time of computation  $t_0$  (due to causality).

The time derivative of the currents will be simply expressed as the derivative with respect to  $\tau$  of the interpolated value, which will give the following formula:

$$\frac{\partial J_{s,\phi}(t)}{\partial t} = \sum_{n=1}^4 \frac{\partial}{\partial t} \left[ \prod_{\substack{i=1 \\ i \neq n}}^4 \left( \frac{t-t_i}{t_n-t_i} \right) J_{s,\phi}(t_n) \right] \quad (4.6)$$

Defining:

$$T_1 = g - g_1$$

$$T_2 = g - g_2$$

$$T_3 = g - g_3$$

$$T_4 = g - g_4$$

The interpolation formulas for the current and its time derivative can be written in their numerical form as follows:

$$\begin{aligned} J_{s,\phi}(i,g) &= \frac{T_1 \times T_2 \times T_3}{6} J_{s,\phi}(i,g_4) - \frac{T_2 \times T_3 \times T_4}{6} \\ &\quad \cdot J_{s,\phi}(i,g_1) + \frac{T_3 \times T_4 \times T_1}{2} J_{s,\phi}(i,g_2) \\ &\quad - \frac{T_4 \times T_1 \times T_2}{2} J_{s,\phi}(i,g_3) \end{aligned} \quad (4.7)$$

and

$$\begin{aligned} DJ_{s,\phi} &= \frac{\partial J_{s,\phi}(i,g)}{\partial t} = \frac{T_1 T_2 + T_2 T_3 + T_1 T_3}{6 \Delta T} J_{s,\phi}(i,g_4) \\ &\quad - \frac{T_2 T_3 + T_3 T_4 + T_2 T_4}{6 \Delta T} J_{s,\phi}(i,g_1) \\ &\quad + \frac{T_3 T_1 + T_4 T_1 + T_3 T_4}{2 \Delta T} J_{s,\phi}(i,g_2) \\ &\quad - \frac{T_4 T_1 + T_1 T_2 + T_2 T_4}{2 \Delta T} J_{s,\phi}(i,g_3) \end{aligned} \quad (4.8)$$

Now we can write the numerical expression for the currents in equations (3.8) and (3.9) by representing the continuous integration by numerical summation, and expressing the currents in terms of their space-time samples.

For simplicity, we will write first the expression for the integral part of equation (3.8) and (3.9) which will be denoted by  $J_{cs}$ , and  $J_{cp}$ .

$$J_{cs}(k,n) = \frac{1}{2\pi} \sum_{i=1}^{NS} \Delta\beta_i \rho_i \Delta s_i \sum_{\substack{m=1 \\ m \neq i \text{ for } i=k}}^{NP} \frac{1}{R_{kim}^2} \cdot \left[ \frac{V \cdot s_i^2(m) J_{\phi}(i,g) + F_1 CO(m) J_s(i,g)}{R_{kim}} \right. \\ \left. + \frac{V \cdot s_i^2(m) DJ_{\phi}(i,g) + F_1 CO(m) DJ_s(i,g)}{C} \right] \quad (4.9)$$

$$J_{cp}(k,n) = \frac{1}{2\pi} \sum_{i=1}^{NS} \Delta\beta_i \rho_i \Delta s_i \sum_{\substack{m=1 \\ m \neq i \text{ for } i=k}}^{NP} \frac{1}{R_{kim}^2} \cdot \left[ \frac{U \cdot s_i^2(m) J_s(i,g) + F_2 CO(m) J_{\phi}(i,g)}{R_{kim}} \right. \\ \left. + \frac{U \cdot s_i^2(m) DJ_s(i,g) + F_2 CO(m) DJ_{\phi}(i,g)}{C} \right] \quad (4.10)$$

where:

$J_{s,\phi}(i,g)$  are given by equation (4.7) and  $DJ_{s,\phi}(i,g)$  by equation (4.8).

$$R_{kim} = (\rho_k^2 + \rho_i^2 - 2\rho_k \rho_i CO(m) + (z_i - z_k)^2)^{1/2}$$

$$CO(m) = \cos[(m-1)\Delta\beta_i]$$

$$SI(m) = \sin[(m-1)\Delta S_i]$$

$$V = z_i - z_u$$

$$U = V \sin \alpha_k \sin \alpha_i + v_k \cos \alpha_k \sin \alpha_i - v_i \sin \alpha_k \cos \alpha_i$$

$$F_1 = V \cdot CO(m) \cdot \sin \alpha_i + (v_k - v_i CO(m)) \cos \alpha_i$$

$$F_2 = \cos \alpha_k (v_k \cos(m) - v_i) + V \sin \alpha_k CO(m)$$

NS represents the total number of segments

$NP_i$  represent the total number of patches at the  $i$ th ring.

The total currents can now be expressed in terms of  $J_{cs}$  and  $J_{cs}$ , which yields:

$$J_s(k, n) = -2H^i(z_{k,n}) + J_{cs}(k, n) \quad (4.11)$$

$$J_s(k, n) = -2H^i(z_{k,n}) \cdot \sin(\alpha_k) + J_{cs}(k, n) \quad (4.12)$$

$J_s$  and  $J_s$  are the values of the current components stored and used for computation of the backscattered far field, which will be expressed in numerical form as follows:

$$H^s(n) = -\frac{1}{4r_0 C} \sum_{i=1}^{NS} [DJ_s(i, g) \sin \alpha_i + DJ_{s\phi}(i, g)] \Delta S_i \cdot v_i \quad (4.13)$$

where

$$g = n - \frac{z_i}{c \Delta t}$$

and  $DJ_{s,\phi}(i, g)$  are given by equation (4.8).

Equations (4.7) and (4.8) used for interpolation of the currents and their time derivative are given for the general case where:

1.  $g_1 \sim 1$  (after the incident field had reached the specific point  $i$  on the scatterer)
2.  $g_4 \sim n$  (so that no interpolation in the future occurs).

In cases where these two conditions are not met the interpolation must be adjusted to include only those points which satisfy causality with no interpolation in the future.

The numerical formulations derived in this section were programmed in FORTRAN to compute the currents and the back-scattered field, due to the excitation of a body of revolution by an impulse type field (or a ramp). The input data to the program is the function  $\psi(z)$  along with the length of the spatial segment  $\Delta S$  and the time increment  $\Delta T$ . The program is given in Appendix E.

#### C. NUMERICAL EXAMPLES

The first example to be considered is a sphere of radius 1 meter. This special example was chosen since its result appears in various publications and comparison can hence be made.

For the present example, use is made of the guidelines set in Section (I.B) for the choice of the incident field, the sampling rate and the space sampling. The incident field for the case of the impulse response is represented by the gaussian shape

$$H^1(z, t) = \begin{cases} e^{-A^2(t-t_{\max}-z/c)^2}, & \frac{2a}{c} \leq t \leq 0 \\ 0, & \text{otherwise} \end{cases}$$

where:

$$A = 5 \cdot 10^8 \text{ sec}^{-1}$$

which yields

$$\Delta T = 0.2, C \text{ sec}$$

The pulse is described in figure 4.3.

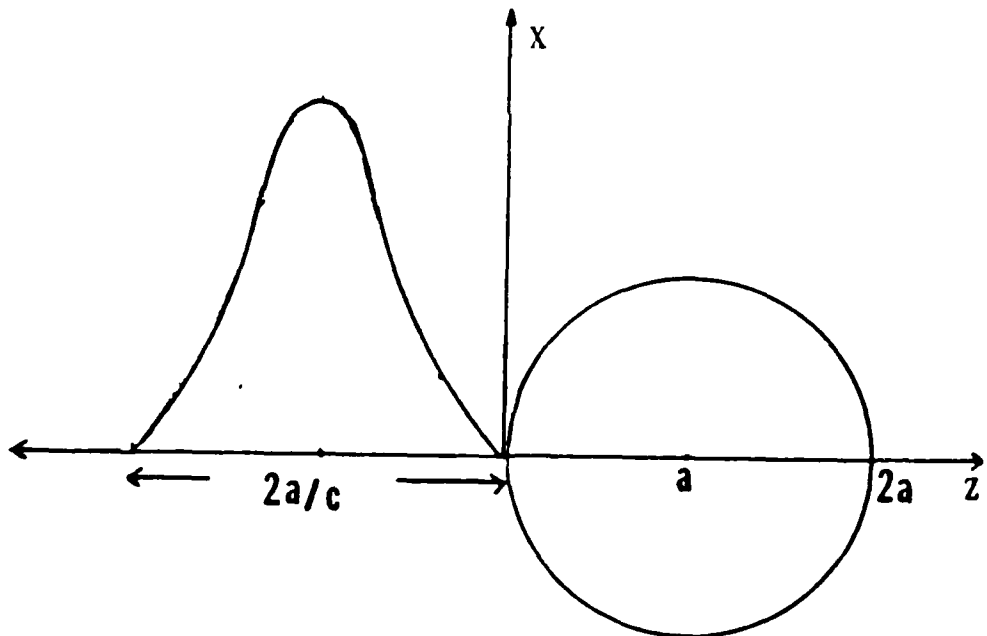


Figure 4.3. Gaussian shaped pulse incident on a sphere

The pulse reaches its maximum value at the center of the sphere:

$$t_{\max} = a/c$$

The spatial segment, with 15 segments

$$\Delta S = \frac{a}{15} = 0.209 \text{ m} < C \cdot \Delta T$$

The number of time increments observed was such that it covers 6 times the transit time across the whole sphere ( $60 \cdot \Delta T$ ). The results obtained for the backscattered field are given in figure 4.4, on which the results of Bennett [7] are superimposed for comparison.

Observation of the impulse response of the sphere shows the following results:

1. The first peak appears after a transit time across one radius of the sphere (which is the time where the incident pulse reaches its peak value), and is due to the return from the leading edge of the sphere.

2. The second peak appears at about  $5.2 a/C$  and is due to the return from the back side of the sphere, after a transit time of:

$$\frac{a}{C} + \frac{a}{C} + \frac{a}{C} \approx 5.2 \frac{a}{C}$$

which corresponds to twice the free space transit time up to the shadow boundary plus the transit time around the back of the sphere. This second peak is the creeping wave return.

3. The response as expected, starts decaying after some time equivalent to 5-6 times the transit time across the sphere.

The ramp response for the same sphere is given in figure 4.5. The first positive incursion of the response waveform

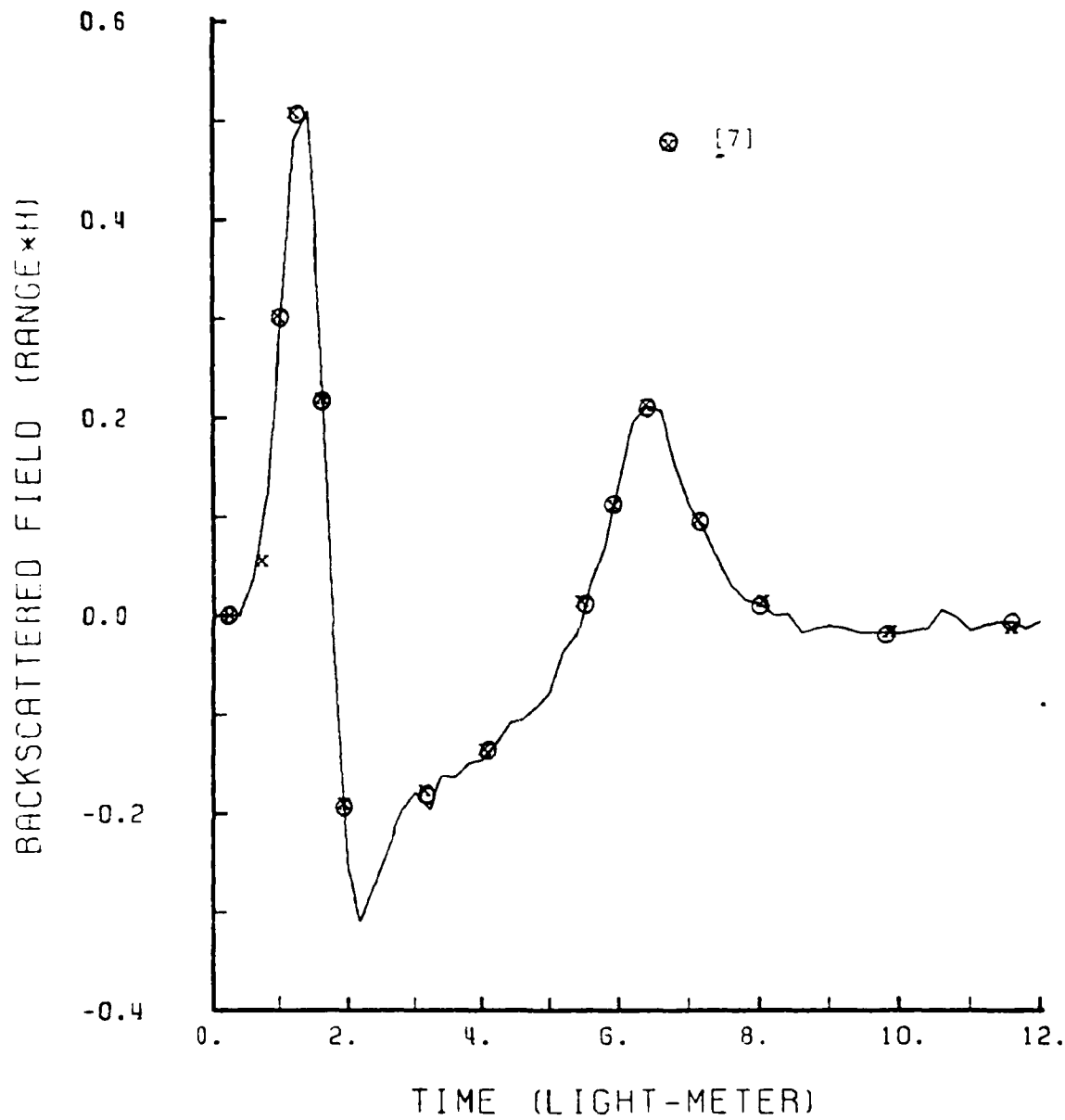


Figure 4.4. Smoothed impulse response of a 1 meter radius sphere

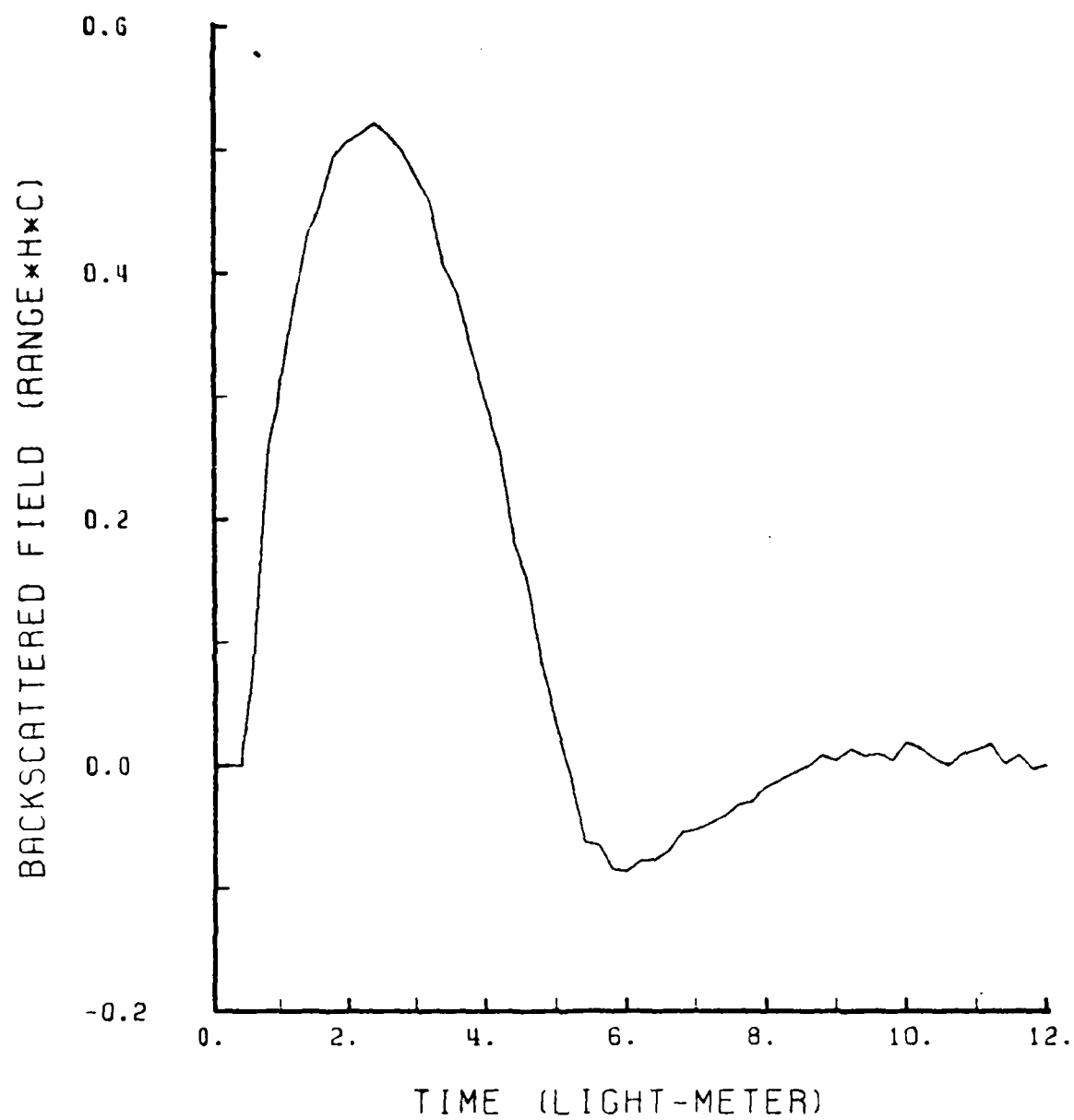


Figure 4.5. Ramp response of a 1 meter radius sphere

extends to about 5 times the transit time across the radius which corresponds to 1.25 round trips across the target. The impulse response of a 30 cm diameter sphere was measured in the NPS scattering range lab. The waveform obtained is shown in figure 4.6. The response appears here with a reversed sign since vertical polarization is used (instead of the horizontal polarization considered for the computations). The waveform shows very good agreement with the form obtained for the 2 meter diameter sphere.

The second example considered was the cone-sphere whose geometry is shown in figure 4.7. The target contour was divided into 12 segments while all other parameters remained the same as for the sphere. The impulse response of the cone-sphere target is given in figure 4.8. The waveforms show two positive peaks, corresponding to the leading edge and creeping wave returns. The separation between them is equivalent to the two way free space transit time up to the shadow boundary plus the transit time across the rear of the sphere.

$[(2 \times 1.3 + \pi \times 0.7) \approx 4.7 \text{ light-meters}]$  The ramp response of the same cone-sphere target is given in figure 4.9, and the remarks made on the sphere apply here too.

The third example was the capped cylinder target shown in figure 4.10. The contour of the target was divided into 12 segments, the sampling time was  $\Delta T = 0.025 \text{ m/sec}$  and  $A = 4 \cdot 10^9 \text{ sec}^{-1}$ . The smoothed impulse (gaussian) response of this target is given in figure 4.11. The waveform shows

clearly the responses from the leading edge and the rear of the cylinder, with the same amplitudes, while from the flat horizontal region of the cylinder the response is zero as expected from the analytical expressions of the field.

The ramp response for the capped cylinder is shown in figure 4.12. The first positive incursion of the response clearly exhibits a shape comparable to the shape of the target.

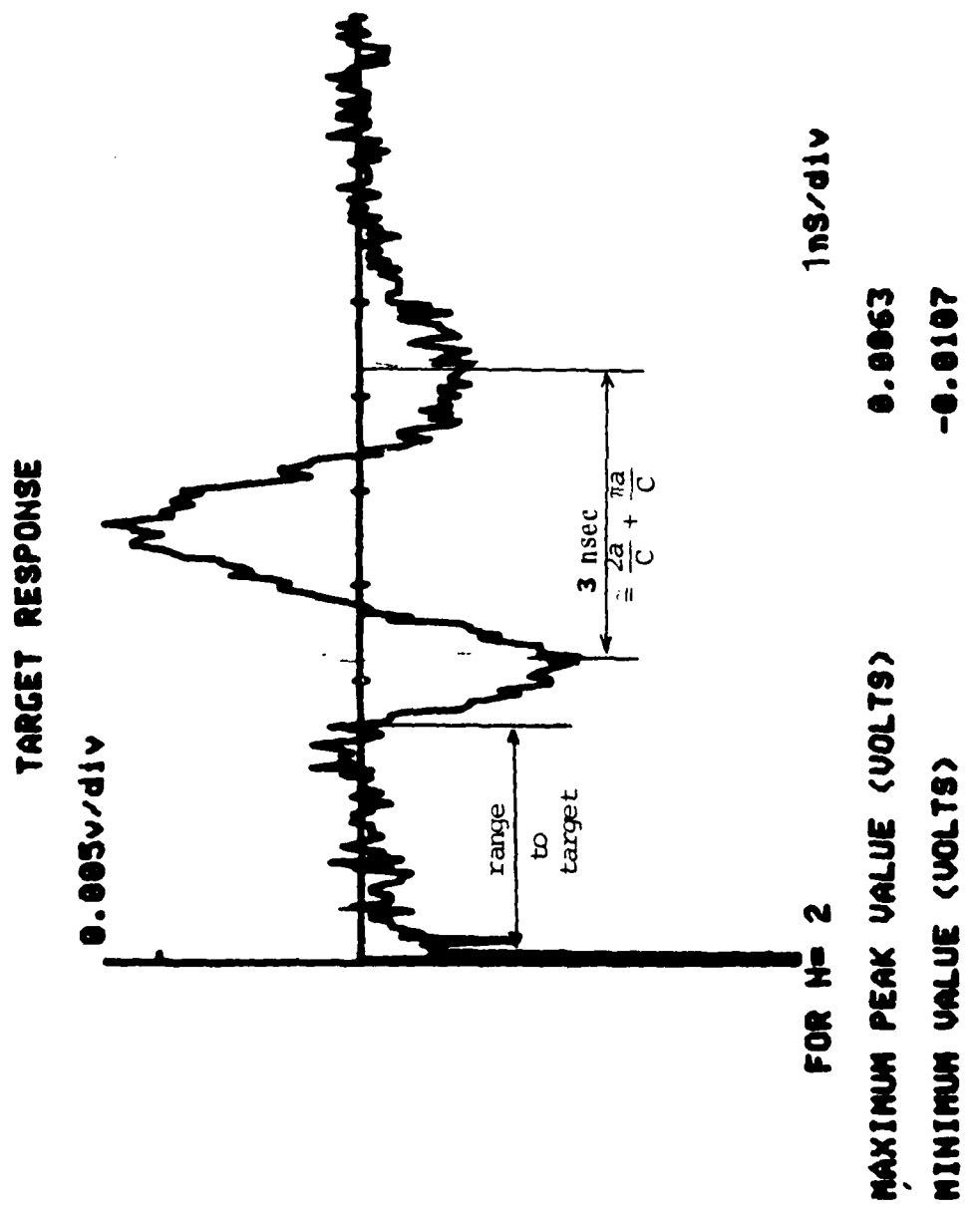


Figure 4.6. Measured impulse response of a 30 cm diameter sphere (incident field vertically polarized)

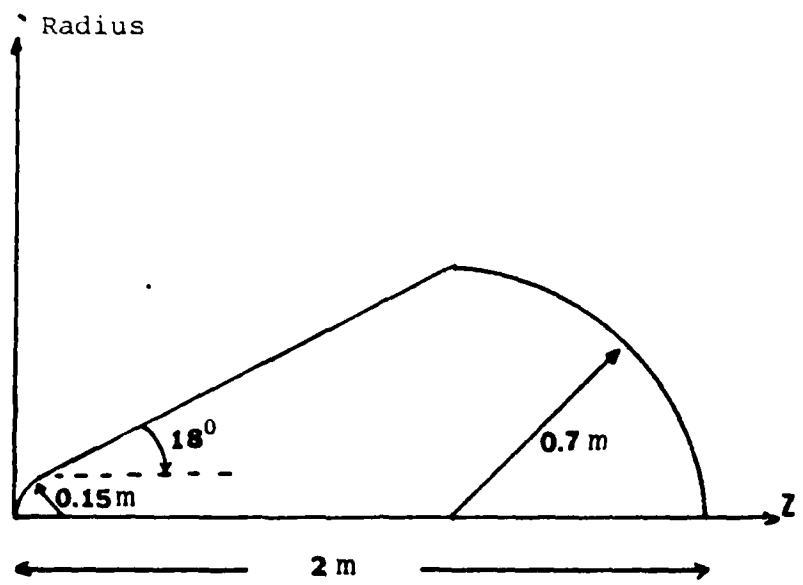


Figure 4.7. Geometry of the cone-sphere target (half-target)

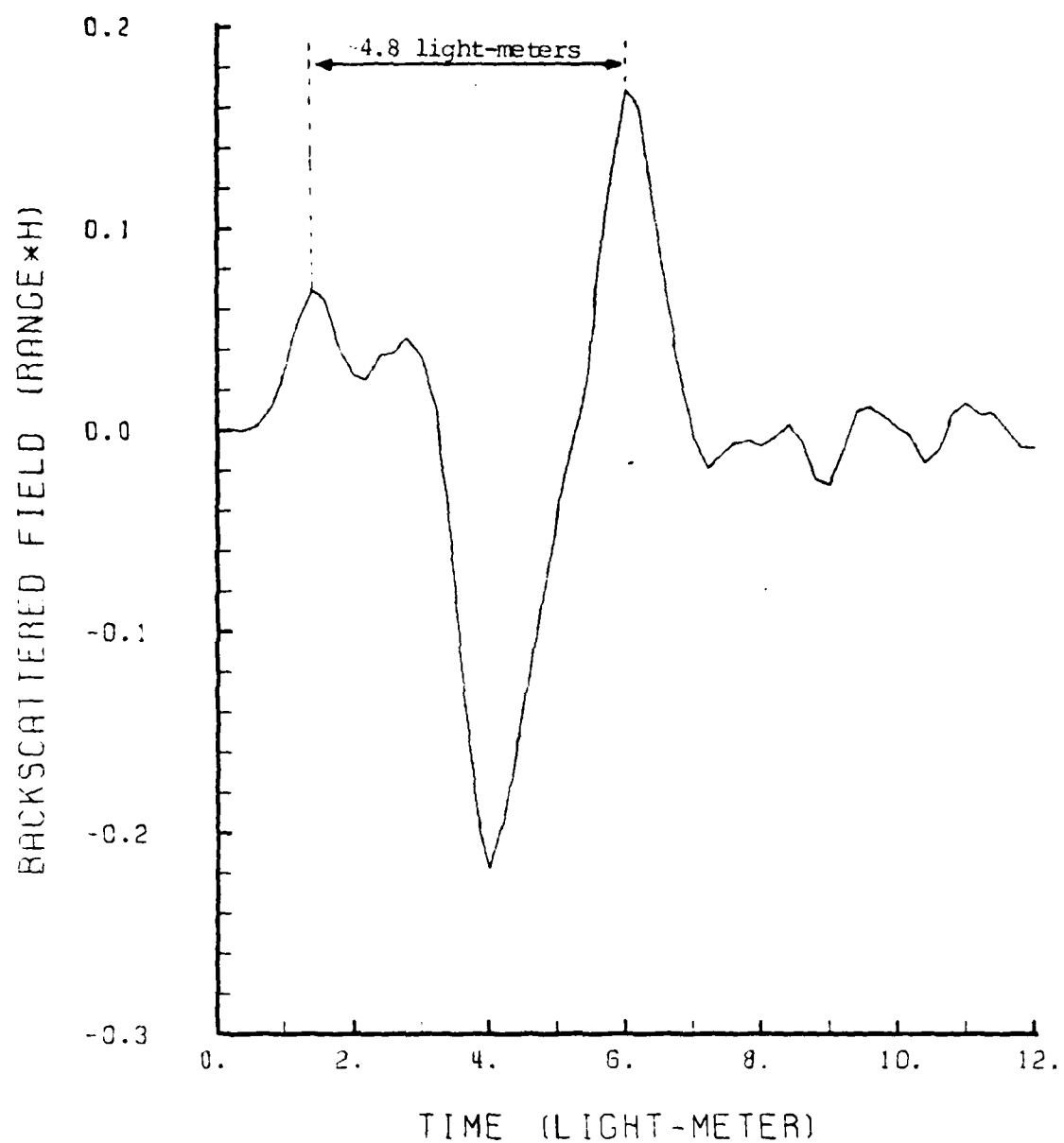


Figure 4.8. Smoothed impulse response of the cone-sphere

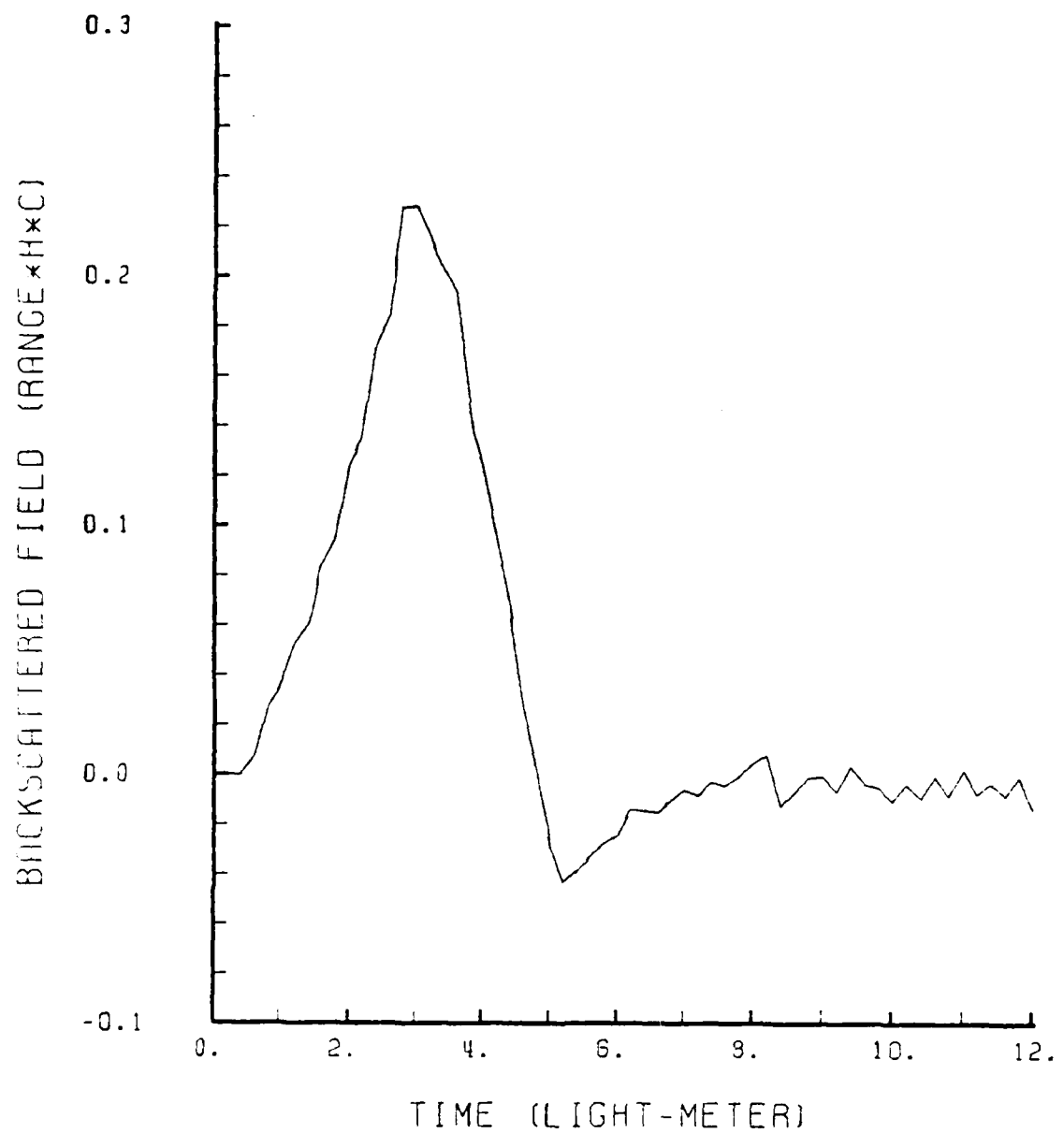


Figure 4.9. Ramp response of the cone-sphere

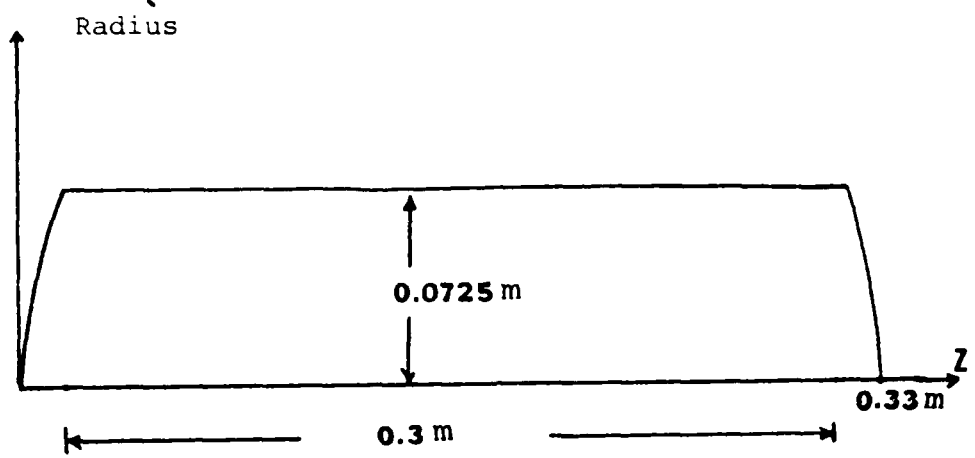


Figure 4.10. Geometry of the capped cylinder target (half-target)

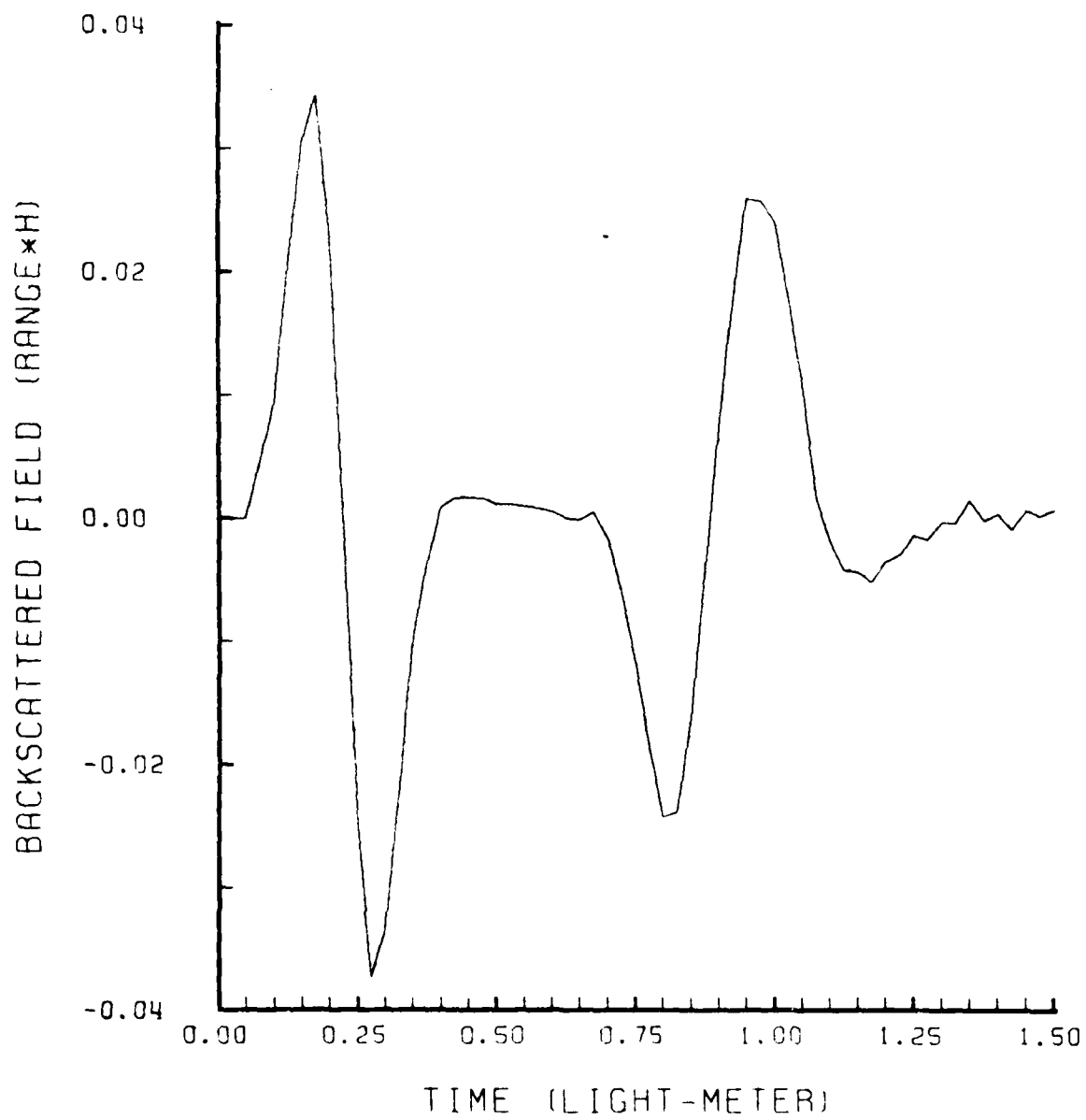


Figure 4.11. Smoothed impulse response of a capped cylinder (length ~ 0.33 m)

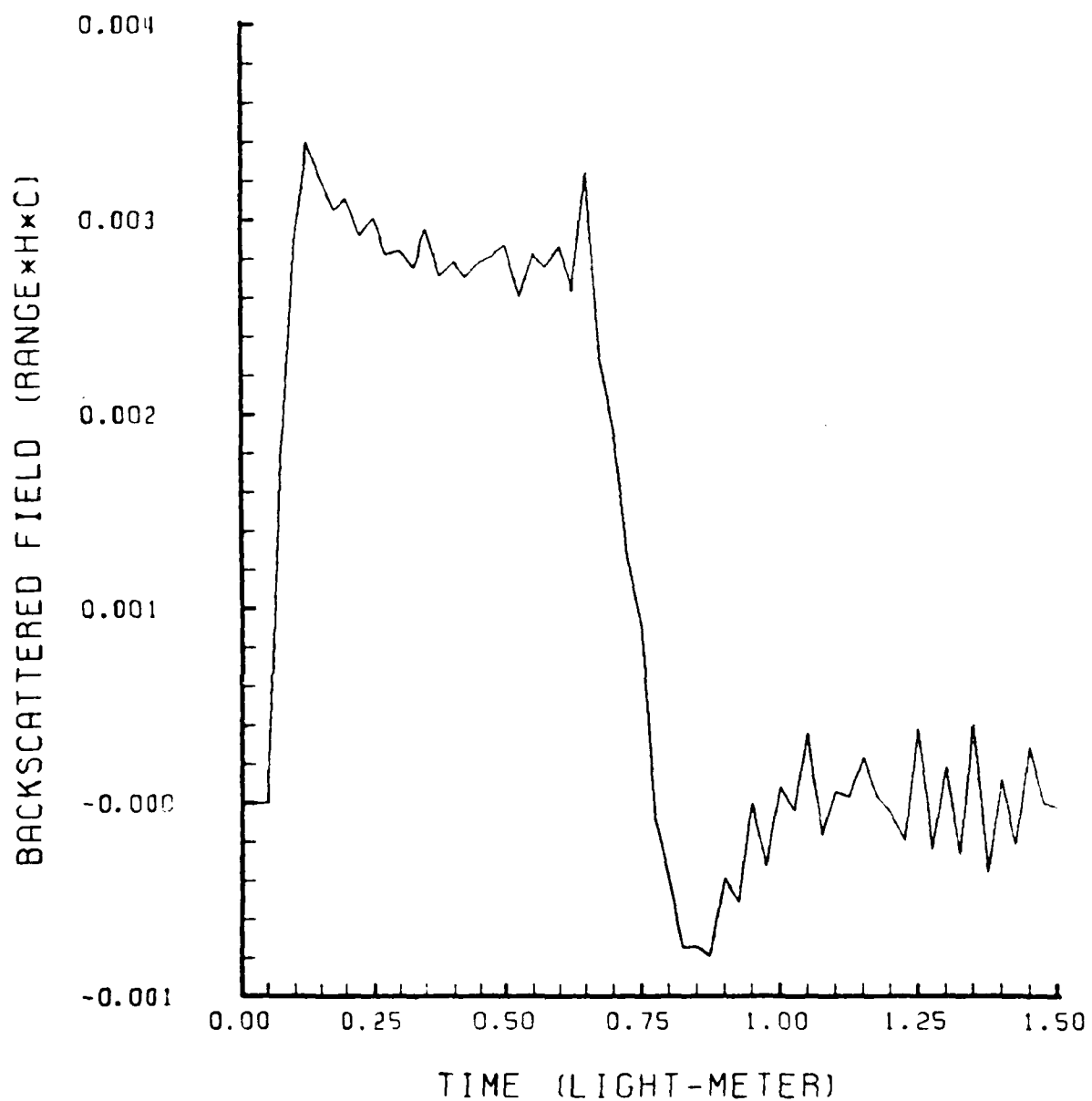


Figure 4.12. Ramp response of the capped cylinder (total length  $\sim 0.33$  m)

## V. INVERSE SCATTERING

### A. PROBLEM DEFINITION

Given the incident field and the scattered field from an unknown target, it is desired in the most general case to retrieve the shape, size, orientation, and, perhaps, composition of the target. This is known as inverse scattering, or target imaging.

For the present case, the problem is restricted to a metallic body of revolution illuminated by a field propagating along the axis of symmetry, and the scattered field is measured in the backscattered direction, as shown in figure 5.1.

The solution of this problem is approached here directly in the time-domain.

### B. FORMULATION OF THE PROBLEM

In [6], Kennaugh and Moffatt derive the relationship between the physical-optics impulse response of a body and its area function  $A(z)$ , projected in the plane orthogonal to the direction of propagation of the field (z-axis).

The impulse response is given by:

$$F_I(t) = \frac{C}{8\pi r_0} \frac{d^2 A(z)}{dz^2} \Big|_{z=ct/2} \quad (5.1)$$

where  $r_0$  is the range from the observation point to the scatterer, as shown in figure 5.1. Integrating twice (5.1) with respect to time gives the ramp response as follows:

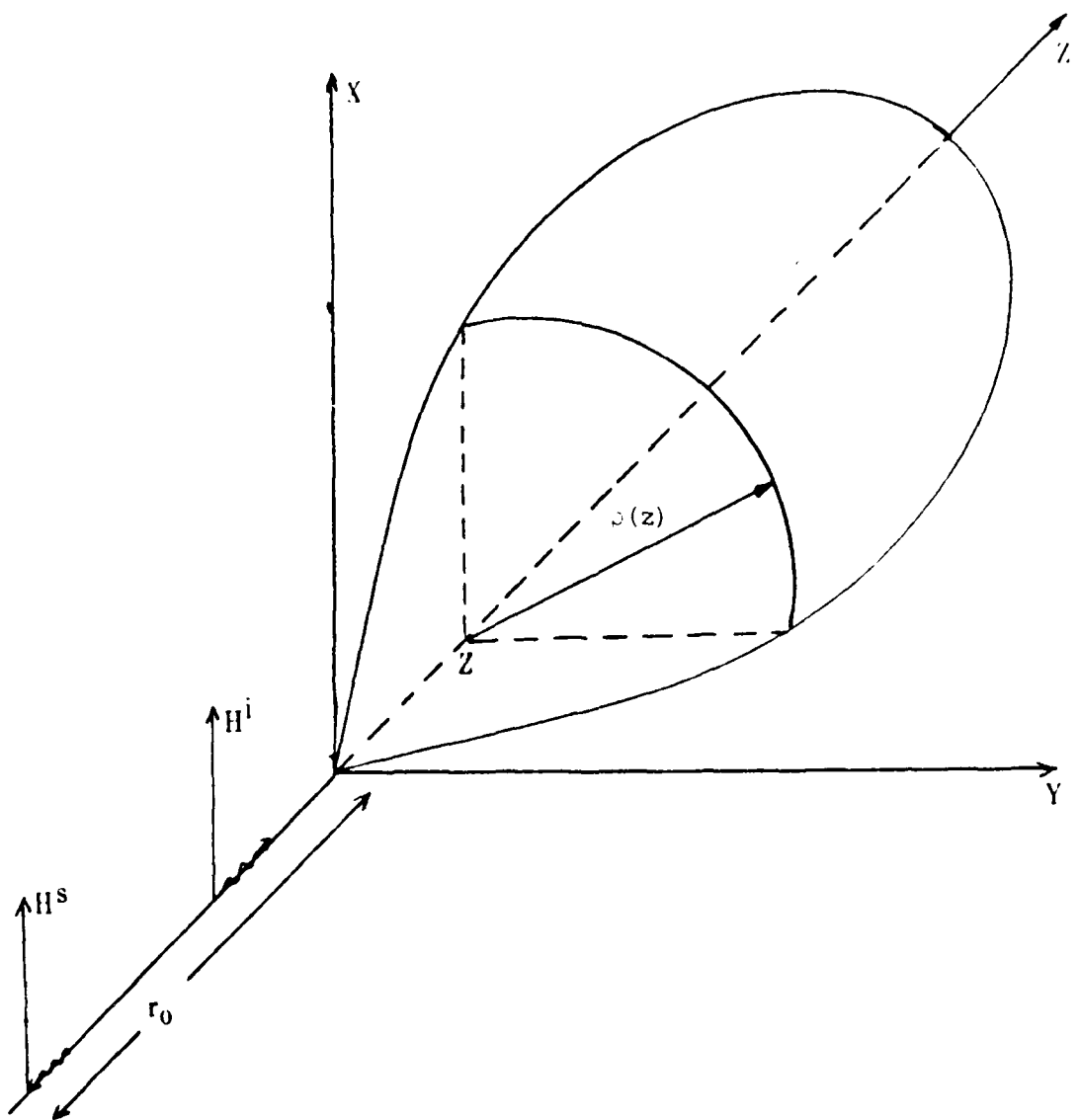


Figure 5.1. Inverse scattering geometry

$$F_R(t) = \frac{1}{2\pi r_o C} A(z) \Big|_{z=ct/2} \quad (5.2)$$

Equations (5.1) and (5.2) were proven to be valid for bodies having a monotonic area function with a limiting value at the shadow boundary. This relationship between the ramp response and  $A(z)$  is derived in Appendix F for the body of revolution.

The total backscattered field that would be measured will consist of the physical optics term plus an additional term due to the field induced interactions between the currents at different parts of the body. The total current induced on the body is given by equation (3.1). The first term of the R.H.S. of the equation represents the physical-optics current, which we will denote by  $\vec{J}_p$ , and the second term expressed by the integral represents the additional current, which we will denote by  $\vec{J}_C$ . The total current will then be:

$$\vec{J}_{\text{total}}(\vec{r}, t) = \vec{J}_p(\vec{r}, t) + \vec{J}_C(\vec{r}, t) \quad (5.3)$$

Expressed in terms of (5.3) the total backscattered field for a ramp excitation will be:

$$\begin{aligned} H_R^S(t) &= \frac{1}{4\pi r_o C} \int_A \frac{\partial}{\partial \tau} (\vec{J}_p + \vec{J}_C) \times \hat{a}_R \, dA' \\ &= \vec{H}_p^S(t) + \vec{H}_C^S(t) \end{aligned} \quad (5.4)$$

where:

$H_p^S(t)$  is the physical optics ramp response,

$H_C^S(t)$  is the additional response,

and

$H_R^S(t)$  is the total ramp response.

Using the relationship between the physical-optics response and the area function, (5.4) can be rewritten as:

$$H_R^S(t) = \frac{1}{2r_0 C} \rho^2(z) + H_C^S(t) , \quad z = ct/2 \quad (5.5)$$

which leads to

$$\rho^2(z) = 2r_0 C (H_R^S(t) - H_C^S(t)) \quad (5.6)$$

Equation (5.6) is the basis for the solution of the inverse scattering problem for the body of revolution.

#### C. INVERSE SCATTERING SOLUTION PROCEDURE

Equation (5.6) relates the contour function of the body,  $\rho(z)$ , to its ramp response. Solution of that equation leads to the shape of the body. The only term known in equation (5.6) is the measured value of the total ramp response  $H_R^S(t)$  while  $H_C^S(t)$  is not known.

Moreover, all the terms in the equation are functions of  $\rho(z)$ , hence there results a non-linear equation that will be solved by an iterative procedure. As a first approximation, the unknown term  $H_C^S(t)$  will be neglected and so the first estimate of the contour function will be given by:

$$\rho_1(z) = [2r_0 C H_R^S(t)]^{1/2} \quad (5.7)$$

Once a body is defined its ramp response can be computed since we know the incident field. The ramp response computed for the first estimate of the body will be denoted by  $H_{R_1}^s(t)$  and is expressed as:

$$H_{R_1}^s(t) = \frac{\rho_1^2(z)}{2r_0 C} + H_{C_1}^s(t) \quad (5.8)$$

A new estimate of the shape  $\rho_2(z)$  can be found using (5.6) and (5.7), and is given by

$$\rho_2^2(z) = 2r_0 C [H_{R_1}^s(t) - H_{R_1}^s(t)] + \rho_1^2(z) \quad (5.9)$$

or equivalently by

$$\rho_2^2(z) = 2r_0 C [2H_{R_1}^s(t) - H_{R_1}^s(t)] \quad (5.10)$$

The new estimate  $\rho_2(z)$  serves to compute a new ramp response,  $H_{R_2}^s(z)$ , from which an updated estimate of  $\rho(z)$  is extracted. Following this iterative procedure, the  $k$ -th estimate of the contour function will be given by:

$$\rho_k^2(z) = \rho_{k-1}^2(z) + 2r_0 C [H_{R_{k-1}}^s(t) - H_{R_{k-1}}^s(t)] \quad (5.11)$$

or by:

$$\rho_k^2(z) = 2r_0 C [k \cdot H_{R_1}^s(t) - \sum_{\ell=0}^{k-1} H_{R_\ell}^s(t)] \quad (5.12)$$

The iterations are continued up to the point where the difference between the true measured response and the last computed

response reaches a minimum. Several runs of the program for various bodies has shown that, as the iterations go on, the mean squared error is decreasing, reaches a minimum then starts oscillating. In one case observed, the error is diverging after reaching the minimum. Some representative results are shown in the next section.

The normalized mean squared error will be defined as follows:

$$\varepsilon_k^2 = \frac{(H_R^S(t) - H_{R_{k-1}}^S(t))^2}{(H_R^S(t))^2} \quad (5.13)$$

$\varepsilon_k^2$  is the value that must be minimized in order to obtain the most accurate representation of the shape of the body. As it is defined, the error is equivalent to the difference between the successive shapes, as shown by equation (5.11). Once the difference  $H_R^S(t) - H_{R_{k-1}}^S(t)$  is minimized, the difference  $\varepsilon_k^2(z) - \varepsilon_{k-1}^2(z)$  is also minimized.

#### D. NUMERICAL SOLUTION AND EXAMPLES

For the numerical solution we will use equation (5.12), which is more suitable for the algorithm developed.

We will incorporate the following terminology:

$H_{RM}(n\Delta T)$  is the time sample of the measured ramp response while  $H_{R_k}(n\Delta T)$  is the time sample of the computed ramp response for the  $k$ -th estimate of the body, and  $\rho_k(z)$  is the  $k$ -th estimate of the contour function. In discrete numerical form, equation (5.12) becomes:

$$\varepsilon_k^2(z_n) = 2r_o C [k \cdot H_{RM}(n\Delta T) - \sum_{\ell=0}^{k-1} H_{R_\ell}(n\Delta T)] \quad (5.14)$$

where

$$z_n = n C \Delta T / 2$$

and for  $\ell = 0$ ,  $H_{R_0}(n\Delta T) \equiv 0$ . The mean squared error is:

$$\varepsilon_k^2 = \frac{\sum_{n=1}^N [H_{RM}(n\Delta T) - H_{R_{k-1}}(n\Delta T)]^2}{\sum_{n=1}^N H_{RM}^2(n\Delta T)} \quad (5.15)$$

where  $N$  is the total number of time samples observed and computed.

The ramp response of the body defined by  $\phi_{k-1}(z_n)$  will be computed using the integral equation solution to the forward scattering problem, as already described in Chapter IV.

The Fortran program, given in Appendix E, has been extended with a subroutine named "SHAPE", in order to implement the inverse scattering algorithm. In this subroutine the shape of the body is computed iteratively, using (5.14).

The space samples given by (5.14) are defined at equal increments on the  $z$ -axis, while the program developed for the computation of the ramp response has been proven to work best when the contour was divided into equal length segments. Consequently, one of the tasks of subroutine "shape" is to find the space-samples at the points delimiting segments of

approximately equal length. This is done using a "cut and try" method which converges to the desired length of segment.

The iterative approach for solving the inversion equation (5.14) was tested in a simulative way for the three types of bodies already considered for the forward scattering solution in the previous chapter.

The ramp response of the body is first computed and is used to simulate the response that would have been measured (without noise or error). Then the shape of the body is retrieved from that ramp response.

The shape of the body is retrieved from the first positive incursion of the ramp response, which as it will be seen extends beyond the length of the target for the shapes considered.

The first example was the 1 meter radius sphere. Figure 5.2 shows the 1-st, 3-rd, 6-th estimates of the contour function of the sphere. The 6-th estimate gives the least error and is shown superimposed on the original shape in figure 5.3.

The second example was the cone-sphere, used in two configurations. The first one when the contour of the body was originally cut to 12 segments. Figure 5.4 shows the successive estimates (1,3,6) of the contour, and figure 5.5 shows the minimum error estimate (estimate 6). The second version, when the body was cut to 11 segments, gave a much more accurate result, as shown in figures 5.6 and 5.7.

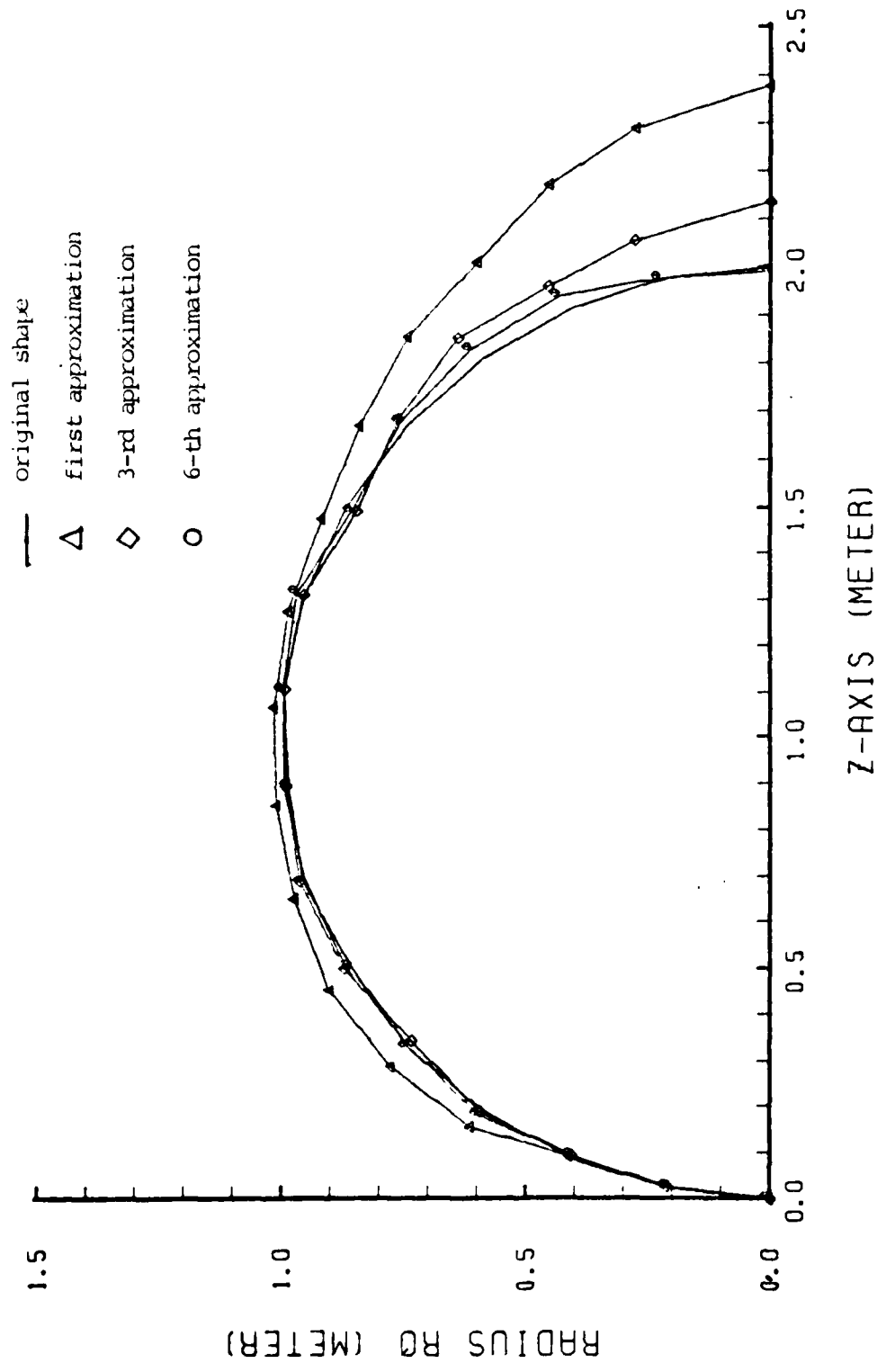


Figure 5.2. Contour estimates of the sphere

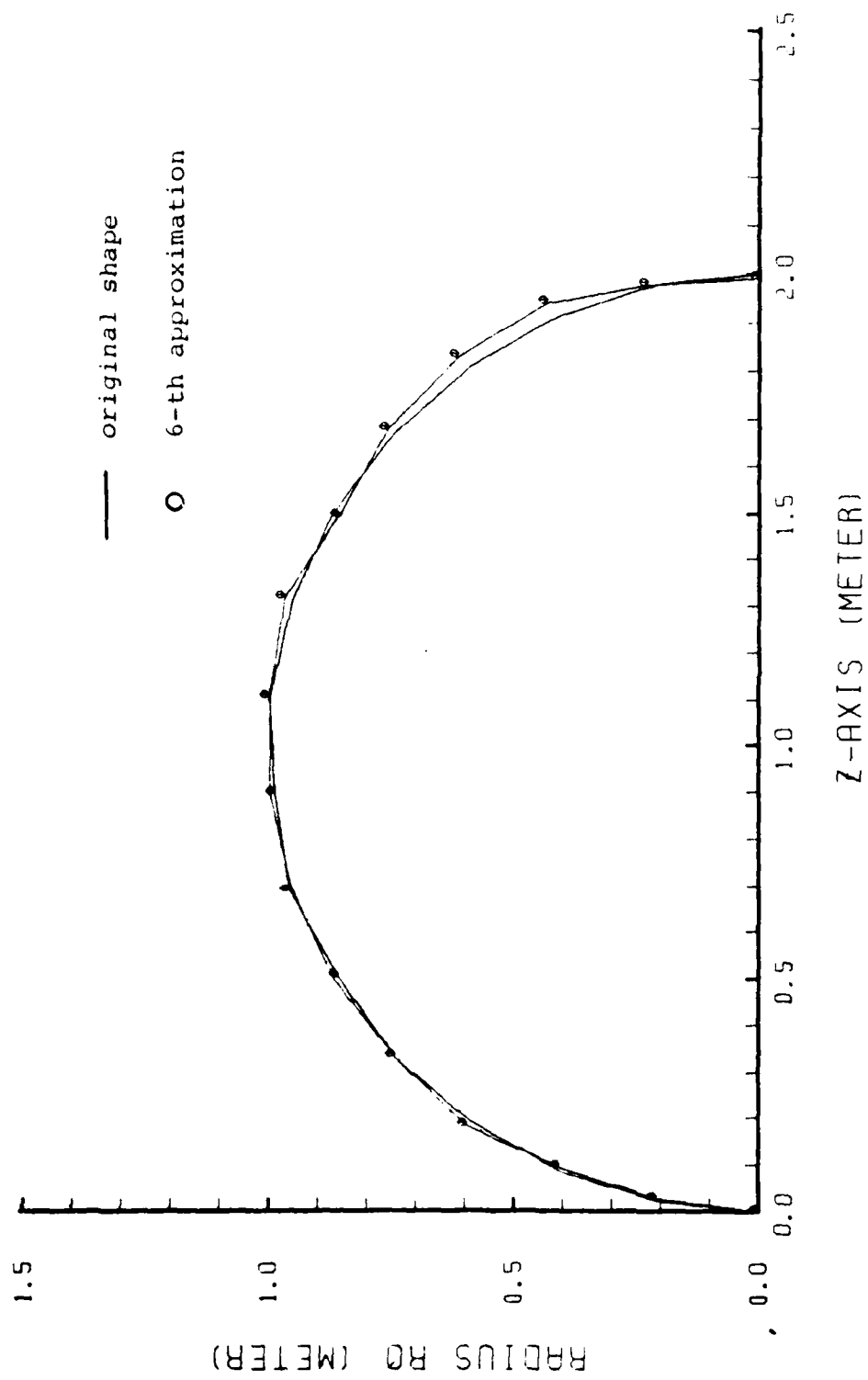


Figure 5.3. 6-th estimate of the contour of the sphere

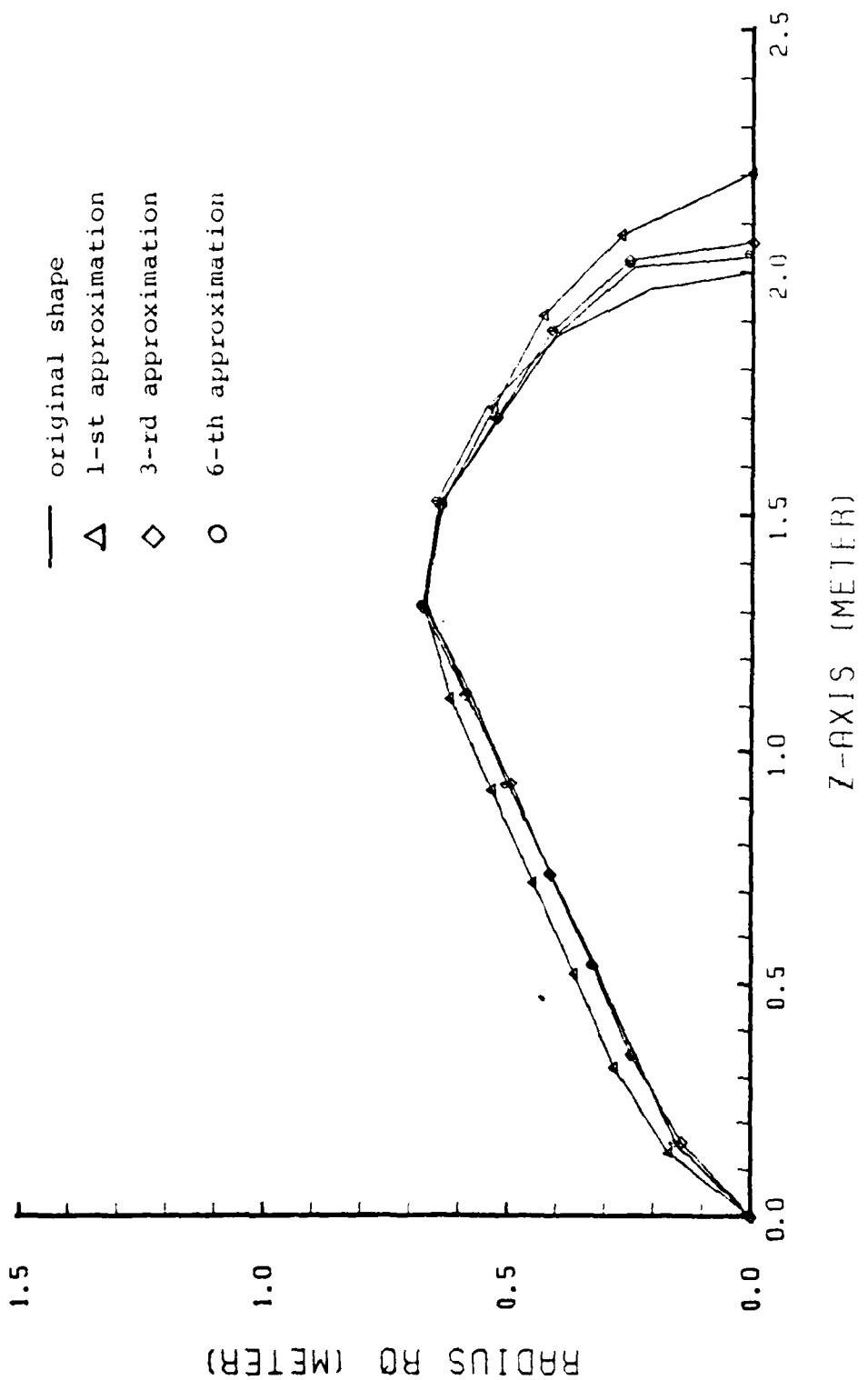


Figure 5.4. Contour estimates of a cone-sphere  
(cut to 12 segments)

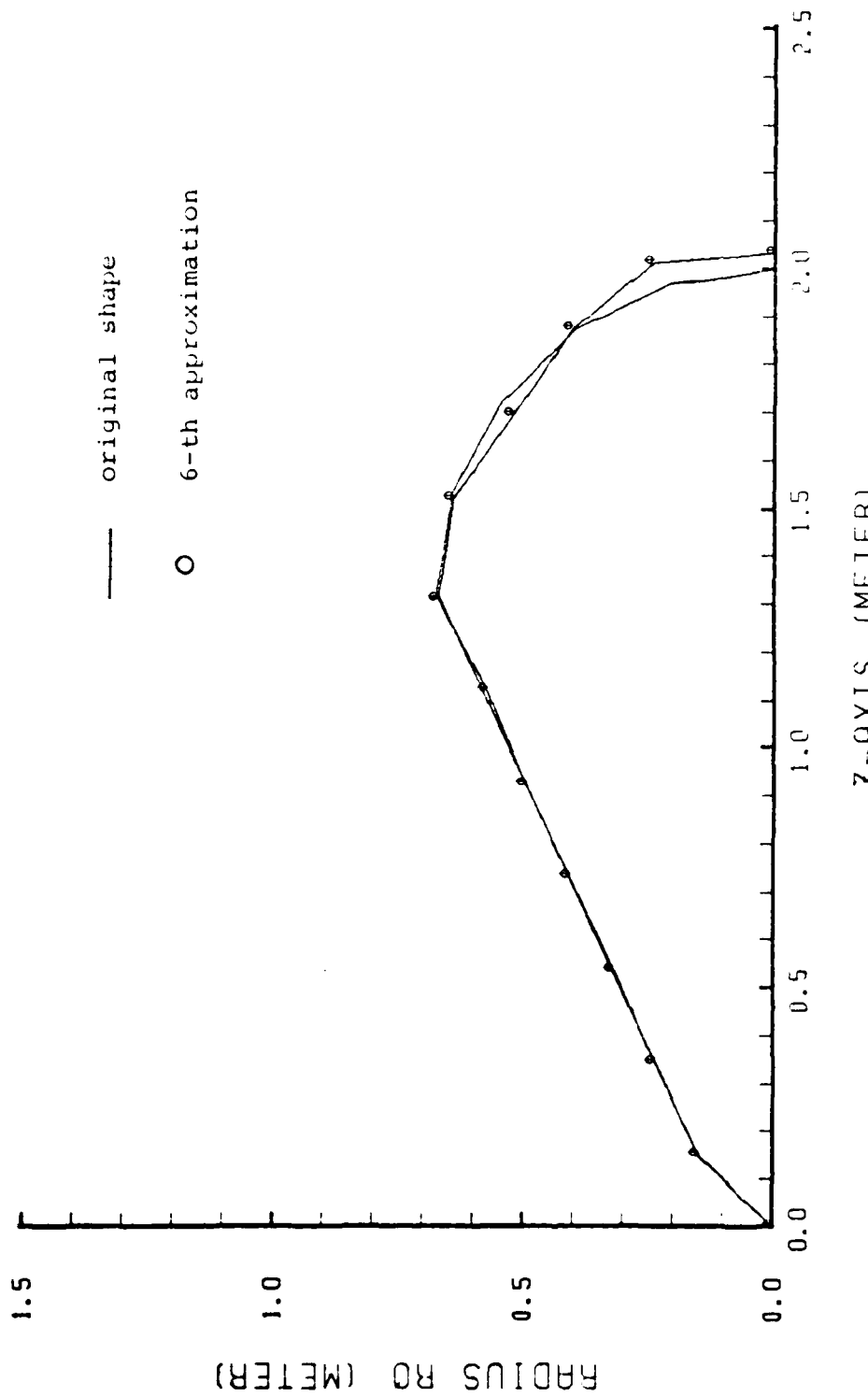


Figure 5.5. 6-th estimate of the contour of a cone-sphere (cut to 12 segments)

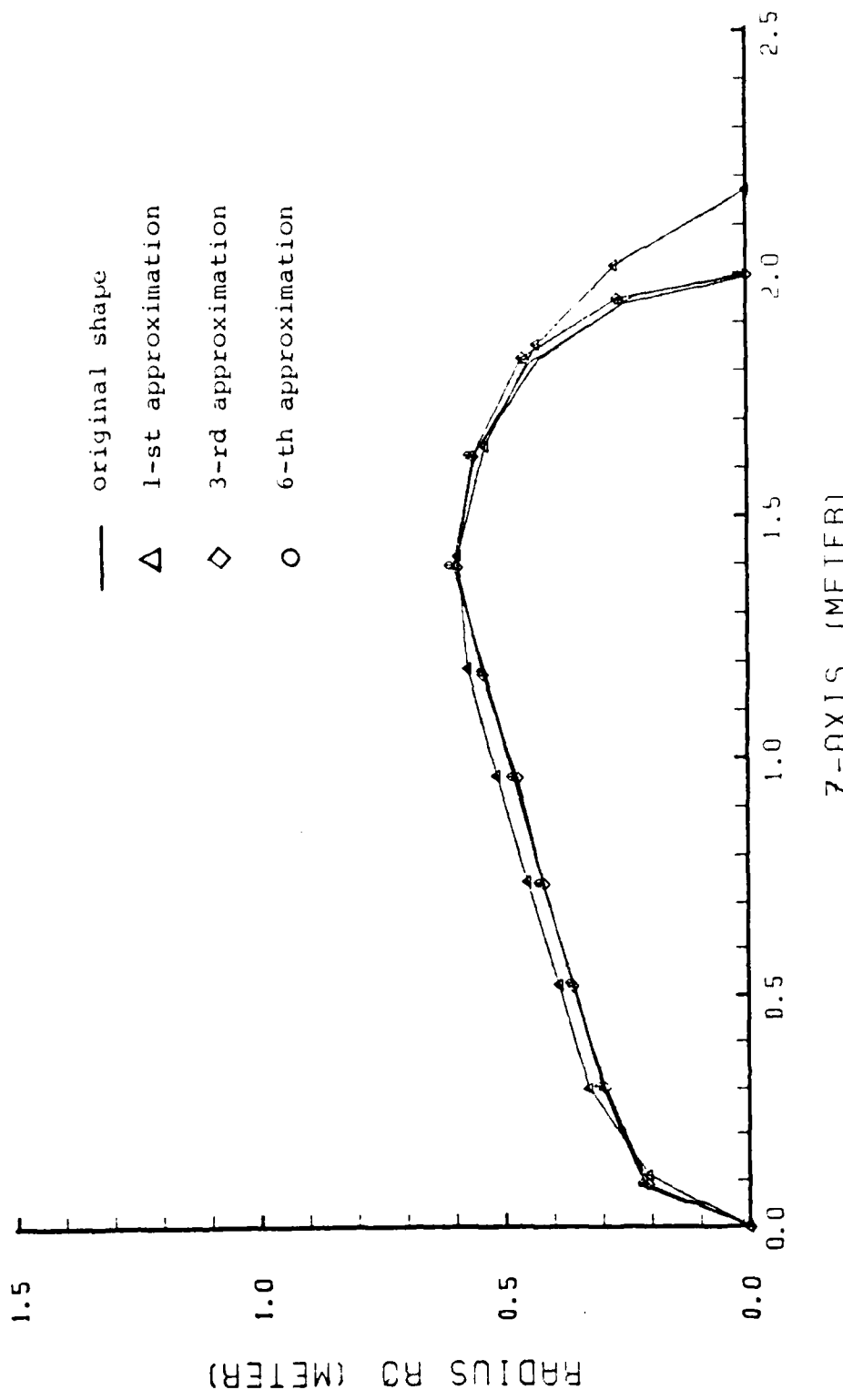


Figure 5.6. Estimates of the contour of the cone sphere (cusp to 11 segments)

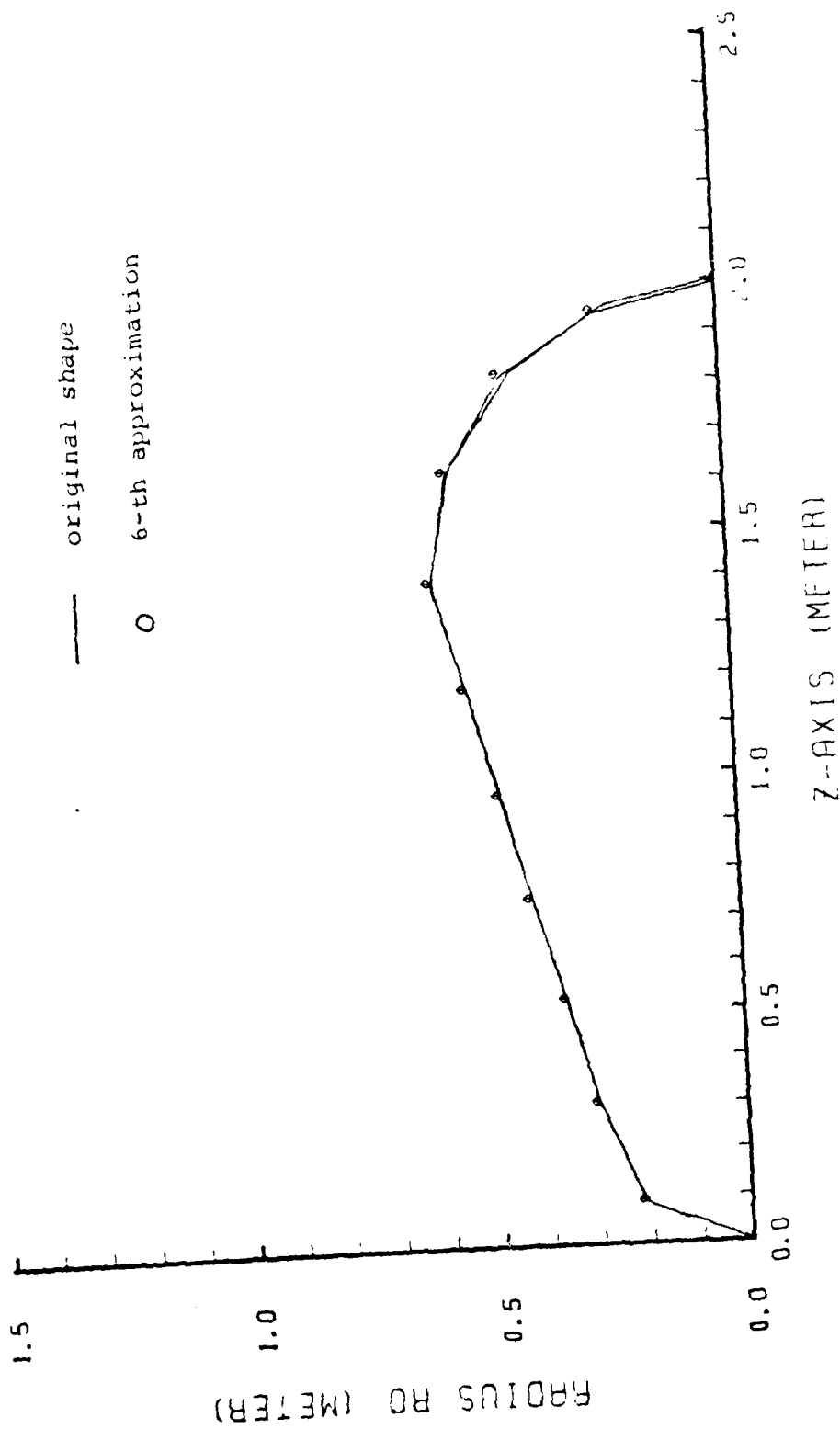


Figure 5.7. Sixth estimate of the contour of the cone sphere (cut to 11 segments)

The last example was the capped-cylinder. Figure 5.8 shows the successive estimates of the shape (estimates 1, 3, 4), and figure 5.9 shows the 4-th estimate which gives the minimum error.

For the case of the capped cylinder, after reaching the minimum error at the 4-th iteration, the imaged shaped of the body started to diverge considerably, and appeared more shortened than the actual shape.

Common to all examples, the error appears mostly at the shadowed region of the body, but in general the shape is retrieved with quite a good fidelity, which proves that the iterative direct time domain solution is working, subject to certain caveats which will be discussed in the conclusions.

#### E. INFLUENCE OF NOISE

In the examples considered in the previous section the only noise appearing in the ramp response is the numerical noise generated by sampling and computational round-off. In this section the measurement noise will be tested with a ramp response to which noise is added. In this simulation, each noise sample is obtained by the sum of a large number of zero-mean, uniformly distributed random numbers, which, by use of the central limit theorem, approximate the statistics of gaussian noise. The noise samples are normalized in order to remain within a certain voltage signal to noise ratio, and are added to the computed ramp response.

The body considered for the noise test was the sphere, and the signal to noise ratios tested were:

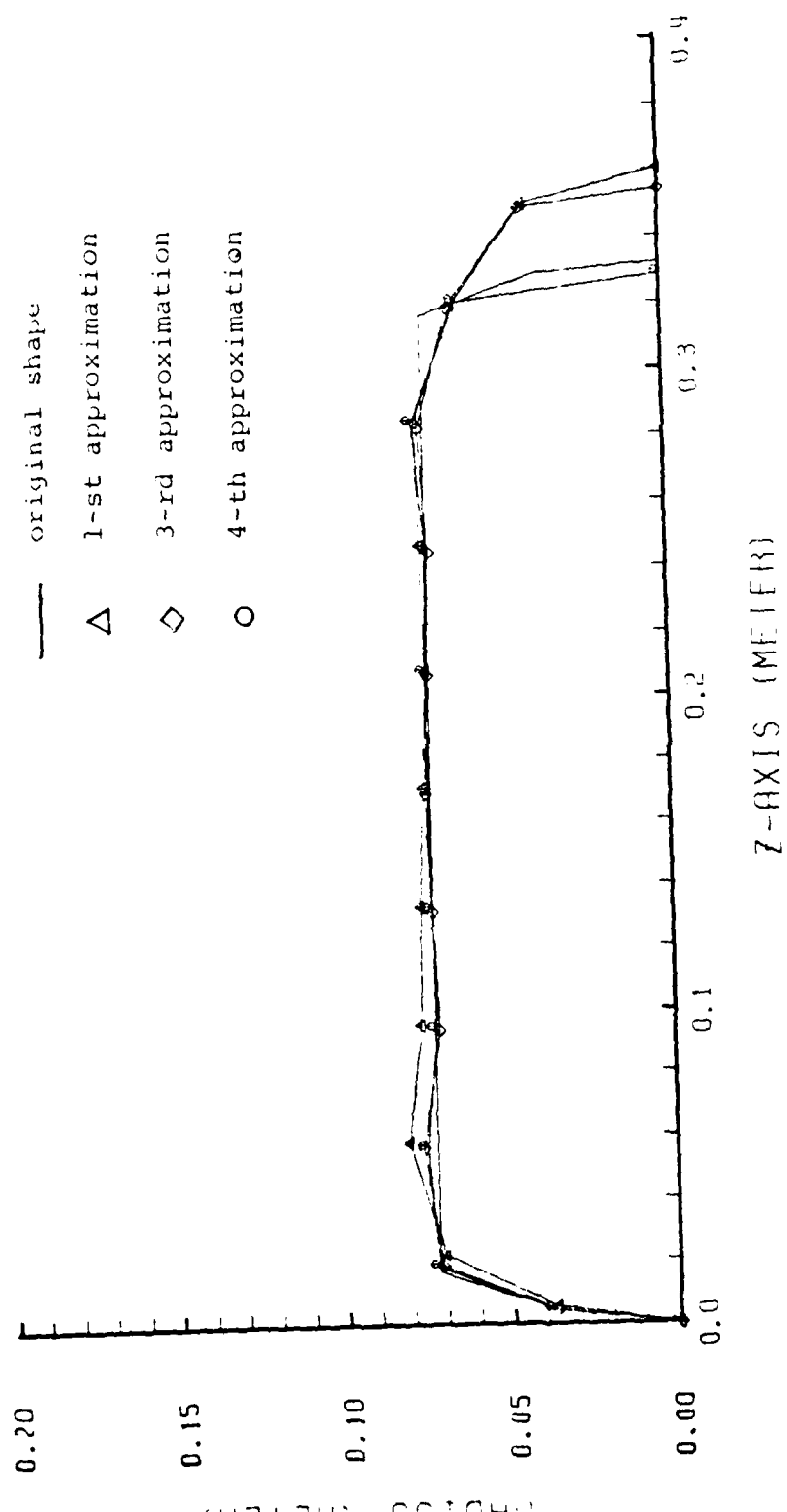


Figure 5.8. Contour estimates of the capped cylinder

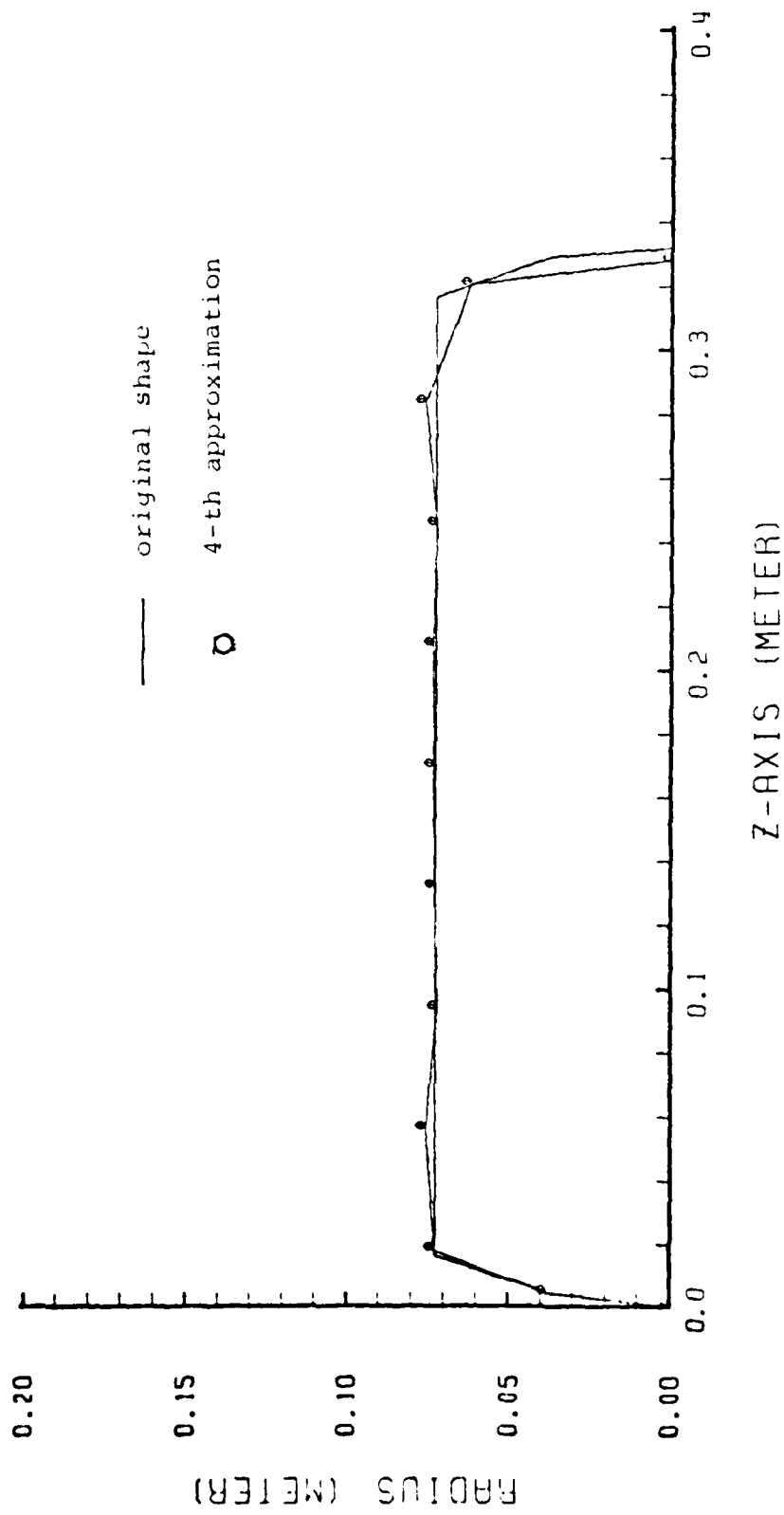


Figure 5.9. 4-th contour estimate of the capped cylinder

$$20 \log \frac{V_{\max}}{V_{\text{noise}}} = 10, 20, 30 \text{ and } 40 \text{ dB}.$$

The sphere ramp responses with the noise added are shown in figures 5.10, 5.11, 5.12 and 5.13 for the successive signal to noise ratios.

For the 10 dB S/N case, the appearance of spikes and discontinuities on the ramp response causes the shape of the body to diverge considerably since the first iteration, and the shape cannot be recovered.

For the 20 dB S/N case, the computed shape starts to converge, with the minimum error shape obtained at the third iteration. Then the imaged shape proceeds to diverge and to shorten.

Figure 5.14 shows the successive estimates of the shape up to the 3-rd, and figure 5.15 shows the sixth estimate, which is clearly different of the actual shape.

For the 30 dB S/N case, the minimum error shape was obtained at the 5-th iteration, as shown by figure 5.16. Then again, the computed shape diverges as shown in figure 5.17. Common to all cases of divergence, the wrong estimates start as soon as the last computed shape exhibits a strong discontinuity in its contour. A very important conclusion from the noise analysis is that before starting the inverse scattering procedure the ramp response used must be smoothed so that no spikes or sudden discontinuities appear on it.

We should normally expect that the true measured response will have a 20 dB S/N ratio, so that the problem of divergence

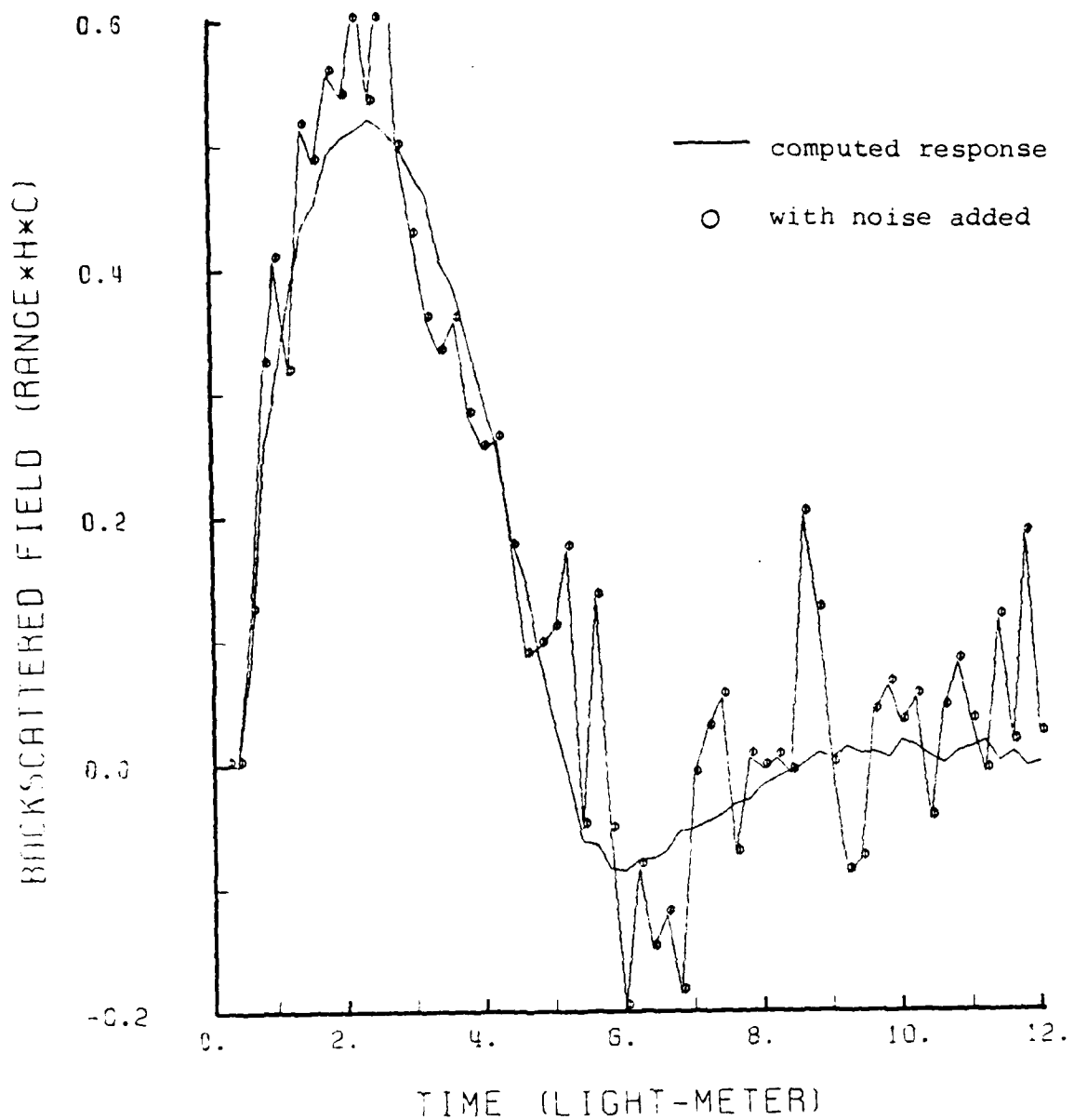


Figure 5.10. Ramp response of the sphere with noise added ( $S/N = 10$  dB)

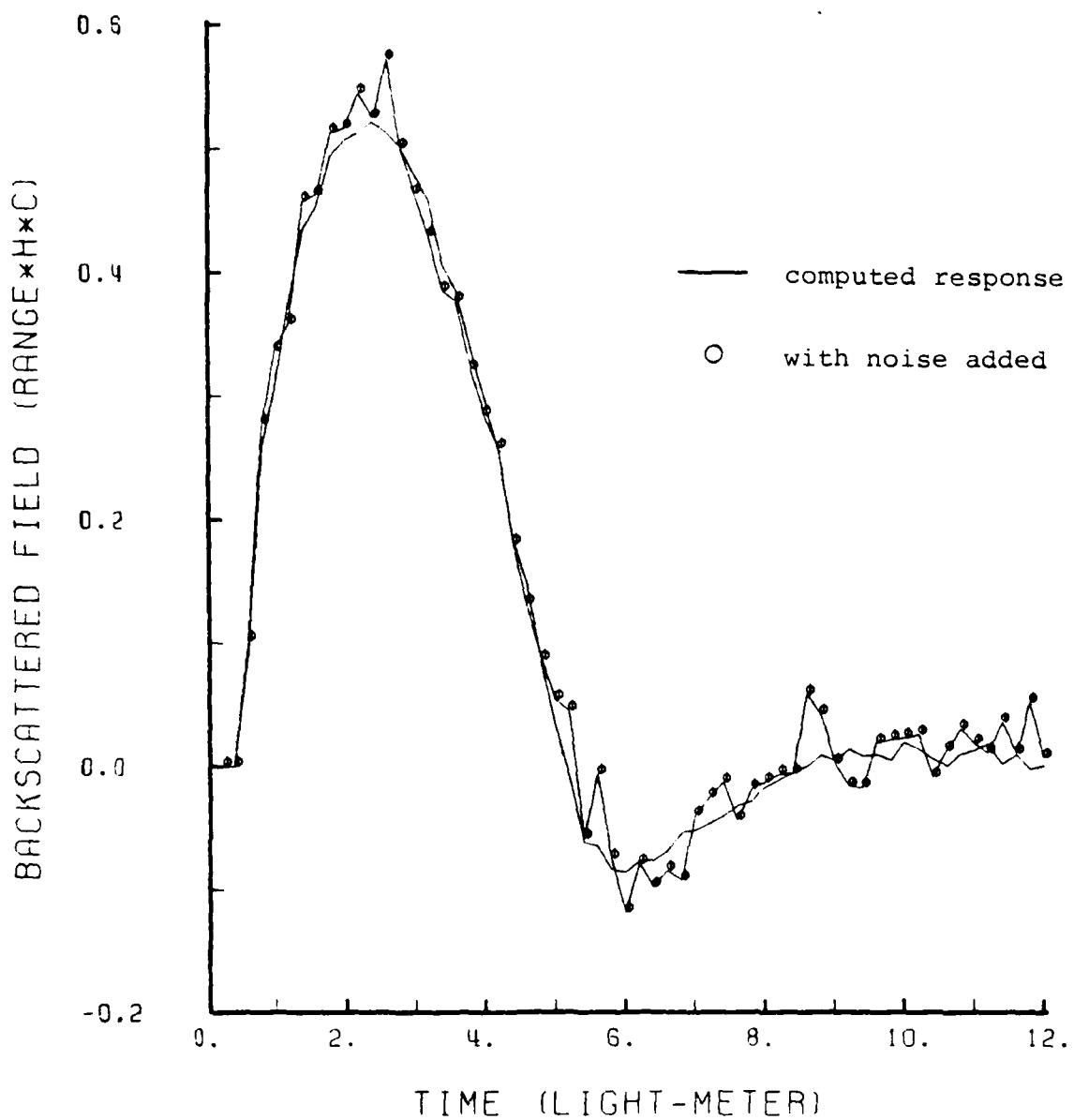


Figure 5.11. Ramp response of the sphere with noise added ( $S/N = 20$  dB)

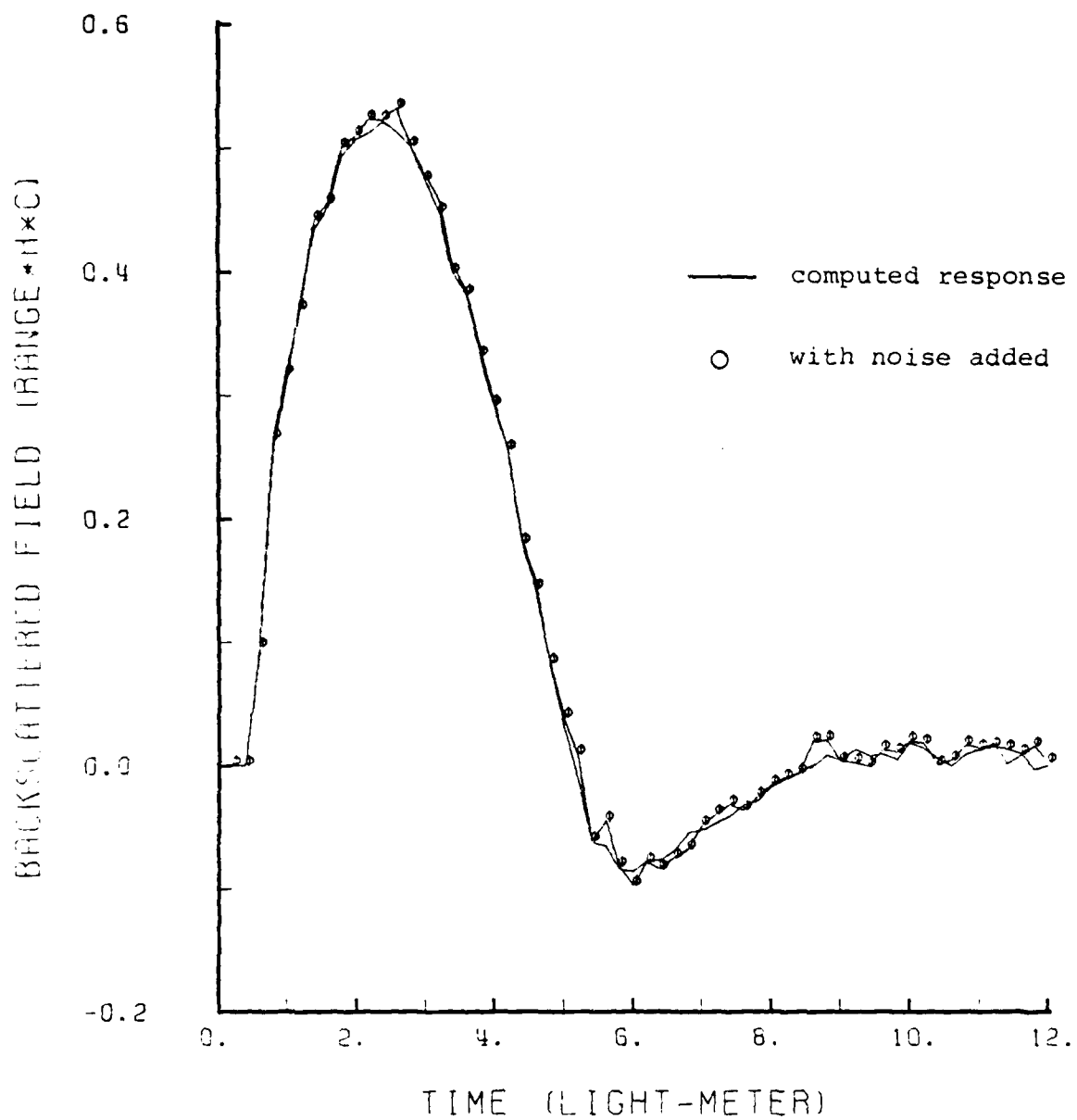


Figure 5.12. Ramp response of the sphere with noise added (S/N = 30 dB)

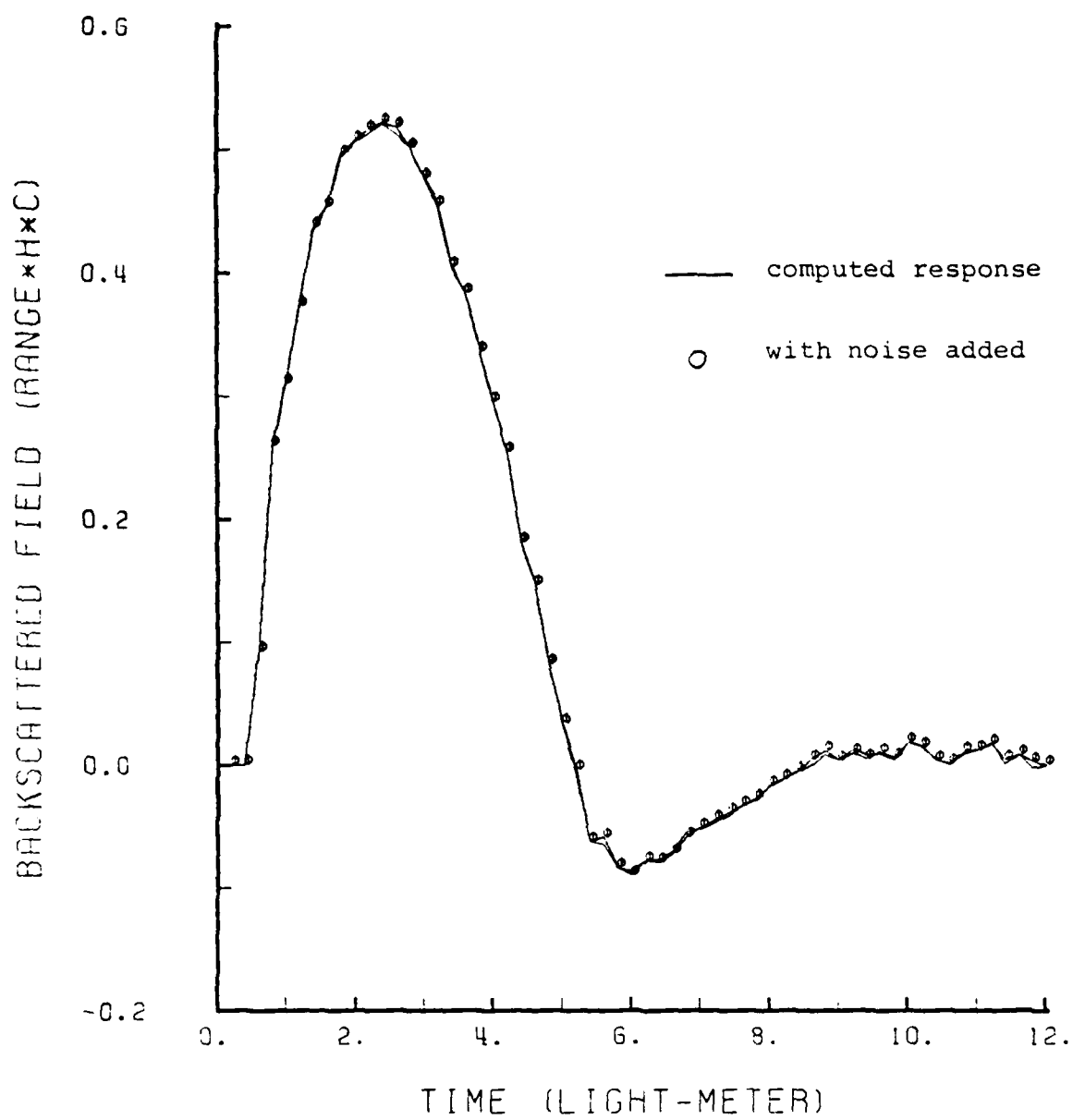


Figure 5.13. Ramp response of the sphere with noise added ( $S/N = 40$  dB)

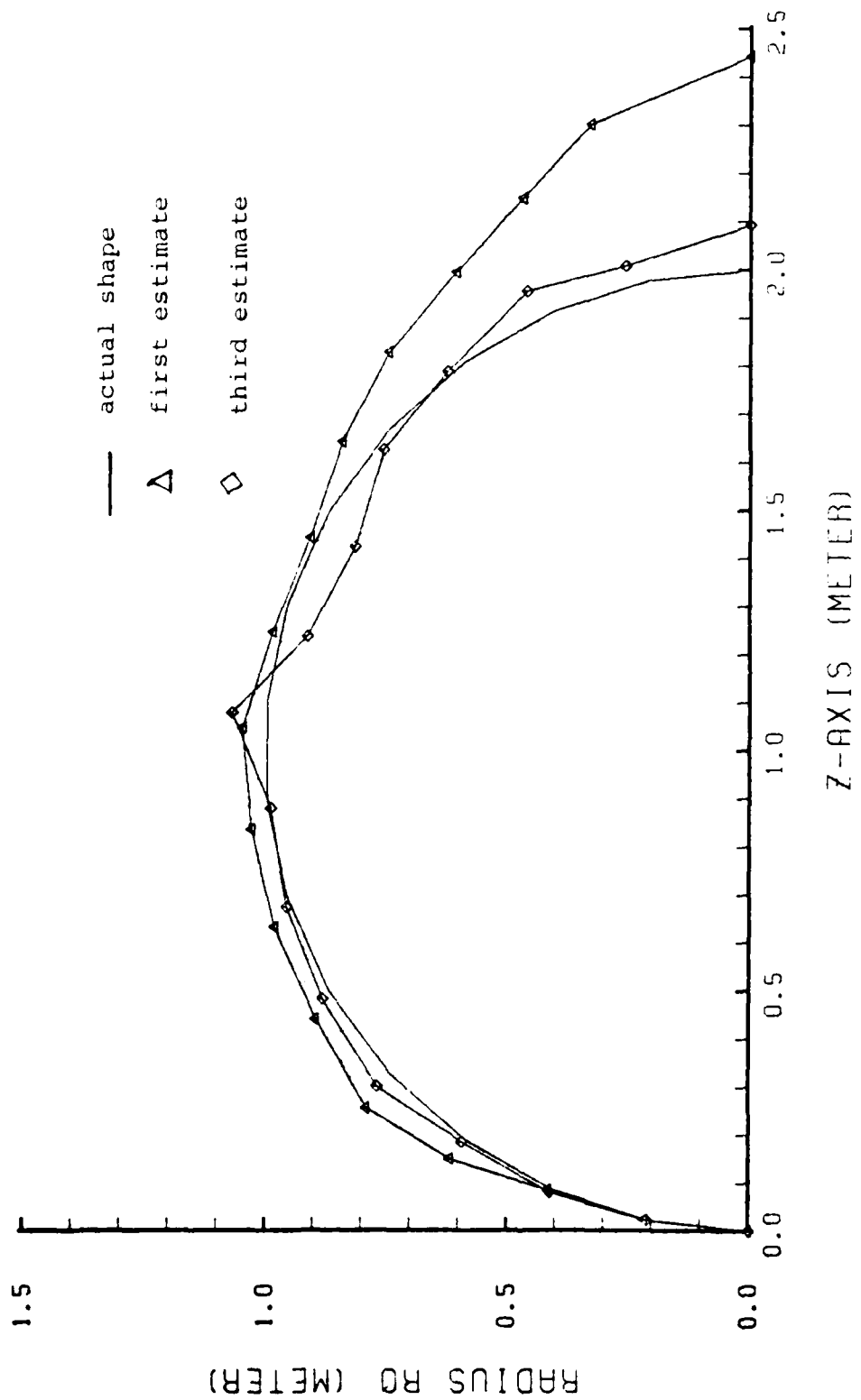


Figure 5.14. Estimates of the shape of the sphere  
(S/N = 20 dB)

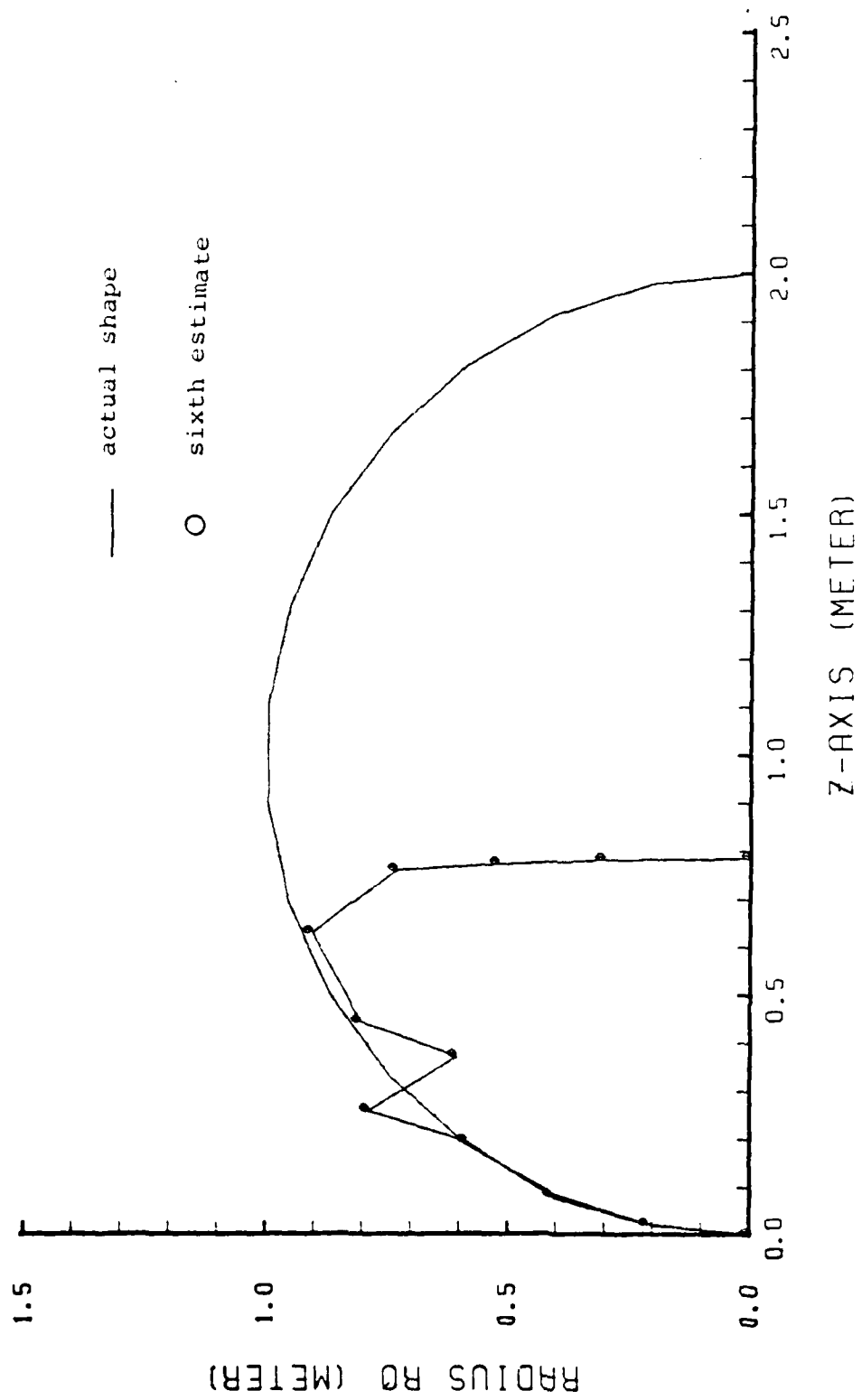


Figure 5.15. Sixth estimate of the shape of the sphere ( $S/N = 20$  dB)

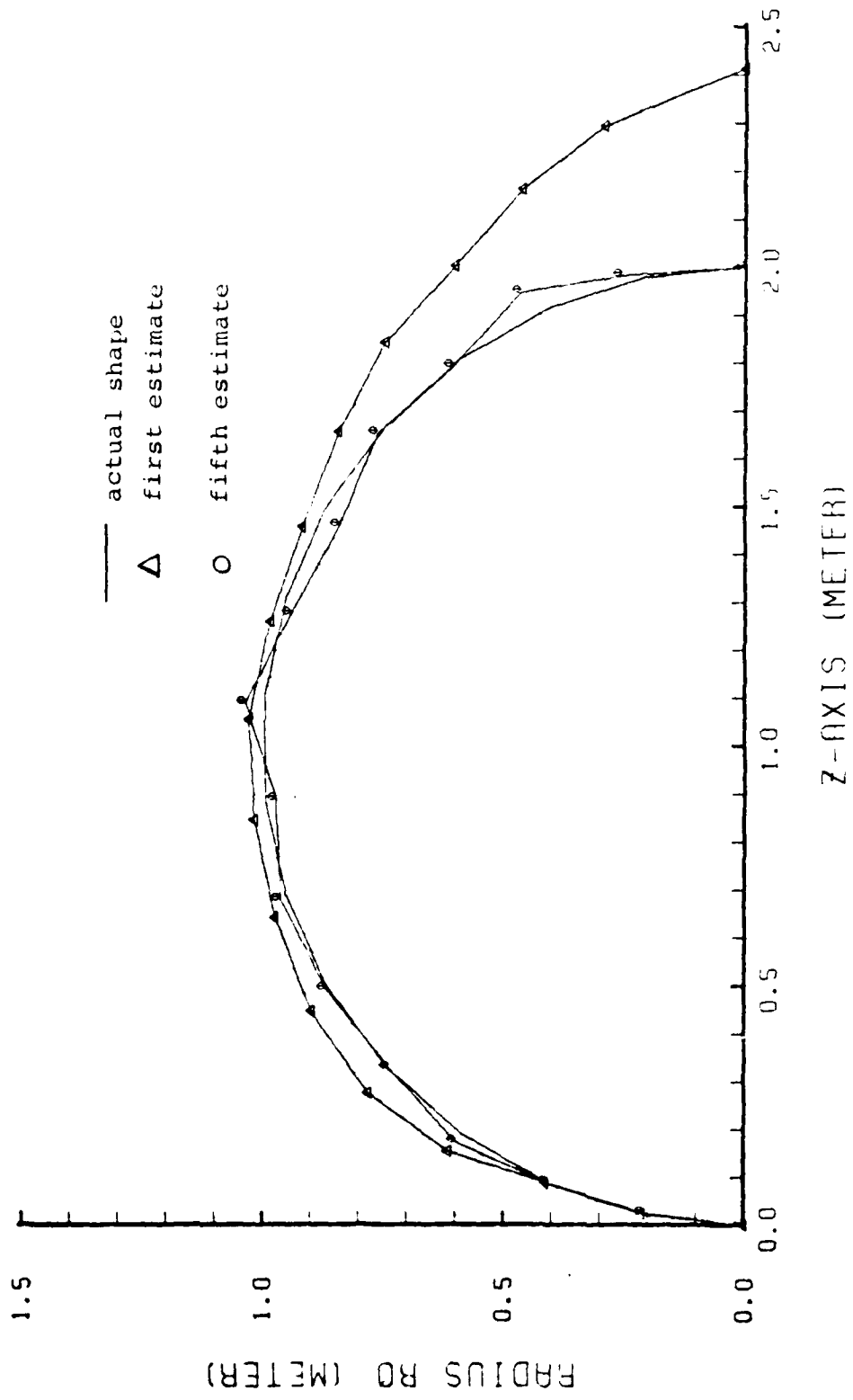


Figure 5.16. Estimate of the shape of the sphere  
(S/N = 30 dB)

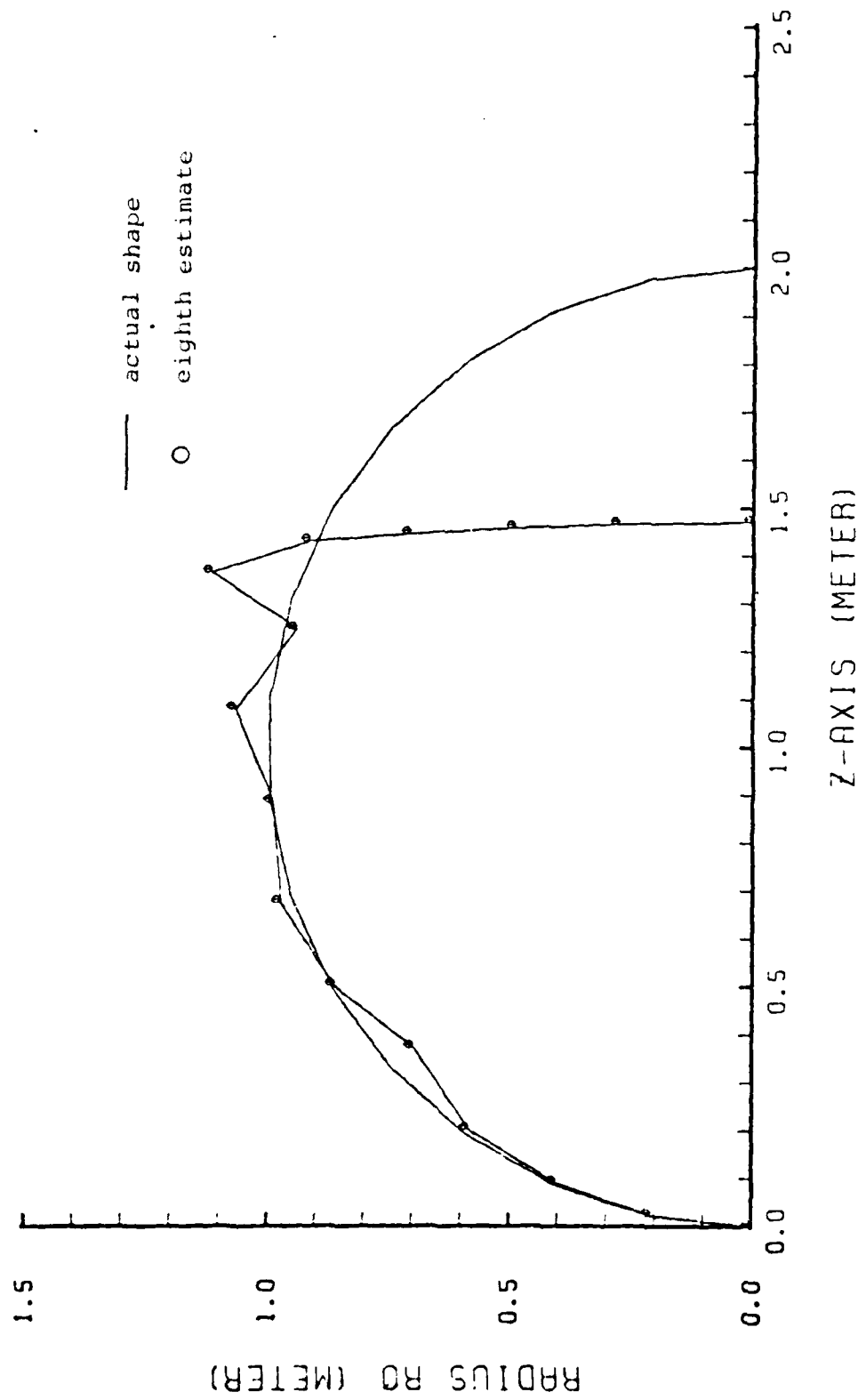


Figure 5.17. Eighth estimate of the shape of the sphere ( $S/N = 30$  dB)

must be investigated. In any case, before diverging the shape that gives the minimum error is quite a good approximation of the true shape.

An additional test with 40 dB S/N was made, and no significant deviation, from the case without noise added, was observed. Figure 5.18 shows the first and 6-th estimates of the shape. The minimum error shape was the 6-th estimate. Up to the 12-th iteration the shape of the body remained stable, with minor variations.

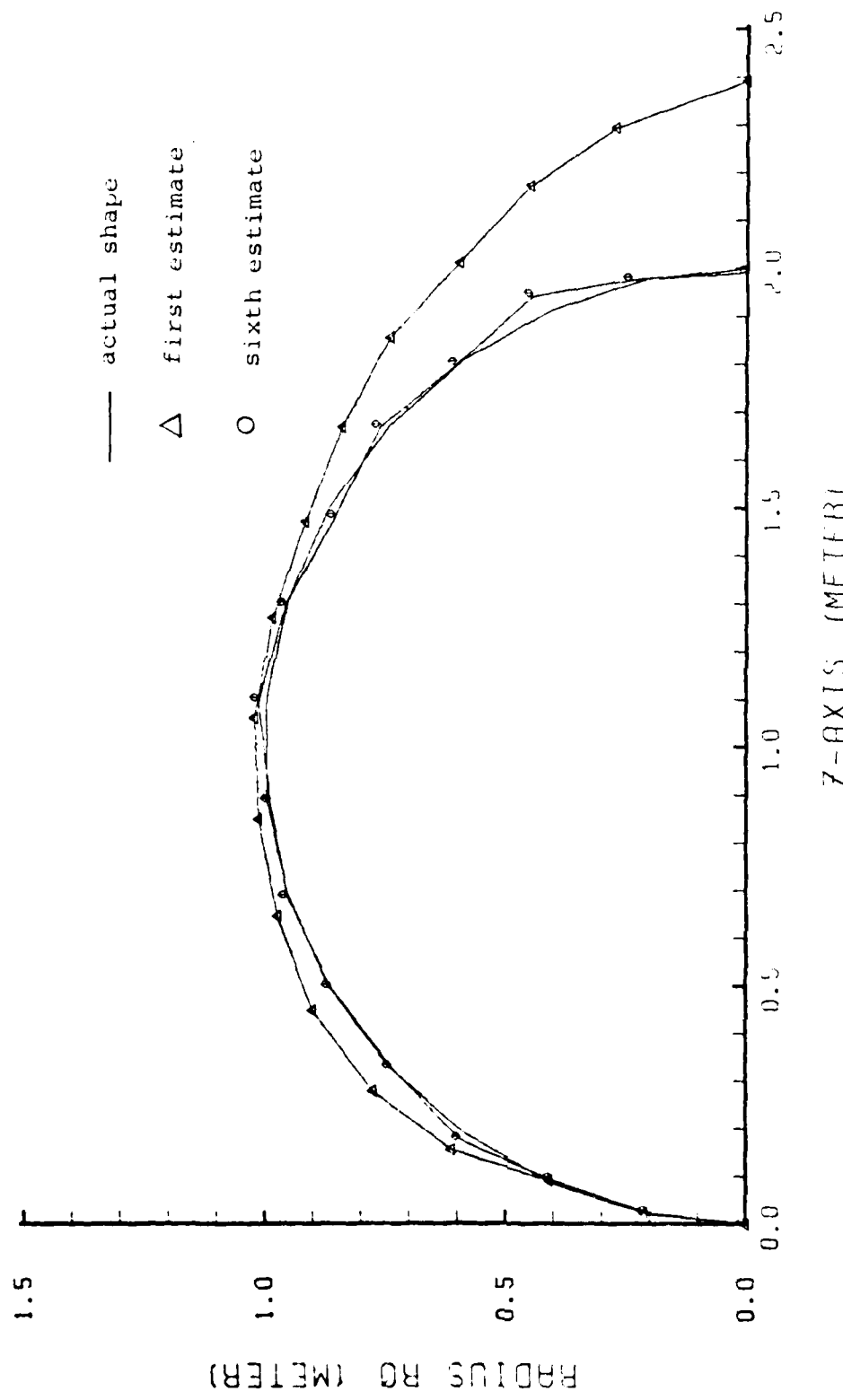


Figure 5.18. Estimates of the shape of the sphere  
(S/N = 40 dB)

AD-A102 660

NAVAL POSTGRADUATE SCHOOL MONTEREY CA  
RADAR TARGET IMAGING BY TIME-DOMAIN INVERSE SCATTERING. (U)  
MAR 81 M MORAG

F/G 17/9

UNCLASSIFIED

NL

2 OF 2  
AD-A102 660

END  
DATE  
9 81  
DTIC

## VI. SUMMARY

### A. SUMMARY OF RESULTS

The inverse scattering method for radar target imaging was the main topic addressed in this work. The inverse scattering algorithm developed uses the time domain solution of the integral equation. The class of targets considered included the conducting bodies of revolution whose important symmetry property reduces considerably the computation time and the computer storage needed for the solution of the inverse scattering problem.

The use of the ramp response for retrieving the shape of the target proved to be a very efficient tool, and the examples considered gave generally good results, with initial convergence of the imaged shape. For the case of the long cylinder and the sphere with low signal to noise ratios there appeared an eventual divergence of the imaged shape after many iterations. This is thought to be due to accumulated numerical roundoff errors in repeatedly solving the integral equations. In general it has been shown that the use of the ramp response by itself, without any further computation, gives a close approximation to the shape of the body but up to its shadow boundary which corresponds to the maximum of the area function  $A(z)$  along the line of sight. Beyond that boundary the body is, at the first observation, elongated and the iterative algorithm is needed to compensate for the errors

induced by the wake or "creeping wave" which alters the target response.

As the iterative computation process goes on, some numerical instability that is mainly due to a discontinuity in the computed shape might arise. However, before diverging, the shape of the body always reaches an estimate which has a minimum error relative to the true shape, and is a good approximation of that shape, so that the minimum error criteria set for stopping the iterative process appear to be an attractive way to overcome the instability phenomena. As a continuation of this work it is suggested to carry out a detailed analysis of the error and numerical instabilities that have been observed while testing the iterative algorithm.

#### B. RECOMMENDATIONS

The algorithm developed for target imaging by transient inverse scattering, has been tested numerically by simulating additive physical noise. It must now be evaluated in a real laboratory environment where the true measured response is used. The transient scattering range at NPS should be used to test and finalize the algorithm for the class of targets addressed in this thesis.

The first step to be done is to obtain the measured ramp response of the target. The range uses an impulse generator which exhibits a gaussian pulse shape characteristic. The true ramp response can be obtained by using either a time domain convolution or a frequency domain computation and I.F.T.

The true ramp response can be obtained, in principle, from the gaussian response of the target using the following relationship:

$$H_R(\omega) = -\frac{H_{IG}(\omega)}{G(\omega)} \cdot \frac{1}{\omega^2}$$

where:

$H_R(\omega)$  is the Fourier transform of the true ramp response of the target,

$H_{IG}(\omega)$  is the gaussian impulse response of the target,

$G(\omega)$  is the Fourier transform of the transmitted gaussian impulse,

and the ramp response will be:

$$h_R(t) = F^{-1}[H_R(\omega)] .$$

Very special care must be given to the choice of space sampling and time sampling intervals. The time sampling is dictated by the sampling rate of the oscilloscope, and the space sampling must be done at a high enough rate such that in every case the distance  $R$  between the closest spatial samples is related to the time sampling  $T$  by:

$$R/C \geq \Delta T .$$

The next step is to translate the FORTRAN program given in Appendix E to fit the computer of the lab. There is a need

to reduce to a minimum the computation time since the laboratory microcomputer is very slow compared to a large mainframe. The use of some additional symmetries of the body can certainly help in this task.

Finally, it is necessary to minimize the noise in measurements, and smooth the response to be used for shape computation.

#### C. AREAS FOR FURTHER STUDY

The ultimate objective of this research program is to aid in determining the feasibility of developing future radar systems having the innate ability to classify targets using their transient scattering response.

In the most general case the target will be of arbitrary shape and the use of the iterative method described in this thesis would be highly impractical and prohibitive for complex targets, due to two principal factors. The first is the time needed to compute the response of a complex body, and the second is that the area function obtained from the ramp response is not sufficient to determine in what way the response is to be computed.

The best technique to deal with such targets would involve a way that does not require the computation of the integral equation, and instead will use only the measured impulse response (or ramp response) to discriminate between targets. The first solution involves measuring the ramp response at multiple look angles. The response waveform will be used up to the shadow boundary to find the area function along each

line of sight. The target image can be approximately reconstructed from the projections of the area functions. Das and Boerner [18], suggested a very interesting approach for target shape estimation using these projections. This method seems attractive and is felt that it could lead to a good solution for target imaging. Its main disadvantage is the need for multiple look angles, requiring either interfaced multiple radars, or long-time dwelling with one radar.

An alternative approach is to classify targets via the complex poles and residues of their time-domain signatures. Once the poles and residues are extracted they could be compared with stored library data corresponding to known targets, and thus would provide a classification of the target under test. This catalogue approach is also being pursued using the NPS transient range, as well as through other independent efforts, and may prove to be the most practically implementable technique available.

Another area which could form the subject of future research includes the time correlation of the shape of the target with its motion.

## APPENDIX A

### DERIVATION OF THE SCALAR INTEGRAL EQUATIONS

In Chapter III, equations (3.3) and (3.4) involve some vector multiplications. The first appearing in the integrals is:

$$\vec{a}_n \times \vec{J}' \times \vec{R} = (\hat{a}_n \times \hat{a}'_s \times \vec{R}) \cdot J'_s + (\hat{a}_n \times \hat{a}'_\phi \times \vec{R}) J'_\phi \quad (A1)$$

We note the following identities:

$$\hat{a}_n \times \hat{a}'_s \times \vec{R} = \hat{a}'_s (\hat{a}_n \cdot \vec{R}) - \vec{R} (\hat{a}_n \cdot \hat{a}'_s) \quad (A2)$$

$$\hat{a}_n \times \hat{a}'_\phi \times \vec{R} = \hat{a}'_\phi (\hat{a}_n \cdot \vec{R}) - \vec{R} (\hat{a}_n \cdot \hat{a}'_\phi) \quad (A3)$$

Expressing  $\vec{R}$ ,  $\hat{a}'_s$  and  $\hat{a}'_\phi$  in terms of the  $(\hat{a}_s, \hat{a}_\phi, \hat{a}_n)$  coordinates system gives:

$$\begin{aligned} \vec{R} &= \hat{a}_\phi (\vec{R} \cdot \hat{a}_\phi) + \hat{a}_s (\vec{R} \cdot \hat{a}_s) \\ \hat{a}'_\phi &= \hat{a}_\phi (\hat{a}'_\phi \cdot \hat{a}_\phi) + \hat{a}_s (\hat{a}'_\phi \cdot \hat{a}_s) \\ \hat{a}'_s &= \hat{a}_\phi (\hat{a}'_s \cdot \hat{a}_s) + \hat{a}_s (\hat{a}'_s \cdot \hat{a}_s) \end{aligned} \quad (A4)$$

For the body of revolutions we note the following relationships:

$$\hat{a}'_\phi \cdot \hat{a}_\phi = \cos \beta$$

$$\hat{a}'_\phi \cdot \hat{a}_s = -\sin \alpha \cdot \sin \beta$$

$$\hat{a}'_\phi \cdot \hat{a}_n = -\cos \alpha \cdot \sin \beta$$

$$\hat{a}'_s \cdot \hat{a}_s = \sin \alpha \sin \alpha' \cos \beta + \cos \alpha \cos \alpha'$$

$$\hat{a}' \cdot \hat{a}_\phi = \sin \alpha' \sin \beta$$

$$\hat{a}' \cdot \hat{a}_n = \cos \alpha \sin \alpha' \cos \beta - \sin \alpha \cos \alpha'$$

where

$$\beta = \phi' - \phi$$

The vectors  $\vec{R}$ ,  $\hat{a}_n$ ,  $\hat{a}_s$ ,  $\hat{a}_\phi$  are given in cartesian coordinates by:

$$\vec{R} = \hat{a}_x (\rho \cos \phi - \rho' \cos \phi') + \hat{a}_y (\rho \sin \phi - \rho' \sin \phi')$$

$$- \hat{a}_z (z' - z)$$

$$\hat{a}_n = \hat{a}_x (\cos \alpha \cdot \cos \phi) + \hat{a}_y (\cos \alpha \cdot \sin \phi) - \hat{a}_z \sin \alpha$$

$$\hat{a}_s = \hat{a}_x (\sin \alpha \cdot \cos \phi) + \hat{a}_y (\sin \alpha \cdot \sin \phi) + \hat{a}_z \cos \alpha$$

$$\hat{a}_\phi = -\hat{a}_x (\sin \alpha) + \hat{a}_y \cdot \cos \alpha$$

Carrying out the dot products gives:

$$\vec{R} \cdot \hat{a}_n = \cos \alpha (\rho - \rho' \cos \beta) + (z' - z) \sin \alpha$$

$$\vec{R} \cdot \hat{a}_s = \sin \alpha (\rho - \rho' \cos \beta) - (z' - z) \cos \alpha \quad (A5)$$

$$\vec{R} \cdot \hat{a}_\phi = -\rho' \sin \beta$$

Using the relationships given by the sets of equations (A4) and (A5), and simplifying, equations (A2) and (A3) become:

$$\begin{aligned}
 \hat{a}_n \times \hat{a}'_s \times \vec{R} = & \hat{a}_\phi \{ \sin \beta [ (z' - z) \sin \alpha \sin \alpha' + \rho \cos \alpha \sin \alpha' \\
 & - \rho' \cos \alpha' \sin \alpha] \} + \hat{a}_s \{ (\rho - \rho' \cos \beta) \cos \alpha' \\
 & + (z' - z) \cos \beta \sin \alpha' \}
 \end{aligned} \tag{A6}$$

$$\begin{aligned}
 \hat{a}_n \times \hat{a}'_\phi \times \vec{R} = & \hat{a}_\phi [ (z' - z) \sin \alpha \cos \beta + \cos \alpha (\rho \cos \beta - \rho') ] \\
 & + \hat{a}_s [-\sin \beta (z' - z)]
 \end{aligned} \tag{A7}$$

Defining:

$$V = z' - z$$

$$F_1 = (z' - z) \cos \beta \sin \alpha' + \cos \alpha' (\rho - \rho' \cos \beta)$$

$$U = (z' - z) \sin \alpha \sin \alpha' + \rho \cos \alpha \sin \alpha' - \rho' \cos \alpha' \sin \alpha$$

$$F_2 = \cos \alpha (\rho \cos \beta - \rho') + \sin \alpha \cos \beta (z' - z)$$

produces from (A6) and (A7)

$$\hat{a}_n \times \hat{a}'_s \times \vec{R} = \hat{a}_\phi U \sin \beta + \hat{a}_s \cdot F_1 \tag{A8}$$

$$\hat{a}_n \times \hat{a}'_\phi \times \vec{R} = \hat{a}_\phi F_2 - \hat{a}_s V \cdot \sin \beta \tag{A9}$$

Note that  $V$ ,  $F_1$ ,  $F_2$  are even functions of  $\beta$  and  $U$  is independent of  $\beta$ . Next we have to carry the second vector multiplication:

$$\hat{a}_n \times \vec{H}^i = -\hat{a}_s H^i \sin \phi - \hat{a}_\phi H^i \cos \phi \sin \alpha \tag{A10}$$

where  $\vec{H}^i$  is given in cartesian coordinates by:

$$\vec{H}^i = \vec{a}_x \cdot \vec{H}^i$$

After substituting equations (A8), (A9), and (A10) into equations (3.3) and (3.4) we obtain the scalar expressions for the components of the current in the  $\hat{s}$  and  $\hat{\phi}$  directions as follows:

$$J_s = -2H^i \sin \phi + \frac{1}{2\pi} \int_A \frac{1}{R^2} \left[ \frac{1}{R} + \frac{1}{C} \frac{\partial}{\partial \tau} \right] [J'_s F_1 - J'_\phi V \sin \beta] dA' \quad (A11)$$

$$J_\phi = -2H^i \cos \phi \sin \alpha + \frac{1}{2\pi} \int_A \frac{1}{R^2} \left[ \frac{1}{R} + \frac{1}{C} \frac{\partial}{\partial \tau} \right] \\ \cdot [J'_s U \sin \beta + J'_\phi F_2] dA' \quad (A12)$$

## APPENDIX B

### DEMONSTRATION OF THE SINUSOIDAL VARIATION OF THE CURRENTS WITH $\phi$

Maxwell's first equation:

$$\nabla \times \vec{H} = \epsilon \dot{\vec{E}} + \vec{J} \quad (B1)$$

In the case of interest, due to symmetry, the field  $\vec{H}$  is independent of  $\phi$  and is given by

$$\vec{H} = \hat{a}_x H_0(\rho, z, t)$$

or in cylindrical coordinates

$$\begin{aligned} \vec{H} &= H_0 \cos \phi \hat{a}_\rho - H_0 \sin \phi \hat{a}_\phi \\ \nabla \times \vec{H} &= \left[ \frac{1}{\rho} \frac{\partial}{\partial z} (\rho H_0) \right] \sin \phi \hat{a}_\rho + \frac{\partial H_0}{\partial z} \cos \phi \hat{a}_\phi \\ &\quad - \hat{a}_z \sin \phi \cdot \frac{\partial H_0}{\partial \rho} \end{aligned} \quad (B2)$$

The currents on the body expressed in cylindrical coordinates are:

$$\vec{J} = \hat{a}_\rho \sin \alpha J_s + \hat{a}_\phi J_\phi + \hat{a}_z \cos \alpha J_s \quad (B3)$$

The electric field:

$$\vec{E} = \hat{a}_y E_0 = a_\rho \sin \phi E_0 + \hat{a}_\phi \cos \phi E_0 \quad (B4)$$

Substituting equations (B2), (B3) and (B4) in Maxwell's equation (B1) and equating the terms in the same direction gives:

$$\sin \alpha \cdot J_s = \left[ \frac{1}{\rho} \frac{\partial}{\partial z} (\rho H_0) - E_0 \right] \sin \phi$$

The term inside the brackets is independent of  $\phi$  so that we can write

$$\sin \alpha \cdot J_s = J_{o_1}(\rho, z, t) \sin \phi \quad (B5)$$

Similarly

$$\begin{aligned} J_\phi &= \left( \frac{\partial H_0}{\partial z} - E_0 \right) \cos \phi \\ J_\rho &= J_{o_2}(\rho, z, t) \cos \phi \end{aligned} \quad (B6)$$

and finally

$$\begin{aligned} J_s \cos \alpha &= - \sin \alpha \frac{\partial H_0}{\partial \rho} \\ &= J_{o_3}(\rho, z, t) \sin \phi \end{aligned} \quad (B7)$$

Equations (B5), (B6), (B7) show clearly that the currents  $J_s$  and  $J_\phi$  vary sinusoidally with the angle  $\phi$  so that we can generalize:

$$J_s(\rho, z, t, \phi) = J_s(\rho, z, t) \sin \phi$$

$$J_\phi(\rho, z, t, \phi) = J_\phi(\rho, z, t) \cos \phi$$

APPENDIX C  
SIMPLIFICATION OF THE SCALAR INTEGRAL EQUATIONS

In Chapter III the scalar equations for the currents components were given by equations (3.4) and (3.5). In these equations we had:

$$dA' = \rho' ds' d\beta$$

and

$$Js = J_s \sin \phi$$

$$J\phi = J_\phi \cos \phi$$

Substituting in equation (3.4) gives

$$J_s \sin \phi = -2H^i \sin \phi + \frac{1}{2\pi} \int_0^s \rho' ds' \int_0^{2\pi} \frac{1}{R^2} \left[ \frac{1}{C} \frac{\partial}{\partial \tau} + \frac{1}{R} \right] \\ \cdot [J'_s \sin \beta' F_1 - J'_\phi \sin \beta' V \cos \phi'] d\beta \quad (C1)$$

As noted in Appendix A, the expressions  $V$ ,  $F_1$  and  $F_2$  appearing in the integral are even and periodic functions of  $\beta$ . We recall that

$$R = (\rho^2 + \rho'^2 - 2\rho\rho' \cos \beta + (z' - z)^2)^{1/2}$$

and

$$\tau = t - R/C$$

so that  $R$ ,  $J'_s(\rho', z, t)$  and  $J'(\rho', z', t)$  are also even and periodic functions of  $\beta$ . Finally  $U$  is independent of  $\beta$ .

We will concentrate on the integral over  $s$  in order to reduce it to its simplest expression. Since

$$\phi' = \phi + \beta$$

we can write

$$\sin \phi' = \sin \phi \cos \beta + \sin \beta \cos \phi$$

$$\cos \phi' = \cos \phi \cos \beta - \sin \phi \sin \beta$$

and substitute this into the integral over  $\beta$  in equation (C1). The integral over  $\beta$  for a complete period, of all terms that contain  $\sin \beta$  will be zero since those terms are periodic and odd functions of  $\beta$ . All the other terms will produce a non-zero integral and will be retained.

After this simplification, equation (C1) will become:

$$\begin{aligned} J_s \sin \phi &= -2H^i \sin \phi + \sin \phi \frac{1}{2\pi} \int_0^s \phi' ds' \\ &\cdot \int_0^{2\pi} \frac{1}{R^2} \left[ \frac{1}{C} \frac{\partial}{\partial \tau} + \frac{1}{R} \right] [J'_s F_1 \cos \beta + V J'_\phi \sin^2 \beta] d\beta \quad (C2) \end{aligned}$$

which after repressing the common term  $\sin \phi$ , leads to the final equation:

$$\begin{aligned} J_s &= -2H^i + \frac{1}{2\pi} \int_0^s \phi' ds' \int_0^{2\pi} \frac{1}{R^2} \left[ \frac{1}{C} \frac{\partial}{\partial \tau} + \frac{1}{R} \right] \\ &\cdot [J'_s F_1 \cos \beta + V J'_\phi \sin^2 \beta] d\beta. \quad (C3) \end{aligned}$$

Following the same reasoning for equation (3.5), and repressing the common term  $\cos \beta$  leads to the following final equation:

$$J_{\phi} = -2H^i \sin \alpha + \frac{1}{2\pi} \int_0^s \rho' ds' \int_0^{2\pi} \frac{1}{R^2} \left[ \frac{1}{C} \frac{\beta}{\beta - \tau} + \frac{1}{R} \right] \\ \cdot [J'_{s,\phi} \sin^2 \beta + J'_{s,\phi} F_2 \cos \beta] d\beta \quad (C4)$$

In both equations (C4) and (C3) the currents are:

$$J_{s,\phi} = J_{s,\phi}(\rho, z, t)$$

$$J'_{s,\phi} = J'_{s,\phi}(\rho', z, \tau)$$

$\tau$  being the retarded time  $t - R/C$ , and the incident field is:

$$H^i = H^i(z, t)$$

SYSIN DD DATA

APPENDIX D

\*\*\*\*\*  
\* TRANSIENT RESPONSE OF A STRAIGHT THIN WIRE \*  
\*\*\*\*\*

PURPOSE:

\*\*\*\*\*  
THIS PROGRAM COMPUTES THE TRANSIENT TIME DOMAIN  
RESPONSE OF A STRAIGHT THIN WIRE.

THE PROGRAM COMPUTES THE CURRENTS INDUCED ON THE  
WIRE BY AN INCIDENT IMPULSE FIELD, AND THE SCATTERED  
FIELD, FOR ANY ANGLES OF INCIDENCE AND SCATTERING.

USAGE:

\*\*\*\*\*  
THE PROGRAM CAN BE USED AFTER PROPER DEFINITION  
OF THE INITIAL PARAMETERS OF THE WIRE, AND DEFINITION  
OF THE DESIRED ANGLES OF INCIDENCE AND REFRACTION.

THE WIRE IS ALIGNED WITH THE Z-AXIS STARTING AT Z=0  
THE ANGLES ARE MEASURED WITH RESPECT TO THE Z-AXIS

PARAMETER DEFINITION

\*\*\*\*\*

BETA(400,40) : ARRAY DEFINING THE CURRENTS FOR UP  
TO 40 SEGMENTS AND 400 TIME INCREMENTS.

GAMMA(400,40) : ARRAY DEFINING THE CHARGES FOR UP  
TO 40 SEGMENTS AND 400 TIME INCREMENTS.

NS: NUMBER OF SEGMENTS IN WHICH THE WIRE IS DIVIDED

SL: TOTAL LENGTH OF THE WIRE IN METERS.

A: RADIUS OF THE WIRE IN METERS.

ITS: NUMBER OF TIME INCREMENTS.  
ITS MUST BE A MULTIPLE OF 80 FOR PLOTTING  
CONVENIENCE

TI: ANGLE OF INCIDENCE IN DEGREES.

TS: ANGLE OF REFRACTION IN DEGREES.

DZ: LENGTH OF A SEGMENT (L/NS)

DT: TIME INCREMENT IN SECONDS (DT=DZ/C)

AA: GAUSSIAN IMPULSE PARAMETER. IN SEC-1.

TMAX: TIME DELAY OF THE IMPULSE FROM THE FIRST TIME OF INCIDENCE TO ITS PEAK.(TYPICALLY DT\*NS/2)

EI: INCIDENT FIELD (GAUSSIAN PULSE).

ES(400): ARRAY CONTAINING THE COMPUTED SCATTERED FIELD UP TO 400 TIME INCREMENTS.

DELAZ : TIME DERIVATIVE OF THE MAGNETIC POTENTIAL.

DELPHI: TIME DERIVATIVE OF THE ELECTRIC POTENTIAL.

C: SPEED OF LIGHT.

C1: CONSTANT ( $\mu/4\pi$ ).

C2: CONSTANT ( $1/4\pi\epsilon$ ).

X(30),Y(30):COORDINATES REQUIRED FOR SUBROUTINE "PLOTP".

REMARKS:

\*\*\*\*\*  
THE ANGLES OF INCIDENCE AND REFRACTION DESIRED ARE ENTERED IN DATA CARDS ACCORDING TO FORMAT 2F6.1. EACH DATA CARD CONTAIN ONE ANGLE OF INCIDENCE AND ONE ANGLE OF REFRACTION.

THE COMPUTATION IS DONE FOR AS MANY DATA INPUTS AS THERE ARE DATA CARDS. THE LAST DATA CARD MUST CONTAIN THE DATA NUMBER 1.0 IN ORDER TO TERMINATE THE PROGRAM.

SUBROUTINES USED:

\*\*\*\*\*  
THE PROGRAM USES A LIBRARY SUBROUTINE NAMED PLOTP FOR THE PLOT OF CURRENTS AND FIELD AS A FUNCTION OF TIME.

METHOD OF SOLUTION:

\*\*\*\*\*  
THIS IS THE SOLUTION OF THE E.F.I.E. EQUATION APPLIED TO A THIN WIRE, ACCORDING TO THE METHOD DESCRIBED BY HARRINGTON AND SAYRE IN 'TIME DOMAIN RADIATION AND SCATTERING BY THIN WIRES' (IN 'APPL. SCI. RES. 26' SEPT 1972)

```

*****
* MAIN PROGRAM *
*****
DIMENSION BETA(400,40), GAMMA(400,40), ES(400)
DIMENSION X(400), Y(400)

CONSTANTS INITIALIZATION
C=3.0E+8
C1=1.0E-7
C2=9.0E+9
PI=3.141592654

PARAMETERS INITIALIZATION
COMPUTATION PARAMETERS
NS=40
ITS=400
NS1=NS-1

WIRE PARAMETERS
SL=1.04
A=7.75 E-4
DZ=SL/NS
DT=DZ/C

GAUSSIAN IMPULSE PARAMETERS
AA=0.67 E+9
TMAX=DT*18.0

CONTINUE
READING OF DESIRED ANGLE OF INCIDENCE TI
AND ANGLE OF REFRACTION TS.
9510 READ(5,9510) TI, TS
FORMAT(2F6.1)
IF(TI.EQ.1.0) GO TO 999

WRITE HEADING
9601 WRITE(6,9601) TI, TS
FORMAT(1H1,10X,'CURRENTS INDUCED WHEN FIELD INCIDENT',
2'AT ANGLE',1F6.1,'//',10X,'FAR FIELD SCATTERED TOWARDS',
3'ANGLE',1F6.1,'///',8X,'TIME',15X,'CURRENT (AMP)',///)

TRANSLATION FROM DEGREES TO RADIANS.
TIR=PI*TI/180.0
TSR=PI*TS/180.0
AI=COS(TIR)
AR=COS(TSR)

```

```

C          START OF CURRENTS COMPUTATION
C
C          S1=0.5
C          S2=-0.5
C          S3=(A/DZ)**2
C          FO= ALOG((S1+SQRT(S1**2+S3))/(S2+SQRT(S2**2+S3)))
C
C          INITIAL CONDITIONS SETTING
C
C          DO 100 L=1,NS1
C          L1=L-1
C          IF(TI.LE.90.0) GO TO 120
C          L2=L-NS
C          GO TO 130
120      CONTINUE
C          L2=L
130      CONTINUE
C          EI= EXP((-AA**2)*(DT*(1-L2*AI)-TMAX)**2) *SIN(TIR)*3.0
C          BETA(1,L)=EI/(2*C1*FO/DT)
C          IF(L.EQ.1) GO TO 110
C          GAMMA(1,L)=-(1.0/C)*(BETA(1,L)-BETA(1,L1))
C          GO TO 100
C
C          BOUNDARY CONDITIONS SETTING
C
110      CONTINUE
C          GAMMA(1,1)=-BETA(1,1)/C
100      CONTINUE
C          GAMMA(1,NS)= BETA(1,NS1)/C
C
C          START ALL CURRENTS COMPUTATION
C          AT EACH TIME INTERVAL, AND FOR ALL SEGMENTS
C
C          DO 200 J=2,ITS
C
C          DO 300 L=1,NS1
C
C          DELPHI      =0.0
C          DELAZ       =0.0
C          DO 310 K=1,NS1
C          K1=IABS(L-K)
C          K2=J-K1
C          S1=K1+0.5
C          S2=K1-0.5
C          S3=(A/DZ)**2
C          F= ALOG((S1+SQRT(S1**2+S3))/(S2+SQRT(S2**2+S3)))
C          IF(K1.EQ.0) GO TO 320
C          IF(K2.LE.0) GO TO 310
C          DELAZ      =DELAZ      +BETA(K2,K)*F
320      CONTINUE
C          K3=K2-1
C          IF(K3.LE.0) GO TO 310
C          DELAZ      =DELAZ      -BETA(K3,K)*F
310      CONTINUE
C          DELAZ      =DELAZ      *C1
C          DO 330 K=1,NS
C          K2=IABS(L-K)
C          K1=IABS(L-K+1)
C          K3=J-1-K1
C          K4=J-1-K2
C          IF(K3.LE.0) GO TO 340
C          S1=K1+0.5
C          S2=K1-0.5
C          F= ALOG((S1+SQRT(S1**2+S3))/(S2+SQRT(S2**2+S3)))
C          DELPHI     =DELPHI     +GAMMA(K3,K)*F

```

```

340  CONTINUE
      IF(K4.LE.0) GO TO 330
      S1=K2+0.5
      S2=K2-0.5
      F=ALOG((S1+SQRT(S1**2+S3))/(S2+SQRT(S2**2+S3)))
      DELPHI=DELPHI-GAMMA(K4,K)*F
330  CONTINUE
      DELPHI=DELPHI*C2
      IF(TI.LE.90.0) GO TO 331
C          FOR ANGLES OF INCIDENCE MORE THAN 90 DEGREES
C
      L2=L-NS
      GO TO 332
C          FOR ANGLES OF INCIDENCE LESS THAN 90 DEGREES
C
331  CONTINUE
      L2=L
332  CONTINUE
      IF(J.GT.50) GO TO 333
      EI=EXP((-AA**2)*(J*DT*(1-L2*AI)-TMAX)**2)*SIN(TIR)*3
      GO TO 334
333  CONTINUE
      EI=0.0
334  CONTINUE
      BETA(J,L)=(EI-DELAZ/DT-DELPHI/DT)/(C1*FO/DT)
      J1=J-1
      L1=L-1
      IF(L.GT.1) GO TO 350
      GAMMA(J,L)=GAMMA(J1,L)-BETA(J,L)/C
      GO TO 300
350  CONTINUE
      GAMMA(J,L)=GAMMA(J1,L)-BETA(J,L)/C+BETA(J,L1)/C
300  CONTINUE
      GAMMA(J,NS)=GAMMA(J1,NS)+BETA(J,NS1)/C
      KK=NS/2
C
C          WRITE THE CURRENT INDUCED AT THE CENTER OF THE WIRE
C
9690  WRITE(6,9690) J,BETA(J,KK)
      FORMAT(10X,I4,21X,E12.5)
200  CONTINUE
C          END OF CURRENTS COMPUTATION
C
C          START OF SCATTERED FIELD COMPUTATION
C
      DO 400 LP=1,ITS
      ES(LP)=0.0
      DO 500 K=1,NS1
      IF(ITS.GT.90.0) GO TO 501
      IF(ITS.EQ.90.0) GO TO 503
C          FOR REFRACTION ANGLE LESS THAN 90 DEGREES
C
      KP=K
      NQ=LP-1-(KP-0.5)*AR
      NQP=LP-1-(KP+0.5)*AR
      GO TO 502
C

```

C FOR REFRACTION ANGLE MORE THAN 90 DEGREES  
 501 CONTINUE  
 KP=K-NS  
 NQP=LP-1-(KP-0.5)\*AR  
 NQ=LP-1-(KP+0.5)\*AR  
 GO TO 502  
 C FOR REFRACTION ANGLE EQ. 90 DEGREES.  
 503 CONTINUE  
 NQ=LP-1  
 NQP=NQ  
 502 CONTINUE  
 NQ1=NQ-1  
 NQ2=NQP-1  
 IF(NQ.LE.0) GO TO 500  
 IF(NQ.EQ.1) GO TO 510  
 IF(NQ.EQ.NQP) GO TO 520  
 ZQ=(LP-1-NQ)/AR +0.5  
 EPS=DZ\*(ZQ-KP)  
 DEL=DZ-EPS  
 ES(LP)=ES(LP)+EPS\*(BETA(NQ,K)-BETA(NQ1,K))  
 IF(NQ.EQ.2) GO TO 530  
 ES(LP)=ES(LP)+DEL\*(BETA(NQP,K)-BETA(NQ2,K))  
 GO TO 500  
 510 CONTINUE  
 ES(LP)=ES(LP)+DZ\*2\*BETA(NQ,K)  
 GO TO 500  
 520 CONTINUE  
 ES(LP)=ES(LP)+DZ\*(BETA(NQ,K)-BETA(NQ1,K))  
 GO TO 500  
 530 CONTINUE  
 ES(LP)=ES(LP)+DZ\*2\*BETA(NQP,K)  
 500 CONTINUE  
 CT=-SIN(TSR)\*(1.0 E-7)/DT  
 ES(LP)=CT\*ES(LP)  
 400 CONTINUE

END OF FIELD COMPUTATION

PLOT OF CURRENT AT CENTER OF THE WIRE  
 PLOT EVERY 44 POINT.

4M=ITS/100  
 DO 600 I=MM,ITS,MM  
 K=I/MM  
 X(K)=I\*DZ  
 KK=NS/2  
 Y(K)=BETA(I,KK)\*1000.0  
 600 CONTINUE  
 MM=ITS/80  
 WRITE(6,9630)  
 9630 FORMAT(1H1)  
 MODCUR=0  
 CALL PLOTP(X,Y,80,MODCUR)  
 WRITE(6,9600) TI  
 9600 FORMAT(//,5X,'CURRENT INDUCED AT CENTER OF WIRE',  
 2 SCATTERER',/5X,'FIELD INCIDENT AT ANGLE',1F6.1,/,  
 3 10X,'X-AXIS TIME IN LIGHT-METERS',  
 4 //,10X,'Y-AXIS CURRENT IN MILLIAMPS')

```

C          PLOT OF SCATTERED FIELD
C
C          DO 700 I=MM,ITS,MM
C          K=I/MM
C          Y(K)=ES(I) *1000.0
C          CONTINUE
C          700      WRITE (6,9640)
C          9640      FORMAT(1H1)
C          MODCUR=0
C          CALL PLOTP(X,Y,80,MODCUR)
C          WRITE (6,9620) TS
C          9620      FORMAT(//,,5X,'NORMALIZED FAR FIELD BACK SCATTERED',:
C          2BY WIRE',/,5X,'AT ANGLE',1F6.1,/,10X,'X-AXIS TIME',
C          3 LIGHT METERS',/,10X,'Y-AXIS FAR FIELD MILLIVOLTS')
C
C          END OF PROGRAM GO BACK TO NEXT ANGLE IF ANY
C
C          GO TO 10
C          CONTINUE
C          STOP
C          END

EXAMPLE OF DATA CARDS

90.0 90.0
1.0

```

APPENDIX E

\*\*\*\*\*  
\* TIME DOMAIN RESPONSE AND INVERSE SCATTERING \*  
\* FOR A PERFECT CONDUCTOR BODY OF REVOLUTION \*  
\*\*\*\*\*

NAME OF PROGRAM : GAIL  
\*\*\*\*\*

PURPOSE:  
\*\*\*\*\*

THIS PROGRAM COMPUTES THE TRANSIENT TIME DOMAIN  
RESPONSE OF A PERFECT CONDUCTOR BODY OF REVOLUTION,  
AND APPLIES IT TO THE SOLUTION OF THE INVERSE  
SCATTERING PROBLEM. (COMPUTATION OF THE SHAPE OF THE  
BODY FROM ITS TIME DOMAIN RAMP RESPONSE)

USAGE:  
\*\*\*\*\*

THE PROGRAM CAN BE USED IN ONE OF FOUR WAYS  
DEPENDING OF THE DESIRED OUTPUT AND CONSEQUENTLY OF  
THE VALUE ASSIGNED TO THE INITIATING PARAMETERS 'INC'  
AND 'INVER'.

THE POSSIBLE USES ARE:

1. COMPUTATION OF THE TRANSIENT TIME DOMAIN IMPULSE  
RESPONSE (BACKSCATTERED FIELD), WHEN THE INCIDENT  
FIELD IS A GAUSSIAN IMPULSE. (INC=1)  
THE CURRENTS INDUCED ON THE BODY CAN BE MADE AVAILABLE  
AT THE OUTPUT IF DESIRED (FOR EMP PROBLEMS).

THE INPUTS REQUIRED ARE:

- A. THE SPACE SAMPLES OF THE CONTOUR FUNCTION OF  
THE BODY,  $R_0(z)$ , ENTERD IN DATA CARDS.
- B. THE NUMBER OF SEGMENTS SUBDIVIDING THE CONTOUR  
OF THE BODY (NS<20).
- C. THE LENGTH OF A TIME INCREMENT (DT).
- D. THE NUMBER OF TIME SAMPLES NEEDED (ITS<= 60).
- E. THE LENGTH OF EACH SEGMENT DS(20).
- F. THE PARAMETERS DEFINING THE GAUSSIAN IMPULSE.

2. COMPUTATION OF THE RAMP RESPONSE OF THE BODY  
WHEN THE INCIDENT FIELD IS A RAMP. (INC=2 AND INVER=1)

THE INPUTS REQUIRED ARE:

SAME AS A THRU E LISTED ABOVE.

3. INVERSE SCATTERING SOLUTION STARTING FROM THE  
BODY ITSELF. (THIS CASE IS A SIMULATION PROCEDURE,  
WHERE THE PROGRAM RETRIEVES BY INVERSE SCATTERING  
THE SHAPE OF THE KNOWN BODY. (INC=2 AND INVER=1).

THE INPUTS REQUIRED ARE:

SAME AS A THRU E LISTED ABOVE, PLUS THE LENGTH OF  
A SEGMENT FOR NEW SUBDIVISION OF THE BODY. (DS0)

4. INVERSE SCATTERING SOLUTION STARTING FROM THE  
MEASURED GIVEN RAMP RESPNSE OF AN UNKNOWN BODY (HSFM).  
THIS CASE IS THE TRUE COMPUTATION OF THE SHAPE OF THE  
BODY WHEN ONLY ITS RAMP RESPONSE IS KNOWN.  
(INC=2 AND INVER=2)

THE INPUTS REQUIRED ARE:

- A. THE TIME SAMPLES OF THE RAMP RESPONSE. (ENTERED  
IN DATA CARDS)
- B. THE LENGTH OF THE DESIRED SEGMENTS. (DS0)
- C. B THRU D LISTED ABOVE.

NOTE: NO INVERSE SCATTERING IS COMPUTED WHEN INC=1 .

PARAMETER DEFINITION:  
\*\*\*\*\*

INC: DEFINES THE TYPE OF INCIDENT FIELD

INC=1 THE INCIDENT FIELD IS A GAUSSIAN IMPULSE.  
INC=2 THE INCIDENT FIELD IS A RAMP.

INVER : DEFINES THE TYPE OF PROGRAM REQUIRED

INVER=0 NO INVERSE SCATTERING  
INVER=1 THE PROGRAM COMPUTES THE INVERSE SCATTERING,  
STARTING FROM A GIVEN BODY SHAPE.  
INVER=2 THE PROGRAM COMPUTES THE INVERSE SCATTERING  
FROM A GIVEN RAMP RESPONSE OF THE BODY.

NS: NUMBER OF SEGMENTS SUBDIVIDING THE CONTOUR (<=20)

ITS: NUMBER OF TIME SAMPLES NEEDED (<= 60)

DT: LENGTH OF THE TIME INCREMENT (SECONDS)

DS(20) : LENGTH OF THE SEGMENTS SUBDIVIDING THE  
CONTOUR OF THE BODY. (MAXIMUM 20 SEGMENTS)  
TO BE ENTERED IN DATA STATEMENT.

Z(21): Z-COORDINATE OF THE SPACE SAMPLE POINTS ON THE  
CONTOUR OF THE BODY. (MAXIMUM 21 POINTS ENTERED  
DELIMITING 20 SEGMENTS). (METER)

R0 (21) : RADIUS OF THE BODY AT THE SPACE SAMPLE POINTS  
DEFINED BY Z. (MAX. 21). (METER)

CJS(20,60): SPACE TIME SAMPLES OF THE S COMPONENT OF  
THE CURRENTS INDUCED ON THE BODY. (UP TO  
20 SPACE SAMPLES AND 60 TIME SAMPLES EACH)

CJPHI(20,60): SPACE TIME SAMPLES OF THE PHI COMPONENT  
OF THE CURRENTS INDUCED ON THE BODY. (UP TO  
20 SPACE SAMPLES AND 60 TIME SAMPLES EACH)

HSF (60): TIME SAMPLES OF THE SCATTERED FIELD. UP TO  
60 SAMPLES.

HSFM(60): TIME SAMPLES OF THE INITIAL RAMP RESPONSE.  
( THE MEASURED RAMP RESPONSE)

HSFC(60): TIME SAMPLES OF THE COMPUTED RAMP RESPONSE  
OF THE BODIES OBTAINED BY INVERSE SCATTERING

NP(20): NUMBER OF PATCHES ON THE RINGS DEFINED BY  
EACH SEGMENT.

B(20): ANGLE SUSTAINED BY THE PATCHES ON EACH RING.

ALFAK: SLOPE OF THE CONTOUR OF THE BODY CONTOUR  
FUNCTION, MEASURED AT THE CENTER OF THE  
EACH SEGMENT.

SI (20): SIN(ALFAK) FOR EACH SEGMENT.

CO (20): COS(ALFAK) FOR EACH SEGMENT.

EPS: NORMALIZED MEAN SQUARED ERROR ON THE BODY SHAPE  
COMPUTED BY INVERSE SCATTERING PROCEDURE.

ITER: NUMBER OF ITERATIONS EXECUTED FOR INVERSE SCATTERING SOLUTION.

C: SPEED OF LIGHT (METER/SEC)

CP : CONSTANT C\*DT.

OTHER PARAMETERS USED ARE DEFINED IN THE PROPER SUBROUTINE.

REMARKS:  
\*\*\*\*\*

1. THE SHAPE OF THE BODY IS ENTERD IN DATA CARDS WITH THE FORMAT 2F10.5

2. THE TIME SAMPLES OF THE MEASURED RAMP RESPONSE HSFM ARE ENTERD IN DATA CARDS WITH THE FORMAT 1F10.5  
THE VALUES OF THE SAMPLES MUST BE NORMALIZED, THAT MEANS MULTIPLIED BY C AND R (RANGE TO TARGET)

3. IN THIS PROGRAM THE INCIDENT FIELD H IS ASSUMED TO BE VERTICAL (HORIZONTAL POLARIZATION). THE DIFFERENCE BETWEEN THE RESPONSE TO THE TWO POLARIZATIONS IS ONLY THE SIGN OF THE RESPONSE.  
( SEE ALSO REMARKS IN SUBROUTINE SHAPE)

SUBROUTINES USED:  
\*\*\*\*\*

1. SUBROUTINE 'FIELD' : COMPUTES THE BACK SCATTERED FIELD FOR BOTH RAMP AND IMPULSE EXCITATION.

2. SUBROUTINE 'SHAPE' : COMPUTES WITH A METHOD OF ITERATIONS, THE SHAPE OF THE BODY FROM ITS RAMP RESPONSE. (SEE SUBROUTINE SHAPE FOR DETAILS.)

3. LIBRARY SUBROUTINE 'PLOTP' FOR PLOTS OF FIELDS AND SHAPE OF THE BODY.

METHOD OF SOLUTION:  
\*\*\*\*\*

SEE SUBROUTINE FIELD FOR THE COMPUTATION OF IMPULSE AND RAMP RESPONSES.

SEE SUBROUTINE SHAPE FOR THE COMPUTATION OF THE SHAPE OF THE BODY.

INVERSE SCATTERING: THE FIRST APPROXIMATION OF THE SHAPE IS OBTAINED FROM ITS MEASURED RAMP RESPONSE. A NEW RAMP RESPONSE IS COMPUTED FOR THAT APPROXIMATE BODY. THE PHYSICAL OPTICS PART OF THE RESPONSE IS EXTRACTED, AND IS USED TO COMPUTE A NEW SHAPE, AND SO ON, UNTILL A MINIMUM MEAN SQUARED ERROR IS OBTAINED BETWEEN THE LAST COMPUTED RESPONSE AND THE MEASURED.  
(SEE ALSO SECTION 5 OF THIS THESIS)

```

*** **** * * * * * * * * * * *
*          *
*  MAIN PROGRAM  *
*          *
*** **** * * * * * * * * * * *

SPHERE EXAMPLE

DIMENSION X(60)
DIMENSION CJS(20,60),CJPHI(20,60), HSF(60)
DIMENSION Z(21),RO(21),NP(20)
DIMENSION SI(20),CO(20),B(20),DS(20)
DIMENSION HSFM(60),HSFC(60)
COMMON HSF,Z,RO,ITS,NS,NS1
COMMON XMAX
DATA HSFM/60*0.0/
DATA HSFC/60*0.0/
DATA DS/20*0.20900/

START PROGRAM

DEFINE TYPE OF PROGRAM,INVER AND INC

INC=2
INVER=1

COMPUTATION PARAMETERS

NS=15
NS1=NS+1
ITS=60
IT=ITS
DS0=0.209
C=3.0E+8
DT=0.2/C
CP=C*DT

IF (INC.EQ.1) GO TO 11
IF (INVER .EQ.2) GO TO 15

STARTING POINT FOR INVER=1 AND INVER=0

CONTINUE

READ THE SHAPE OF THE BODY

DO 10 K=1,NS1
9510 READ(5,9510) Z(K),RO(K)
FORMAT(2F10.5)
CONTINUE

PLOT THE INITIAL SHAPE OF THE BODY

NS2=NS1+1
XMAX = Z(NS1)*1.25
Z(NS2)= XMAX
RO(NS2)= Z(NS2)
9620  WRITE(6,9620)
      FORMAT(1H1)
      'MODCUR=0
      CALL PLOTP(Z,RO,NS2,MODCUR)
      WRITE(6,9621)
      FORMAT(//,20X,'INITIAL SHAPE OF BODY',//,21X,
2 'X-AXIS Z, Y-AXIS RADIUS (RO)')

```

```

C      COMPUTE THE BACK-SCATTERED FIELD
C
C      CALL FIELD (DS,CP,DT,INC)
C
C      END OF PROGRAM FOR INVER=0 AND INVER=1
C
C      IF (INC.EQ.1) GO TO 99
C      IF (INVER .EQ.0) GO TO 99
C      IF (INVER .EQ.1) GO TO 19
15    CONTINUE
C
C      STARTING POINT FOR INVER=2
C
C      INC=2
C
C      READ THE GIVEN RAMP RESPONSE
C
C      DO 12 N=1,ITS
C      READ (5,9520) HSFM (N)
9520  FORMAT (1F10.5)
      HSF(N)=HSFM(N)
12    CONTINUE
      GO TO 920
C
19    CONTINUE
C
C      STORE THE COMPUTED RAMP RESPONSE
C
C      DO 910 N=1,ITS
C      HSFM(N)=HSF(N)
910   CONTINUE
920   CONTINUE
C
C      STARTING POINT FOR INVERSE SCATTERING COMPUTATION
C
C      ITER=1
C
C      COMPUTATION OF THE FIRST APPROXIMATION OF THE SHAPE
C
C      CALL SHAPE (DS,ITER,CP,DS0,IT)
C
C      COMPUTE SUM OF SQUARES OF THE TIME SAMPLES OF THE
C      ORIGINAL RAMP RESPONSE.
C
C      ITS=IT+10
C      SIGMA1=0.0
C      DO 940 N=1,ITS
C      SIGMA1=SIGMA1+HSFM(N)**2
940   CONTINUE
C
950   CONTINUE
C
C      COMPUTE THE RESPONSE OF THE APPROXIMATE BODY.
C
C      CALL FIELD (DS,CP,DT,INC)
C
C

```

```

C      COMPUTE NORMALIZED MEAN SQUARED ERROR.
C
C      SIGMA2=0.0
C      DO 960 N=1,ITS
C      SIGMA2=SIGMA2+(HSFM(N)-HSF(N))**2
960      CONTINUE
C      EPS=SIGMA2/SIGMA1
C
C      WRITE ERROR
C
C      WRITE (6,9666) EPS
9666      FORMAT ( //,15X,'NORMALIZED MEAN SQ. ERROR',1F10.5)
      IF (ITER.GT.1) GO TO 961
      EPS1=1.
961      CONTINUE
C
C      END THE PROGRAM WHEN THE ERROR IS MINIMUM
C
C      IF(EPS.GT.EPS1) GO TO 999
      EPS1=EPS
C
C      CONTINUE WHEN THE ERROR IS NOT YET MINIMIZED
C
C      ITER=ITER+1
C
C      EXTRACTION OF THE PHYSICAL OPTICS RESPONSE
C
9649      WRITE (6,9649)
      FORMAT (1H1, 10X,'PHYSICAL OPTICS RESPONSE',//,9X,'N',
2      10X,'H(N)',//)
      DO 970 N=1,ITS
      HSFC(N)=HSFC(N)+HSF(N)
      HSF(N)=ITER*HSFM(N)-HSFC(N)
      WRITE (6,9651) N,HSF(N)
9651      FORMAT(5X,15,5X,E12.5)
970      CONTINUE
C
C      USE PHYSICAL OPTICS RESPONSE TO COMPUTE A NEW SHAPE
C
C      CALL SHAPE (DS,ITER,CP,DS0,IT)
C
C      RETURN TO COMPUTE THE RESPONSE TO THE NEW BODY
C
999      GO TO 950
      CONTINUE
C
C      END OF PROGRAM WHEN MINIMUM ERROR ACQUIRED
C      WRITE FINAL ERROR
C
9625      WRITE (6,9625) ITER,EPS1
      FORMAT ( //,20X,'FINAL SHAPE AFTER',I4,'ITERATIONS',//,
2      '20X,'NORMALIZED MEAN SQUARED ERROR IS',1F10.5)
99      CONTINUE
C
C      END OF PROGRAM
C
      STOP
      END
C

```

\*\*\*\*\*  
\*  
\* SUBROUTINE FIELD \*  
\*  
\*\*\*\*\*

PURPOSE:  
\*\*\*\*\*

THIS SUBROUTINE PROVIDES THE SOLUTION TO THE  
MAGNETIC FIELD INTEGRAL EQUATION APPLIED TO A  
BODY OF REVOLUTION, EXCITED BY A GAUSSIAN PULSE  
OR A RAMP FIELDS. THE CURRENTS INDUCED ON THE BODY  
AND THE BACK-SCATTERED FIELD ARE COMPUTED.

USAGE:  
\*\*\*\*\*

CALL FIELD (DS,CP,DT,INC)

PARAMETER DEFINITION:  
\*\*\*\*\*

HI: INCIDENT FIELD

C3,C4: CONSTANTS.

METHOD OF SOLUTION:  
\*\*\*\*\*

THE METHOD OF SOLUTION IS DESCRIBED IN SECTION 4  
OF THIS THESIS.

```

C
C      SJROUTINE FIELD (DS,CP,DT,INC)
C
C      DIMENSION X(60)
C      DIMENSION CJS(20,60),CJPHI(20,60), HSF(60)
C      DIMENSION Z(21),RO(21),NP(20)
C      DIMENSION SI(20),CO(20),B(20),DS(20)
C      COMMON HSF,Z,RO,ITS,NS,NS1
C
C      CONSTANT DEFINITION
C
C      PI=3.141592654
C      C=3.0E+8
C      C+=-1./(DT*4.0*C)
C      C3=1./(PI*2.0)
C
C      GAUSSIAN IMPULSE PARAMETERS
C
C      AA=0.6 E+9
C      TMAX=DT*5.0
C      A2=AA*AA
C
C      DO 20 K=1,NS
C      K1=K+1
C
C      COMPUTE THE SLOPE OF THE SEGMENTS
C
C      WK=(RO(K1)-RO(K))/(Z(K1)-Z(K))
C      ALFAK=ATAN(WK)
C      SI(K)=SIN(ALFAK)
C      CO(K)=COS(ALFAK)
C
C      COMPUTE THE CENTRAL SPACE SAMPLE POINTS
C
C      Z(K)=(Z(K1)+Z(K))/2.0
C      RO(K)=(RO(K1)+RO(K))/2.0
C
C      COMPUTE THE NUMBER OF PATCHES IN EACH RING
C
C      PK=      PI*RO(K)/DS(K)
C      VP(K)=2*IFIX(PK)
C      IF (NP(K).GT.0) GO TO 23
C      NP(K)=1
C
C      COMPUTE THE ANGLE SUSTAINED BY THE PATCHES OF EACH
C      RING.
C
C      23  CONTINUE
C      B(K)=2.0*PI/NP(K)
C
C      INITIAL CONDITIONS OF THE CURRENTS
C
C      TZK=1.0+Z(K)/CP
C      DO 25 N=1,2
C      IF (N.LT.TZK) GO TO 25
C      IF (INC.EQ.1) GO TO 24
C
C      WHEN INCIDENT FIELD IS A RAMP
C
C      HI=(N-1)*CP-Z(K)
C      GO TO 27
C      CONTINUE
C
C      WHEN INCIDENT FIELD IS AN IMPULSE
C
C      ARG=(N-1)*DT-TMAX-Z(K)/C
C      HI=(N-1)*EXP(-A2*ARG*ARG)

```

```

26      GO TO 27
CONTINUE
HI=0.0
27      CONTINUE
      INITIAL CURRENTS INDUCED
      CJPHI(K,N)=-2.0*HI*SI(K)
      CJS(K,N)=-2.0*HI
25      CONTINUE
20      CONTINUE
      COMPUTE THE CURRENT COMPONENTS
      COMPUTE FIRST THE INTEGRAL PART OF THE EQUATION
      AT TIME N
      DO 100 N=3,ITS
      AT THE K-TH SAMPLE
      DO 200 K=1,NS
      CJS(K,N)=0.0
      CJPHI(K,N)=0.0
      INFLUENCE OF ALL OTHER SPACE CURRENTS
      DO 300 I=1,NS
      NP2=NP(I)
      DO 400 M=1,NP2
      IF (M.EQ.1) GO TO 410
410      GO TO 420
      CONTINUE
      IF (I.EQ.K) GO TO 400
420      CONTINUE
      COMPUTE DISTANCE BETWEEN SAMPLES
      CM=COS((M-1)*B(I))
      SM=SIN((M-1)*B(I))
      V=Z(I)-Z(K)
      R2=(RO(K)*RO(K)+RO(I)*RO(I)+V*V-2.0*RO(I)*RO(K)*CM)
      R=SQRT(R2)
      COMPUTE RETARDATION TIME
      Q=N-R/CP
      INTERPOLATION OF THE CURRENT AND THEIR TIME
      DERIVATIVE AT THE RETARDED TIME
      NQ=IFIX(Q)
      NQP=NQ+1
      NQM=NQ-1
      NQ2=NQ+2
      T1=Q-NQ2
      T2=Q-NQP
      T3=Q-NQ
      T4=Q-NQM
      IF (Q.LE.1.0) GO TO 400
      IF (Q.LE.2.0) GO TO 435
      IF (N.EQ.NQP) GO TO 430
      IF (N.EQ.NQ2) GO TO 432

```

FCUR POINT LAGRANGIAN INTERPOLATION

```

Y1=T2*T3*T4*CJS(I,NQ2)/6.0-T3*T4*T1*CJS(I,NQP)/2.0
2 +T4*T1*T2*CJS(I,NQ)/2.0-T1*T2*T3*CJS(I,NQM)/6.0
Y2=T2*T3*T4*CJPHI(I,NQ2)/6.0-T3*T4*T1*CJPHI(I,NQP)/2.0
2 +T4*T1*T2*CJPHI(I,NQ)/2.0-T1*T2*T3*CJPHI(I,NQM)/6.0
CJS=(T2*T3+T2*T4+T3*T4)*CJS(I,NQ2)/6.0
2 -(T3*T4+T4*T1+T1*T3)*CJS(I,NQP)/2.0
3 +(T4*T1+T4*T2+T1*T2)*CJS(I,NQ)/2.0
4 -(T1*T3+T2*T3+T2*T1)*CJS(I,NQM)/6.0
DJPHI=(T2*T3+T2*T4+T3*T4)*CJPHI(I,NQ2)/6.0
2 -(T3*T4+T4*T1+T1*T3)*CJPHI(I,NQP)/2.0
3 +(T4*T1+T4*T2+T1*T2)*CJPHI(I,NQ)/2.0
4 -(T1*T3+T2*T3+T2*T1)*CJPHI(I,NQM)/6.0
GO TO 440
430 CONTINUE

```

TWO POINT LAGRANGIAN INTERPOLATION

```

Y1=T4*CJS(I,NQ)-T3*CJS(I,NQM)
Y2=T4*CJPHI(I,NQ)-T3*CJPHI(I,NQM)
CJS=CJS(I,NQ)-CJS(I,NQM)
DJPHI=CJPHI(I,NQ)-CJPHI(I,NQM)
GO TO 440
432 CONTINUE

```

THREE POINT LAGRANGIAN INTERPOLATION

```

Y1=T4*T3*CJS(I,NQP)/2.0-T2*T4*CJS(I,NQ)
2 +T2*T3*CJS(I,NQM)/2.0
Y2=T4*T3*CJPHI(I,NQP)/2.0-T2*T4*CJPHI(I,NQ)
2 +T2*T3*CJPHI(I,NQM)/2.0
CJS=(T4+T3)*CJS(I,NQP)/2.0-(T2+T4)*CJS(I,NQ)
2 +(T2+T3)*CJS(I,NQM)/2.0
DJPHI=(T4+T3)*CJPHI(I,NQP)/2.0-(T2+T4)*CJPHI(I,NQ)
2 +(T2+T3)*CJPHI(I,NQM)/2.0
GO TO 440
435 CONTINUE
IF (N.EQ.NQP) GO TO 400
IF (N.EQ.NQ2) GO TO 433

```

THREE POINT LAGRANGIAN INTERPOLATION

```

Y1=T2*T3*CJS(I,NQ2)/2.0-T3*T1*CJS(I,NQP)
2 +T2*T1*CJS(I,NQ)/2.0
Y2=T2*T3*CJPHI(I,NQ2)/2.0-T3*T1*CJPHI(I,NQP)
2 +T2*T1*CJPHI(I,NQ)/2.0
CJS=(T2+T3)*CJS(I,NQ2)/2.0-(T3+T1)*CJS(I,NQP)
2 +(T2+T1)*CJS(I,NQ)/2.0
DJPHI=(T2+T3)*CJPHI(I,NQ2)/2.0-(T3+T1)*CJPHI(I,NQP)
2 +(T2+T1)*CJPHI(I,NQ)/2.0
GO TO 440
433 CONTINUE

```

TWO POINT LAGRANGIAN INTERPOLATION

```

Y1=T3*CJS(I,NQP)-T2*CJS(I,NQ)
Y2=T3*CJPHI(I,NQP)-T2*CJPHI(I,NQ)
CJS=CJS(I,NQP)-CJS(I,NQ)
DJPHI=CJPHI(I,NQP)-CJPHI(I,NQ)

```

440 CON- INUE

```

C
C          FINAL COMPUTATION OF THE INTEGRAL
C
V=Z(I)-Z(K)
    F1=V*CM*SI(I)+(RO(K)-R0(I)*CM)*CO(I)
    X1=F1*CM
    X2=V*(SM*SM)
    U=V*SI(I)*SI(K)+RO(K)*CO(K)*SI(I)-RO(I)*SI(K)*CO(I)
    F2=(RO(K)*CM-R0(I))*CO(K)+CM*V*SI(K)
    Y11=Y1*X1
    Y22=Y2*X2
    XP1=F2*CM
    XP2=U*(SM*SM)
    YP1=Y2*XP1
    YP2=Y1*XP2
    C1=DS(I)*RO(I)*B(I)/(CP*R2)
    R3=R*R2
    C2=DS(I)*RO(I)*B(I)/R3
    CJPHI(K,N)=CJPHI(K,N)+C1*(DJPHI*XP1+DJS*XP2)
    +C2*(YP1+YP2)
2  CJS(K,N)= CJS(K,N)+C1*(DJPHI*X2 +DJS*X1 )+C2*(Y11+Y22)
    CONTINUE
C
300  CONTINUE
    CJS(K,N)=CJS(K,N)*C3
    CJPHI(K,N)=CJPHI(K,N) *C3
C
C          END OF COMPUTATION OF THE INTEGRAL
C
C          ADDITION OF THE CURRENT INDUCED BY THE INCIDENT
C          FIELD AT THE COMPUTATION POINT. (PHYSICAL OPTICS PART
C
TZK=1.0+Z(K)/CP
TD=TZK+2.*TMAX/DT
IF (N.LT.TZK) GO TO 200
IFI (INC.EQ.1) GO TO 240
C
C          WHEN INCIDENT FIELD IS A RAMP
C
HI=(N-1)*CP-Z(K)
GO TO 250
240  CONTINUE
IFI (INC.GT.TD) GO TO 200
C
C          WHEN INCIDENT FIELD IS AN IMPULSE
C
ARG=(N-1)*DT-TMAX-Z(K)/C
    HI=EXP(-A2*ARG*ARG)
250  CONTINUE
C
C          FINAL CURRENT AT THE K-TH SPACE SAMPLE AT TIME N
C
CJS(K,N)=CJS(K,N)-2.0*HI
    CJPHI(K,N)=CJPHI(K,N)-2.0*HI*SI(K)
C
C          NEXT SPACE SAMPLE
C
200  CONTINUE
    NEXT TIME
C
100  CONTINUE
C
C          END OF COMPUTATION OF ALL SPACE-TIME CURRENTS

```

```

      IF (INC.EQ.1) GO TO 110
      WRITE(6,9623)
9623  FORMAT(1H1,10X,'NORMALIZED FIELD (H*C*R)',//,
2      10X,'RAMP RESPONSE',//,9X,'N',10X,'H(N)',//)
      GO TO 111
110   CONTINUE
      WRITE(6,9723)
9723  FORMAT(1H1,10X,'NORMALIZED FIELD (H*R)',//,
2      10X,'IMPULSE RESPONSE',//,9X,'N',10X,'H(N)',//)
C
C
      START COMPUTATION OF THE BACK-SCATTERED FIELD
C
C
111   CONTINUE
C
C
      AT THE N-TH TIME
C
      DO 500 N=1,ITS
      HSF(N)=0.0
      IF (N.EQ.1) GO TO 650
C
C
      FROM EACH SAMPLE
C
      DO 600 K=1,NS
C
C
      COMPUTATION OF THE RETARDATION TIME
C
      Q=N-Z(K)/CP
      NQ=IFIX(Q)
C
C
      INTERPOLATION OF THE TIME DERIVATIVE OF THE CURRENT
      AT THE RETARDED TIME
C
      NQP=NQ+1
      NQ4=NQ-1
      NQ2=NQ+2
      T1=Q-NQ2
      T2=Q-NQP
      T3=Q-NQ
      T4=Q-NQM
      IF (Q.LE.1.0) GO TO 600
      IF (Q.LE.2.0) GO TO 601
          IF (N.EQ.NQP) GO TO 602
          IF (N.EQ.NQ2) GO TO 603
C
C
      FCUR POINT LAGRANGIAN INTERPOLATION
C
      DJS=(T2*T3+T2*T4+T3*T4)*CJS(K,NQ2)/6.0
2      -(T3*T4+T4*T1+T1*T3)*CJS(K,NQP)/2.0
3      +(T4*T1+T4*T2+T1*T2)*CJS(K,NQ)/2.0
4      -(T1*T3+T2*T3+T2*T1)*CJS(K,NQM)/6.0
      DJPHI=(T2*T3+T2*T4+T3*T4)*CJPHI(K,NQ2)/6.0
2      -(T3*T4+T4*T1+T1*T3)*CJPHI(K,NQP)/2.0
3      +(T4*T1+T4*T2+T1*T2)*CJPHI(K,NQ)/2.0
4      -(T1*T3+T2*T3+T2*T1)*CJPHI(K,NQM)/6.0
      GO TO 620
      CONTINUE
C
C
      TWO POINT LAGRANGIAN INTERPOLATION
C
      DJS = CJS(K,NQ) - CJS(K,NQM)
      DJPHI=CJPHI(K,NQ) - CJPHI(K,NQM)
      GO TO 620
      CONTINUE

```

```

C      THREE POINT LAGRANGIAN INTERPOLATION
C
2      DJS=(T4+T3)*CJS(K,NQP)/2.0-(T2+T4)*CJS(K,NQ)
2      +(T2+T3)*CJS(K,NQM)/2.0
2      DJPHI=(T4+T3)*CJPHI(K,NQP)/2.0-(T2+T4)*CJPHI(K,NQ)
2      +(T2+T3)*CJPHI(K,NQM)/2.0
GO TO 620
601  CONTINUE
IF (N.EQ.NQP) GO TO 600
IF (N.EQ.NQ2) GO TO 604
C      THREE POINT LAGRANGIAN INTERPOLATION
C
2      DJS=(T2+T3)*CJS(K,NQ2)/2.0-(T3+T1)*CJS(K,NQP)
2      +(T2+T1)*CJS(K,NQ)/2.0
2      DJPHI=(T2+T3)*CJPHI(K,NQ2)/2.0-(T3+T1)*CJPHI(K,NQP)
2      +(T2+T1)*CJPHI(K,NQ)/2.0
GO TO 620
604  CONTINUE
C      TWO POINT LAGRANGIAN INTERPOLATION
C
DJS = CJS(K,NQP) - CJS(K,NQ)
DJPHI=CJPHI(K,NQP)-CJPHI(K,NQ)
620  CONTINUE
C      CONTRIBUTION OF THE K-TH SPACE SAMPLE
C
HSF(N)=HSF(N)+RO(K)*(SI(K)*DJS+DJPHI)*DS(K)
C      NEXT SPACE SAMPLE
C
600  CONTINUE
650  CONTINUE
C      FINAL VALUE OF THE N-TH TIME SAMPLE OF THE FIELD
C
HSF(N)=C4*HSF(N)
X(N)=N*CP
9610  WRITE(6,9610) N,HSF(N)
FORMAT(5X,I5,5X,E12.5)
C      NEXT TIME SAMPLE
C
500  CONTINUE
C      END OF COMPUTATION OF THE FIELD
C      PLOT BACK-SCATTERED FIELD VERSUS TIME(LIGHT-METERS)
C
9630  WRITE(6,9630)
FORMAT(1H1)
MODCUR=0
CALL PLOT(X,HSF,ITS,MODCUR)
IF (INC.EQ.1) GO TO 112
WRITE(6,9624)
9624  FORMAT(//,14X,' NORMALIZED BACK SCATTERED FIELD',//,
2 14X,'RAMP RESPONSE',//,14X,
3 'X-AXIS TIME (C*DT)',10X,'Y-AXIS FIELD (H*C*R) ')
GO TO 113
112  CONTINUE
WRITE(6,9724)
9724  FORMAT(//,14X,' NORMALIZED BACK SCATTERED FIELD',//,
2 14X,'IMPULSE RESPONSE',//,14X,
3 'X-AXIS TIME (C*DT)',10X,'Y-AXIS FIELD (H*R) ')
113  CONTINUE
RETURN
END

```

\*\*\*\*\*  
\*  
\* SUBROUTINE SHAPE  
\*  
\*\*\*\*\*

PURPOSE:  
\*\*\*\*\*

THIS SUBROUTINE COMPUTES THE SHAPE OF THE BODY FROM ITS APPROXIMATE COMPUTED PHYSICAL-OPTICS RESPONSE. IT FINDS THE CONTOUR FUNCTION  $R_0(z)$  AND DIVIDES IT INTO APPROXIMATELY EQUAL SEGMENTS (DS).

USAGE:  
\*\*\*\*\*

CALL SHAPE (DS,ITER,CP,DS0,IT)  
THE DATA NEEDED AT THE INPUT ARE DS0, AND HSF.

PARAMETER DEFINITION:  
\*\*\*\*\*

ZMAX: THE MAXIMUM LENGTH OF THE BODY ON THE Z-AXIS.  
(CORRESPONDING TO THE POINT WHERE THE RAMP RESPONSE CHANGES ITS SIGN)

IT: THE TRANSIT TIME NEEDED TO OBTAIN THE REFLECTION FROM THE POINT LOCATED AT ZMAX. (IT IS THE NUMBER OF TIME INCREMENTS).

DS0: OPTIMAL LENGTH OF A SEGMENT(NEEDED FOR THE COMPUTED SHAPE SUBDIVISION) .(METER)

ALL OTHER PARAMETERS ALREADY DEFINED IN MAIN PROGRAM

REMARKS:  
\*\*\*\*\*

IN THIS PROGRAM THE RAMP RESPONSE USED ASSUMES A VERTICAL H FIELD INCIDENT (HORIZONTAL POLARIZATION). THIS GIVES A POSITIVE INITIAL RESPONSE. FOR VERTICAL POLARIZATION THE INITIAL RESPONSE IS NEGATIVE. (THE WHOLE RESPONSE CHANGES ITS SIGN) SINCE THE RADIUS OF THE BODY AT EACH POINT IS PROPORTIONAL TO SQRT OF THE INITIAL RAMP RESPONSE, IT MUST BE ENSURED THAT THE RAMP USED HAS PROPER SIGN.

METHOD OF SOLUTION:  
\*\*\*\*\*

FIRST STEP IS TO FIND ZMAX, WHICH CORRESPONDS TO THE POINT WHERE THE RESPONSE CHANGES ITS SIGN.  
THE CONTOUR FUNCTION OF THE BODY  $R_0(z)$  IS PROPORTIONAL TO THE SQRT OF THE PHYSICAL-OPTICS RAMP RESPONSE.  
THE BODY IS DIVIDED INTO APPROXIMATELY EQUAL SEGMENTS, AND THE SPACE SAMPLES DELIMITING THE SEGMENTS ARE FOUND USING A "CUT AND TRY METHOD" WHICH CONVERGES TO THE DESIRED LENGTH OF SEGMENT.  
THE RADIUS AT THE SPACE SAMPLE POINTS ARE INTERPOLATED FROM THE KNOWN SAMPLES OF THE RAMP RESPONSE.  
THE DATA OBTAINED Z,  $R_0$ , DS, NS, IS USED FOR THE NEXT COMPUTATION OF THE FIELD.

```

SUBROUTINE SHAPE (DS,ITER,CP,DS0,IT)
  DIMENSION DS(20),R0(21),Z(21),HSF(60)
  COMMON HSF,Z,R0,ITS,NS,NSI
  COMMON XMAX

  START PROGRAM

  FIND LENGTH OF BODY (ZMAX) AND ITS CORRESPONDING
  TIME OF APPEARANCE IN THE RAMP RESPONSE (IT)

  DSP=DS0
  DO 710 N=1,ITS
  IF(HSF(N).LT.0.0) GO TO 720
  CONTINUE
  CONTINUE
  IT=N-1
  AD=1./(1.-HSF(N)/HSF(IT))
  ZMAX=(IT-2+AD)*CP/2.

  COMPUTE SHAPE OF BODY UP TO ZMAX.

  54  CONTINUE
  Z(1)=0.0
  R0(1)=SQRT(2*HSF(2))
  DO 50 K=1,19
  K1=K+1
  U=DSP/2.0
  CONTINUE
  NN=1

  ADJUST Z TO OBTAIN PROPER DS

  53  Z(K1)=Z(K)+U
  CONTINUE
  IF(Z(K1).GT.ZMAX) GO TO 56
  GO TO 57
  56  CONTINUE
  Z(K1)=ZMAX
  R0(K1)=0.0
  GO TO 51
  57  CONTINUE

  COMPUTE CORRESPONDING RADIUS (R0) OF THE BODY

  G=2*Z(K1)/CP+2.
  M=IFIX(G)
  M1=M+1
  R02=(HSF(M1)-HSF(M))*(G-M)+HSF(M)
  R0(K1)=SQRT(R02*2.)

  COMPUTE LENGTH OF SEGMENT DS

  51  CONTINUE
  DS(K)=SQRT((Z(K1)-Z(K))**2+(R0(K1)-R0(K))**2)
  A=DS(K)/DSP

  ALL OBTAINED SEGMENTS MUST BE WITHIN 1/100 OF DS0

  IF (A.GT.1.01) GO TO 58
  IF (Z(K1).EQ.ZMAX) GO TO 60
  IF (A.LT.0.99) GO TO 58
  GO TO 50

```

```

C          ADJUST Z AND GO BACK TO CHECK FOR DS
C
58      CONTINUE
      NN=NN+1
      IF (A.GT.1.0) GO TO 90
      Z(K1)=Z(K1)+U/NN
      GO TO 53
90      CONTINUE
      Z(K1)=Z(K1)-U/NN
      IF (Z(K1).GT.Z(K)) GO TO 53
      Z(K1)=Z(K1)+U/NN
      NN=NN+1
      GO TO 90
50      CONTINUE
C          NEXT SEGMENT
C
60      CONTINUE
      NS1=K1
      VS=NS1-1
C          ADJUST FOR LAST SEGMENT
C
61      U2=DS(NS)/DSP
      IF(U2.LT.0.10) GO TO 52
      IF(U2.LT.0.95) GO TO 61
      GO TO 70
61      CONTINUE
      U3=(Z(NS1)-Z(NS))/NS
      NS1=NS1-1
      NS=NS1-1
      DO 80 K=1,NS
      K1=K+1
      Z(K1)=Z(K1)+K*U3
      Z(NS1)=ZMAX
      G=2*Z(K1)/CP+2.
      M=IFIX(G)
      M1=M+1
      R02=(HSF(M1)-HSF(M))*(G-M)+HSF(M)
      R0(K1)=SQRT(R02*2.)
      R0(NS1)=0.0
      DS(K)=SQRT((Z(K1)-Z(K))**2+(R0(K1)-R0(K))**2)
80      CONTINUE
      GO TO 70
62      CONTINUE
      Z(NS)=ZMAX
      R0(NS)=0.0
      NS2=NS-1
      DS(NS2)=SQRT((ZMAX-Z(NS2))**2+R0(NS2)**2)
      NS1=NS1-1
      NS=NS1-1
      CONTINUE
C          SHAPE OF BODY COMPLETED AND SUBDIVIDED
C
C          WRITE NUMBER OF SEGMENTS OBTAINED
C
9601  WRITE(6,9601) ITER,NS
      FORMAT(1H1,5X,'NEW NUMBER OF SEGMENTS AFTER ITERATION'
      2,I4,I4,14,10X,Z',10X,R0',10X,DS',14,10X)
      DS(NS1)=99.9
      DO 40 N=1,NS1
      WRITE(6,9602) Z(N),R0(N),DS(N)
      FORMAT(5X,3F10.5)
      CONTINUE
40

```

```
C      PLOT THE CONTOUR FUNCTION OF THE BODY
C
C      NS2=NS1+1
C      Z(NS2)= X MAX
C      RO (NS2)= Z(NS2)
C      WRITE(6,9603)
9603  FORMAT(1H1)
      MODCUR=0
      CALL PLOTP(Z,RO,NS2,MODCUR)
      WRITE(6,9604) ITER
9604  FORMAT(//,20X,'SHAPE OF BODY AFTER ITERATION NUMBER ',
2 14,/,20X,'X-AXIS Z  Y-AXIS RADIUS (RO)')

C      END OF SUBROUTINE SHAPE
C
C      RETURN
C      END
```

CCCCCCCC

EXAMPLE OF DATA CARDS

0.0	0.0
0.02185	0.20791
0.08645	0.40674
0.19098	0.58779
0.33387	0.74314
0.50	0.86603
0.69098	0.95106
0.89547	0.99452
1.10453	0.99452
1.30902	0.95106
1.50	0.86603
1.66913	0.74314
1.80902	0.58779
1.91355	0.40674
1.97815	0.20791
2.0	0.0

APPENDIX F  
RELATIONSHIP BETWEEN RAMP RESPONSE AND SHAPE

The validity of (5.2) will be demonstrated analytically here in the case of a metallic body of revolution. We first express the axially directed incident ramp field as:

$$H_R^i(z, t) = \begin{cases} t - z/C & t \geq z/C \\ 0 & t < z/C \end{cases} \quad (F.1)$$

The physical optics current induced on the body is given by:

$$\vec{J}(\vec{r}, t) = 2\hat{a}_n \times \vec{H}_R^i(\vec{r}, t) \quad (F.2)$$

The backscattered far-zone field is given by equation (3.8) and its scalar equivalent for the body of revolution is expressed by (3.16). Substitution of the current in (3.16) gives the physical optics ramp response as follows:

$$H_R^s(t) = -\frac{1}{4r_0 C} \int_0^s \frac{\partial}{\partial \tau} [-4H_R^i(z', \tau) \sin \alpha'] \rho' ds' \quad (F.3)$$

The time derivative of the incident field expressed by (F.1) is unity:

$$\frac{\partial H_R^i}{\partial \tau} = \frac{\partial H_R^i}{\partial t} = 1 \quad t < z/C \quad (F.4)$$

Substitution of (F.4) into (F.3) gives:

$$H_R^S(t) = \frac{1}{r_o C} \int_0^S \sin \alpha' ds' \quad (F.5)$$

From the geometry of the body of revolution we note that:

$$d\alpha' = \sin \alpha' ds'$$

Substitution in (F.5) gives the following expression:

$$H_R^S(t) = \frac{1}{r_o C} \int_0^{\rho(z)} \rho' d\rho' = \frac{1}{2r_o C} \rho^2(z) \quad (F.6)$$

Since the area function is given by:

$$A(z) = \pi \rho^2(z)$$

the physical optics ramp response (F.6) will be related to  $A(z)$  by

$$H_R^S(t) = \frac{1}{2\pi r_o C} A(z) \quad (F.7)$$

#### LIST OF REFERENCES

1. Baum, C.E., The Singularity Expansion Method, Springer-Verlag (Chapter 3), New York, 1975.
2. Mittra, R., Integral Equation Methods for Transient Scattering, Chapter 2. Springer-Verlag, New York, 1975.
3. Miller, E.K., and Landt, J.A., "Direct time domain techniques for transient radiation and scatterers," Interaction Note 334, July 1976, Lawrence Livermore Laboratory.
4. Hammond, C.W., The Development of a Bistatic Electromagnetic Scattering Laboratory, M.S. Thesis, Naval Postgraduate School, Monterey, Ca., December 1980.
5. Kennaugh, E.M., and Ccxgriff, L., "The use of impulse response in electromagnetic scattering problems," IRE Nat'l Conv. Rec. 1958, pt. 1, p. 72.
6. Kennaugh, E.M., and Moffatt, D.L., "Transient and impulse response approximations," Proc. IEEE 53, p. 893 (1965).
7. Bennett, C.L., and Weeks, A Technique for Computing Approximate Electromagnetic Impulse Response of Conducting Bodies, Ph.D. Dissertation, Purdue University, 1968.
8. Sayre, E.P., and Harrington, R., "Time Domain Radiation and Scattering by Thin Wires," Applied Sci. Res. 26,, p. 413-444 (1972).
9. Miller, E.K., Poggio, A.J. and Burke, G.J., "An integro-differential equation technique for the time domain analysis of thin wire structure," Journal Comput. Phys. 12(1), p. 24-28 and 210-233 (1979).
10. Mittra, R., Computer Techniques for Electromagnetics, Pergamon Press, 1974, Chapter 4.
11. Miller, E.K., "Some computational aspects of transient electromagnetics," Interaction Notes, Note 143, 1972. Lawrence Livermore Laboratory.
12. Bennett, C.L., "Time domain electromagnetics and its applications," Proc. of the IEEE, March 1978, pp. 299-318.
13. Young, J.D., "Radar imaging from ramp response signatures," IEEE Trans. on Ant. and Prop. Vol. AP-24, May 1976.

14. Shubert, K.A., Young, J.D. and Moffatt, D.L., "Synthetic radar imagery," IEEE Trans on Ant. and Prop. Vol. AP-25, No. 4, July 1977.
15. Moffatt, D.L., and Mains, R., "Detection and discrimination of radar targets," IEEE Trans. on Ant. and Prop. May 1975.
16. Bennett, C.L., "Time domain inverse scattering," Sperry Research Center, SRC-RP-80-63, November 80.
17. Standard Mathematical Tables, CRC Press, 25-th Edition.
18. Yogadish, Das and Wolfgang Boemer, "On radar target shape estimation using algorithms for reconstruction from projections," IEEE Transactions on Ant. and Prop. Vol. AP-26, March 1978.

INITIAL DISTRIBUTION LIST

	No. Copies
1. Library, Code 0142 Naval Postgraduate School Monterey, California 93940	2
2. Chairman, Electrical Engineering Department, Code 62 Ki Department of Electrical Engineering Naval Postgraduate School Monterey, Ca 93940	1
3. Professor M.A. Morgan, Code 62Mw Department of Electrical Engineering Naval Postgraduate School Monterey, Ca 93940	12
4. Professor M. Hamid, Code 62Ho Department of Electrical Engineering Naval Postgraduate School Monterey, Ca 93940	3
5. LCDR M. Morag, Israeli Navy 16 shmuuel Hanagid Herzlia, ISRAEL	10
6. Lt. Col A. Feit SMC #1079 Naval Postgraduate School Monterey, California 93940	1
7. Commander R. Antebi, Israeli Navy Defense and Armed Forces Attaché Embassy of Israel 3514 International Drive, NW Washington, D.C. 20008	1
8. Defense Technical Information Center Cameron Station Alexandria, Virginia 22314	2

END

DATE

FILMED

9-81

DTIC